Investigation of the properties of SiGe islands by selective wet chemical etching and scanning probe microscopy

Untersuchung der Eigenschaften von SiGe Halbleiterinseln durch selektives nasschemisches Ätzen und Rastermikroskopie

Dissertation zur Erlangung des akademischen Grades
des Doktors der Naturwissenschaften (Dr. rer. nat.)
an der Universität Konstanz
Fachbereich Physik

vorgelegt von

Georgios Katsaros

Dissertation der Universität Konstanz
Tag der mündlichen Prüfung: 13. April 2006
Referenten: Prof. Dr. Klaus Kern
Prof. Dr. Günter Schatz

Zusammenfassung

In der vorliegenden Arbeit werden mittels selektiven nasschemischen Ätzens und Rastermikroskopie Germanium/Silizium Halbleiterinseln untersucht.

Durch selektives Ätzen von Ge über Si und Rasterkraftmikroskopie wird die Zusammensetzung von freistehenden Inseln untersucht, die durch Abscheidung von reinem Ge auf Si(001) bei unterschiedlichen Wachstumstemperaturen und Abscheidungsraten gewachsen sind. Es zeigt sich, dass sich Si bei niedrigen Temperaturen (560°-600°C) hauptsächtlich in der Peripherie der Inseln befindet, während bei höheren Temperaturen auch das Zentrum der Inseln mehr Si enthält. Die Experimente machen außerdem deutlich, dass das Erhöhen der Wachstumsrate zu einer Erhöhung des Ge Anteils der Inseln führt. Mit Hilfe von Simulationen werden die experimentellen Beobachtungen bestätigt und es wird demonstriert, dass die Komposition der Inseln mittels eines einfachen kinetischen Modells, das nur Oberflächendiffusionen beinhaltet, verstanden werden kann.

Während für die oben genannten Inseln das Kompositionsprofil eine vierfache Symmetrie besitzt, ändert sich dieses drastisch, sobald die Inseln getempert werden. Die Inseln werden nicht mehr symmetrisch geätzt, vielmehr wird eine Seite schneller erodiert als die andere. Dieses inhomogene Kompositionsprofil wird darauf zurückgeführt, dass sich die Inseln während des Temperns bewegen. Diese Bewegung kann durch eine energetisch günstige Vermischung von Ge mit Si erklärt werden. Ge-reiches Material diffundiert von der einen Seite der Insel auf die andere, wo es sich mit Si, das von der Oberfläche dorthin diffundiert, vermischt. Als Folge dieser Bewegung werden die Inseln größer und Si-reicher.

Mit Hilfe des Rastertunnelmikroskops wurden auch Inseln untersucht, die sich während des Wachtums und des Temperns auflösen. Die Inseln schrumpfen nicht selbst-ähnlich, sondern sie folgen einer Reihe von morphologischen Übergängen. Diese Entwicklung ist genau invers zum Wachstumsprozess der Inseln. Das beweißt, dass die Morphologie der Inseln thermodynamisch determiniert ist.

Durch selektives Ätzen von Si über Ge wurden auch die mit Si überwachsenen Inseln untersucht. Die Entfernung von Si durch nasses Ätzen

erlaubt die Untersuchung sowohl der Morphologie als auch der Zusammensetzung der Inseln. Es wird nachgewiesen, dass die Morphologie der Si Oberfläche, die die Inseln bedeckt, nicht immer der der darunter liegenden Inseln entspricht. Außerdem wird demonstriert, dass die Komposition der auf niedrigen Temperaturen überwachsenen Inseln (300°-450°C) die gleiche ist, wie die der freistehenden Inseln. Für die Inseln, die bei 580°C überwachsen worden sind, zeigt es sich, dass trotz morphologischen Änderungen der Gereiche Teil noch existiert. Dieses weisst darauf hin, dass zumindestens bis zur Temperatur von 580°C keine Massendiffusion stattfindet.

Contents

Chapter 1

Introduction

Since the invention of integrated circuits, which can be traced back to 1959, Silicon (Si) has become the most important semiconductor material and still today, after almost 50 years, it holds this position. The main reasons for this are its abundance (it makes 27.5% of Earth's crust weight), its high purity [huge Si crystals can be grown without dislocations and the impurity level is in the low ppt (parts per thousand) range] and its oxide. Silicon oxide (SiO_2) is a very stable dielectric and it can be easily produced in a very good quality by simple thermal oxidation.

In 1961 a circuit build out of four transistors was fabricated on a single Si piece. Since then, the complexity of the circuits has increased dramatically. Very early, in 1964, Gordon Moore predicted that the number of transistors on a chip would double every two years (Moore's law). And indeed the prediction of Moore has come true. This was possible because an enormous decrease in the dimensions of the devices and interconnections contained in a chip has been realized. It is clear that this process cannot continue for ever since at some point the dimensions of the devices will become so small that technological problems will arise. One of the most important problems are the interconnections between the devices included in a chip. By decreasing their dimensions the produced heat is increasing enormously and it can become detrimental for the operation of the chip. A possible solution to this problem is the use of optical interconnects [1]. But for this, a Si-based light emitting device is needed, i.e. a device in which radiative transitions can take place.

Apart from the technological problems which have to be solved, quantum theory starts to become "active" at these small length scales. Thus

additional problems for the function of the devices do arise. In order to overcome these problems there have been intense investigations towards two directions: either Si-devices have to be replaced by others which are based on new concepts or alternatively new materials have to be incorporated in Si-based devices in order to improve their performance.

An ideal material to be incorporated into Si is Germanium (Ge) since it is miscible with it over the entire binary alloy composition range. Indeed, the incorporation of small amounts of Ge in the base of the transistors has led to high performance hetero-bipolar transistors [2] which are compatible with the integrated technology. Due to the lattice mismatch between the two materials, incorporation of bigger amounts of Ge into Si, can lead to spontaneous formation of three-dimensional (3D) Ge nanostructures, which are known as islands. In the beginning there was no interest for these structures, since they were detrimental for the fabrication of thin films. But this situation changed completely after it was reported that these structures can be grown defect free [3, 4]. It was soon recognized that these spontaneously formed Ge islands, embedded in a Si matrix could be employed as quantum dots (QDs). Quantum dots, alternatively called artificial atoms, are structures which due to their small dimensions confine the carries in all three dimensions and thus possess an atom like electronic structure.

Several potential applications have been proposed during the last years for the Ge islands. It has been calculated that for nanostructures a direct band gap can be obtained [5] and thus a Si-based light emitting device could be fabricated. Indeed by embedding them in a Si matrix, electroluminescence [6] and photoluminescence at different wavelengths have been measured [7, 8]. Due to the smaller band gap of Ge compared to Si they can enhance the absorption of near- and mid-infrared radiation of the latter and thus they have been also used as photodetectors [9, 10] and in solar cells [11]. But apart from their opto-electronic applications there are also ideas of using them for increasing the performance of field effect transistors (DOTFet [12]). The strain field created by them could be used to increase the carrier mobility and thus to achieve faster operations in a transistor.

In general, their optical and electronic properties depend on their size, shape, strain and composition, as will be discussed in the next chapter. Therefore, in order to realize any application a detailed control over these characteristics has to be achieved, i.e. the fundamental processes governing their growth have to be understood. This is even more important since the Ge/Si(001) system serves as a model system for studying lattice mismatched

semiconductor heteroepitaxy.

This work aims to contribute to the understanding of these fundamental processes and it is structured as follows:

In Chapter 2 general concepts about film growth are presented and a brief overview of the growth of Ge islands on Si(001) is given. Chapter 3 describes briefly the experimental techniques used in this work. Chapter 4 is dedicated to the compositional study of nominally pure Ge islands grown at various temperatures and with different growth rates. The results of simple simulations, which were performed in order to interpret the experimental results, are presented. It is shown that a simple kinetic model, comprising only surface diffusion processes can explain the experimental observations. Chapter 5 investigates the mechanism by which intermixing is taking place during post growth annealing. It is revealed that, islands intermix by undergoing a lateral motion which is induced by alloying-driven energy minimization. In Chapter 6 the growth and shrinkage of SiGe islands is investigated by scanning tunneling microscopy (STM). It is shown, that while shrinking the islands follow the inverse path of their growth, proving thus that their shape is thermodynamically determined. In Chapter 7 buried SiGe islands are investigated. By means of selective wet chemical etching the Si layers covering the islands were removed and the shape and composition of the disclosed islands are investigated. Finally, Chapter 8 summarizes the obtained results.

Chapter 2

General Concepts

Epitaxy is defined as the growth of a single crystalline film of a material A on a crystal substrate B. If the deposited film is of the same material as the substrate then the process is known as homoepitaxy, otherwise it is called heteroepitaxy.

The epitaxial growth of thin films on solid substrates is of major importance in modern technology. Just for mentioning some examples, almost all modern semiconductor devices include thin films and in information storage, magnetic thin films play a crucial role because they are suitable for creating planar integrated devices. The main growth techniques of thin films, which are also compatible with ultra-high vacuum (UHV), are molecular beam epitaxy (MBE) and chemical vapor deposition (CVD). In the former method the material is supplied to the substrate by beams of atoms or molecules while in the latter in the form of gaseous compounds.

2.1 Growth of Thin Films

During the growth of thin films atoms are deposited on a surface. Once an atom hits the surface it can either re-evaporate or it can be absorbed (adatom) and start to diffuse. This is described by the sticking coefficient which is defined as the ratio of the adsorption to the impingement rate.

The diffusion of adatoms on the surface takes place through hopping from adsorption site to adsorption site and since their motion is usually thermally activated it is descrived by the random walk model. Thus, after time t the mean square displacement of the atom $< \Delta r^2 >$ is:

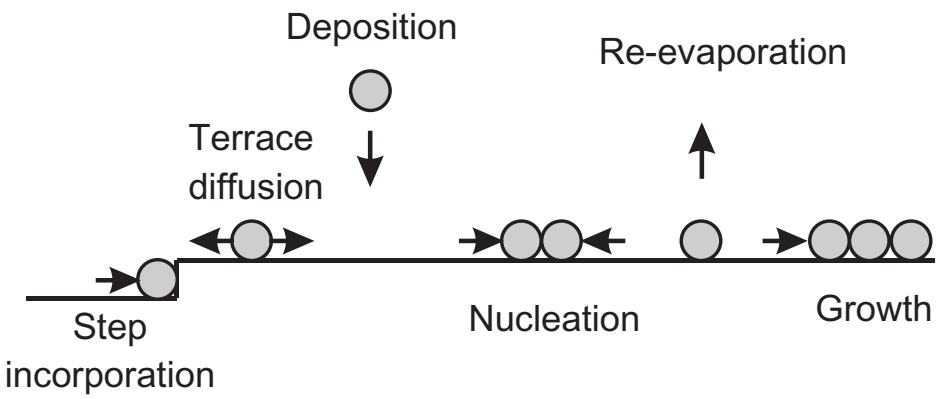

Figure 2.1: Schematic representation of the processes taking place at the surface during growth of thin films.

$$< \Delta r^2 >= \nu \alpha^2 t, \tag{2.1}$$

where ν describes the hopping frequency and α the adsorption site spacing.

The hopping frequency depends strongly on the energy barrier the adatoms have to surpass when moving from one adsorption site to the other, and is given by the following equation:

$$\nu = \nu_o exp(E_b/K_b T), \tag{2.2}$$

where ν_o represents the hopping attempts of the atom and E_b the energy barrier.

While the adatoms are diffusing on the surface, several processes that are shown schematically in Fig. 2.1 can take place. In thermodynamical equilibrium all the above displayed procedures are taking place in both directions with an equal rate. For example, the same amount of atoms which are deposited per unit time are also re-evaporated from the surface. As a consequence, no net growth is taking place. Thus, the growth of thin films is per definition a non-equilibrium kinetic process. The final macroscopic state is therefore not necessarily the most energetically favorable since some paths may be kinetically hindered.

The growth of thin films can be described in a phenomenological way. One distinguishes between three types of film growth, named according to their original investigators. These types depend on the relative strength of

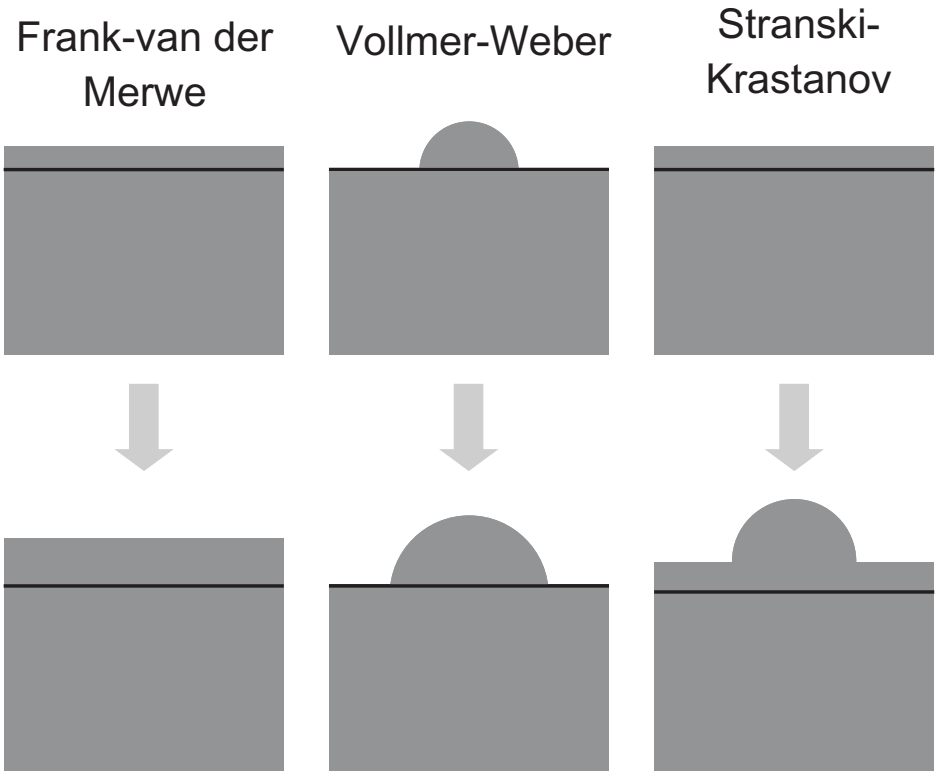

Figure 2.2: Schematic representation of the three growth modes.

the interaction among the adatoms themselves and between them and the atoms of the substrate. We distinguish:

Layer-by-layer (or alternatively called Frank - van der Merwe) growth mode [13]. In this mode the adatom-substrate interaction is stronger than the corresponding adatom-adatom interaction and a new layer starts to grow after the previous has been completed. A typical example of this mode is the homoepitaxial growth of Si on Si(001) [14].

Island (Vollmer - Weber) growth mode [15]. In this mode the adatom/ adatom interaction is stronger than the adatom/substrate interaction and 3D islands form directly on the substrate. An example for this growth mode is the deposition of Fe on Ga(110) [16].

Layer plus island (Stranski - Krastanov) growth mode [17]. In this mode a mixed situation appears and 3D islands form after initially some monolayers (MLs) grow in a layer-by-layer mode. A typical example is the growth of Ge

on the Si(001) and InAs on GaAs(001) [18].

The three different growth modes can be understood in terms of surface energies [19]. Assuming that growth is taking place in vacuum, if γ_s is the surface tension of the substrate/vacuum interface, γ_f the surface tension of the film/vacuum interface and γ_i the surface tension of the substrate/film interface, then after growth of n planar layers the energy of the system changes by:

$$\Delta\gamma_n = \gamma_{f,n} + \gamma_{i,n} - \gamma_s, \tag{2.3}$$

where the two first terms on the right side incorporate the dependance on the strain energy and therefore depend on n.

It is obvious that if $\Delta\gamma_n$ is negative independently of the amount of deposited monolayers, then a layer by layer growth is taking place. On the other hand, if $\Delta\gamma_1$ is positive islands form directly on the substate. The layer plus island growth mode appears when the sign of $\Delta\gamma_n$ depends on n. As long as it is negative a layer-by-layer growth is taking place until at some critical thickness the sign is switching to positive and 3D islands form on the two-dimensional layers.

2.2 Growth of Ge Islands on Si(001)

Lattice mismatched heteroepitaxy has gained a considerable interest during the last fifteen years since it provides a simple route to obtain functional nanostructures. Among the different material combinations which have been investigated, the Ge/Si(001) system is the simplest and it is thus appropriate for studying the fundamental processes taking place during heteroepitaxial growth.

Ge and Si are quite similar semiconductors of the group IV. They have a diamond-like crystal structure and they are miscible over the entire binary alloy composition range. On the other hand, they are characterized by different surface energies, with the one of Ge being lower, and they possess a different lattice constant. The lattice constant of Si is α_{Si}= 5.43Å, while that of Ge is α_{Ge}= 5.66Å, giving thus rise to a mismatch ε of:

$$\varepsilon = (\alpha_{Ge} - \alpha_{Si})/\alpha_{Ge} \simeq 4\%. \tag{2.4}$$

The total free energy of this system is determined by the sum of the elastic strain energy and the surface energy.

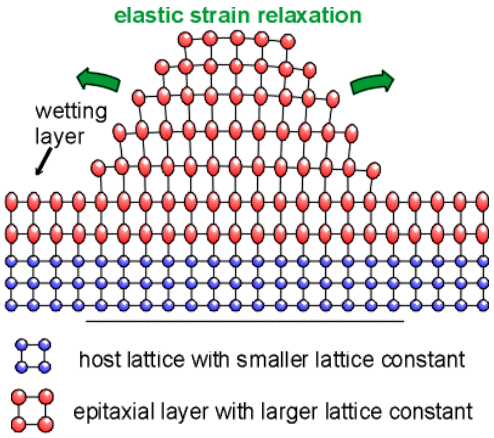

Figure 2.3: Schematic representation of the strain relaxation via the formation of a 3D island. From Ref. [21].

Ge grows for the first MLs pseudomorphically on Si(001). Its in-plane lattice constant has to adjusts its value to the one of Si and as a consequence a biaxial stress is built up in the dislocation free thin film. The accumulated strain energy varies linearly with the film thickness t_{film} according to the formula [20] :

$$E_{strain} \propto \varepsilon^2 t_{film}. \tag{2.5}$$

After some 3-4 MLs the accumulated strain energy in the film is released either through the formation of dislocations or through the formation of 3D structures which are usually called islands. The atoms of the islands can adjust their lateral position and thus partially relax the accumulated strain (Fig. 2.3).

Detailed studies have been performed during the past years addressing the morphology and the evolution of the islands observed on the surface. These studies have shown that different kind of structures exist. It has been found that for a wide range of growth parameters the 3D islands appear in the form of unfaceted mounds [25, 26] (Fig. 2.4). When the Ge coverage increases, these mounds transform first into truncated pyramids and then into pyramids bounded by {105} facets. For samples grown at low temperatures also elongated rectangular islands called 'hut clusters' bounded by {105} facets appear on the surface [4] (Fig. 2.5). These clusters are a specific case

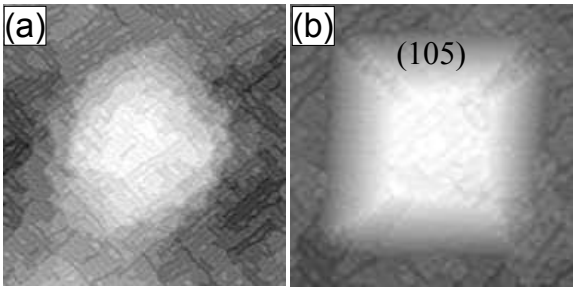

Figure 2.4: STM images of (a) a prepyramid and (b) a truncated pyramid. The size of the images is 125×125 nm^2 and their sides are aligned along the $< 100 >$ directions. From Ref. [22].

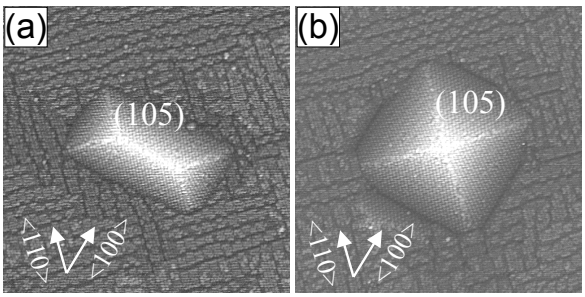

Figure 2.5: STM images of (a) a hut cluster and (b) a pyramid. The size of the images is 60×60 nm^2. From Ref. [23].

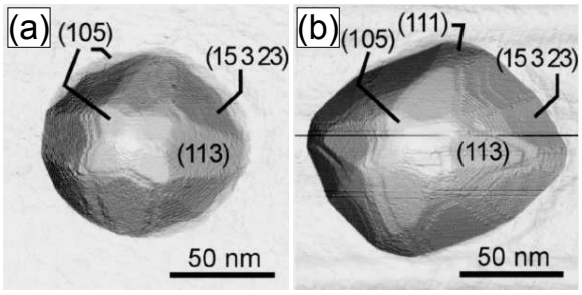

Figure 2.6: STM images of (a) a dome island and (b) a barn. From Ref. [24].

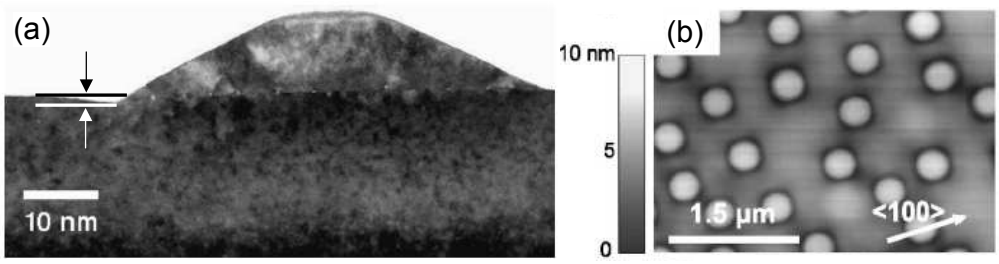

Figure 2.7: (a) Cross sectional Transmission Electron Microscopy image for an island grown at 600°C, showing part of the trench on the left side. From Ref. [29]. (b) Atomic force microscopy (AFM) image of trenches surrounding islands grown at 840°C. From Ref. [30].

of pyramid islands. For even bigger amounts of Ge, multifaceted islands called dome islands [27] and barns [24] appear on the surface (Fig. 2.6). Eventually some of them transform into dislocated islands which are also called "superdomes" [28]. Depending on the chosen growth parameters just one or more types of islands can be observed on the surface.

2.3 Trenches around Islands

In 1997 Kamins et al. [31] showed that for not too low growth temperatures (600°C) there is an additional coherent strain releasing mechanism: the formation of depressions around the islands, the so called trenches (Fig. 2.7). These depressions have been observed since then by many groups and also for lower temperatures [29, 30, 32]. It is agreed that trench formation is the result of the diffusion of the most highly strained material lying close to the perimeter of the island [33, 34] towards regions of lower strain. The highly strained material can diffuse away from this region because strain reduces the activation barrier of diffusion [35, 36]. By the formation of trenches not only the material at the periphery releases its strain by diffusing away, but also the stress of the islands can decrease by as much as 25% [37]. This is so because atoms at the base of the islands can relax by moving laterally outwards.

Trenches do not influence just the strain status of the island but also their composition. Since their depth is usually such that they extend into

the Si substrate, Si-rich material originating from the trenches and diffusing through them can incorporate into the islands [30, 32].

2.4 Theoretical Models of Island Growth

2.4.1 Island Formation Models

Capillary Model

The first theoretical model trying to explain the nucleation of 3D islands on substrates was proposed by Bauer in 1958 [38, 39]. This model is called "capillary theory of nucleation" and it uses only the thermodynamically defined surface tensions of the substrate γ_s, the film (island) γ_f and the interface γ_i. In this model the system which is under consideration includes also the gas phase over the deposited film. The total free enthalpy for the formation of the islands ΔG is a function of the number of atoms n included in the island and consists of two parts. The first includes the energy gain obtained upon condensation of the vapor and the second the cost due to the extra energy needed for forming new surfaces and interfaces. For nucleation of islands the total free enthalpy is thus given by the following formula:

$$\Delta G = -nK_bTln[p/p_o] + n^{2/3}X, \tag{2.6}$$

where p is the vapor pressure, p_o the equilibrium vapor pressure and X includes the contributions of the interface tensions. By assuming that the island is composed by facets of different orientations, X can be written as:

$$X = \sum_k C_k\gamma_f^k + C_i(\gamma_i - \gamma_s). \tag{2.7}$$

C_k and C_i are geometrical constants, γ_f^k represents the surface tension for different facet orientations and k sums over the different facet orientations.

Eq. 2.6 includes two terms, one negative and one positive and therefore ΔG does not change monotonously with the amount of atoms. The sum of the two terms defines a critical nucleus size (nucleation barrier) which has to be overcome in order that the island can nucleate (Fig. 2.8). During growth nuclei of adatoms are formed. If these contain more atoms than the critical size, an island grows; otherwise they are not stable and they dissolve. The

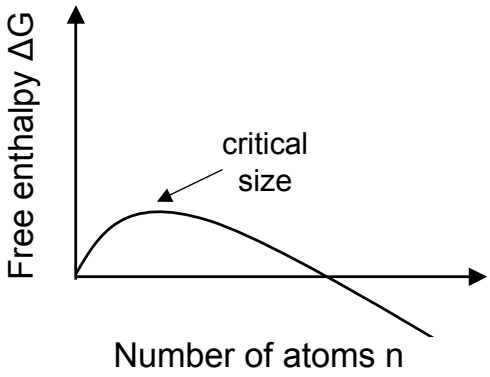

Figure 2.8: Qualitative plot of the free enthalpy change for 3D island growth versus the number of atoms. From Ref. [40].

critical number of atoms and the corresponding value for the enthalpy are obtained by differentiating Eq. 2.6.

It should be pointed out that since the surface tensions are macroscopically determined terms it is questionable whether this classical theory can be applied also for islands including just a few atoms.

Tersoff's Model

A more specific model for pyramidal islands was presented in 1994 by Tersoff and LeGoues [41]; they calculated the difference in energy between a film and a faceted 3D pyramidal island. By including the difference in the surface energy and strain energy they found that, similarly to (2.6), the free energy changes by:

$$E = -6cV \tan\theta + 4\Gamma V^{2/3} \tan^{1/3}\theta, \tag{2.8}$$

where V is the volume of the island, θ the angle between the facet and the substrate and c a constant including the Poisson ratio and shear modulus of the substrate. The term Γ refers to the free energy of the surface. Again a barrier for the nucleation of islands was predicted.

After some years, it was experimentally shown that the pyramidal islands evolve from unfaceted prepyramids [25, 26]. By calculating the energy of unfaceted islands [26] it was shown that these later can form on the substrate without a nucleation barrier. Their energy decreases monotonously with their

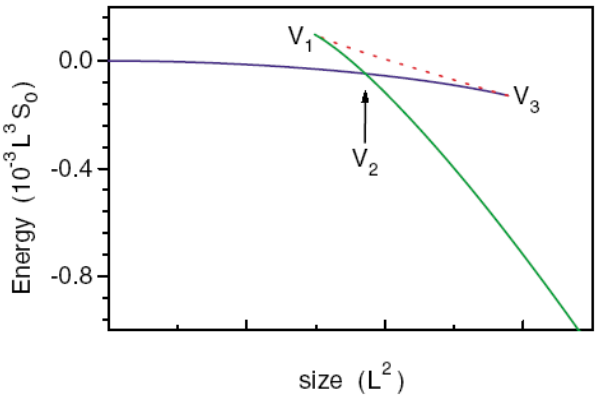

Figure 2.9: Island energy relative to a planar film, versus volume. The blue line represents unfaceted islands while the green faceted ones. From Ref. [26].

volume and they grow unfaceted until they reach a particular volume at which they transform into faceted islands (Fig. 2.9).

2.4.2 Models about Size Distributions of Islands

As already mentioned, the growth of thin films is per definition a not-equilibrium process. Thus, kinetic limitations in the form of low growth temperatures or high deposition rates can substantially influence the size distribution of islands. The experiments have shown that under various growth conditions a bimodal distribution of pyramid and dome islands can be observed on the surface. Mainly two models have been presented in the past years in order to explain these experimental results. The first is a thermodynamical model in which the island sizes correspond to energy minima while the second suggests that the islands evolve according to a coarsening mechanism.

Thermodynamical Model

Shchukin et al. [42] calculated the energy difference between a pseudomorphically grown film and a partially relaxed 3D island containing n atoms. It was shown by Medeiros-Ribeiro et al. [43] that this difference could be parameterized in the form:

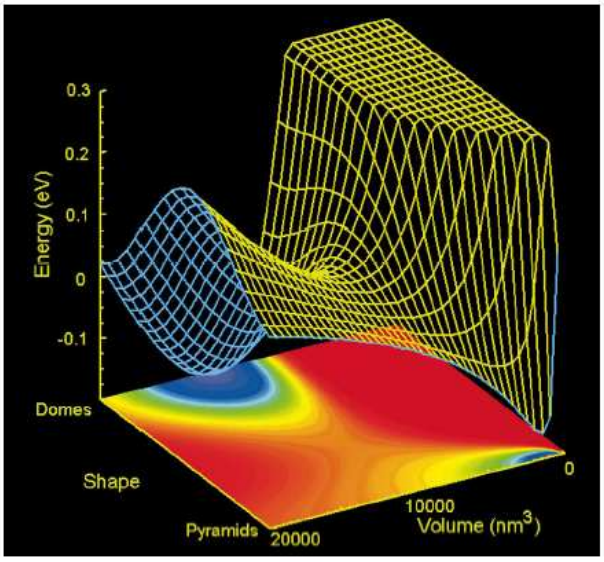

Figure 2.10: Model free-energy surface for Ge nanocrystals with respect to a pseudomorphic 2D island. It is seen that two minima at the positions of the pyramid and dome islands do exist. From Ref. [43].

$$\Delta E(n) = Cn + Bn^{2/3} + An^{1/3} ln[a_c/n^{1/3}], \tag{2.9}$$

where C is a constant determined by the bulk energy of the atoms in the strained island with respect to the pseudomorphic film, B a constant determined by facet and interface energies and A and a_c constants related with the edge energy. This formula is actually very similar to the formulas (2.6) and (2.8) but it includes additionally the edge energy of the islands.

It was shown that for a negative value of the parameter B, there do exist two minima in the energy, each one for a specific number of atoms n_o. Within this model the bimodal distribution of pyramid and dome islands observed in many experiments was explained: the pyramids form and grow to their maximum volume which corresponds to a minimum in the energy, until enough material is present in order that the next minimum which corresponds to the dome islands can be reached (Fig. 2.10). According to this model the pyramid to dome transition should take place abruptly.

Coarsening Model

Already in 1900 Ostwald [44] observed that big clusters are growing to the expense of small ones. He found that although in the beginning many small clusters form, these dissolve slowly and the few bigger do grow. This coarsening behavior is known as Ostwald ripening.

Ross et al. [45, 46] used low energy electron microscopy (LEEM) and transmission electron microscopy (TEM) to investigate the evolution of an ensemble of pyramid and dome islands. It was observed, that while the pyramid islands are dissolving the dome islands are getting bigger. Furthermore it was shown that the transition from pyramid to dome does involve several intermediate transition island shapes, i.e. it is not abrupt (see Fig. 2.11).

In a model which was proposed by them [45] two different kind of islands were assumed, distinguished just by their different facet angle, and their energy was calculated. It was shown that, contrary to the previous model, no energy minimum does exist. As displayed in Fig. 2.12, at some critical

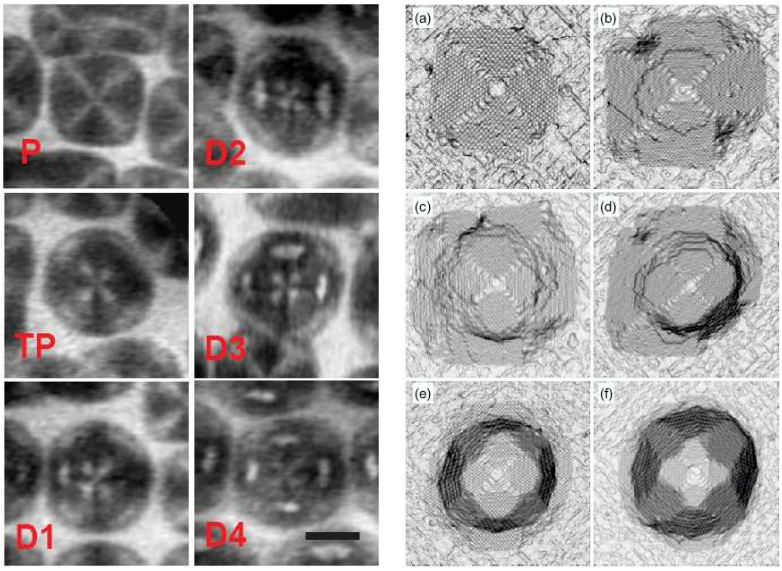

Figure 2.11: (Left) LEEM images showing the pyramid to dome transition through the various transition island shapes. From Ref. [43]. (Right) High resolution STM images showing the same transition. From Ref. [47]. The images sides are parallel to the $< 110 >$ directions.

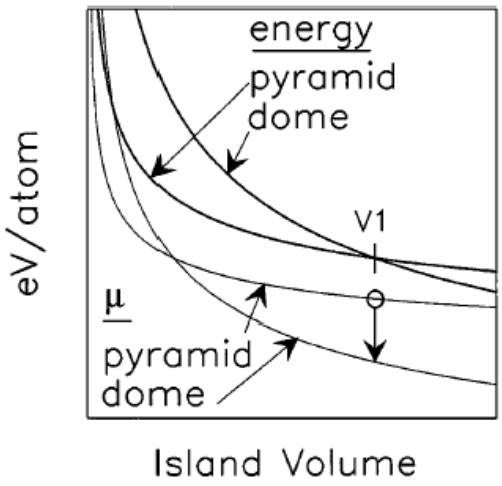

Figure 2.12: Energy per atom and chemical potential of the two types of islands versus their volume. It is seen that at a critical volume V_1 the energies of the islands become equal and that for this critical volume a discontinuous jump appears in the chemical potential. From Ref. [45].

volume V_1 the two shapes become degenerate in energy and it is this particular volume at which the transition takes place. Furthermore, the chemical potential $\Delta\mu$ drops discontinuously (Fig. 2.12). Thus while the small island shrinks, the bigger one acts as a sink of material and the system undergoes a so called anomalous coarsening.

2.5 Electronic and Optical Properties of Ge Islands

Both Si and Ge are indirect semiconductors, i.e. the maximum of their valence band and the minimum of their conduction band are at different points in k-space (Fig. 2.13). For Si the conduction band has six symmetry related minima at points in the $< 100 >$ directions at $\vec{k}$=0.85$\vec{k}_{max}$, while there are two degenerate valence band maxima at k=0 (heavy hole and light hole bands). On the other hand, Ge has six minima for the conduction band in the $< 111 >$ directions at the zone boundaries and again two degenerate valence band maxima at k=0. At room temperature (RT) Ge has a bandgap

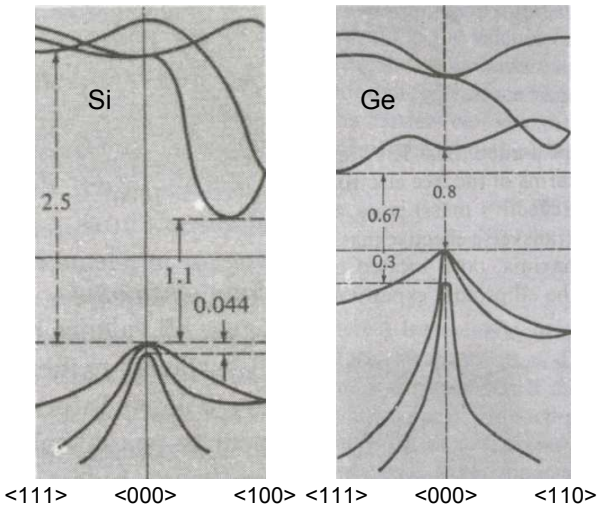

Figure 2.13: Band structure of Si (left) and Ge (right). From Ref. [48].

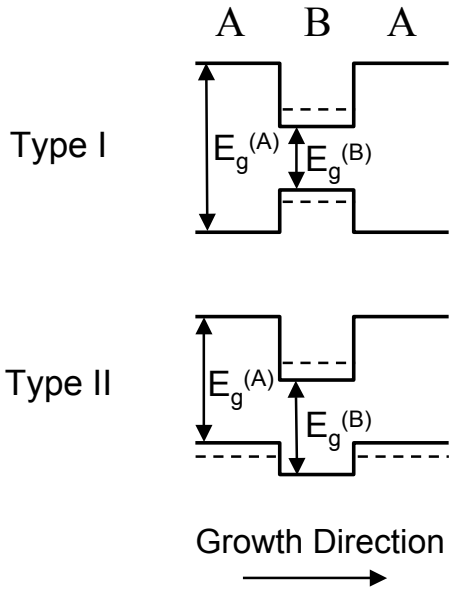

Figure 2.14: Band structures of type I and type II. In the former one the confinement of both electrons and holes is taking place in the same layer contrary to what is happening in the latter one. The dashed lines represent the energies of the confined particles.

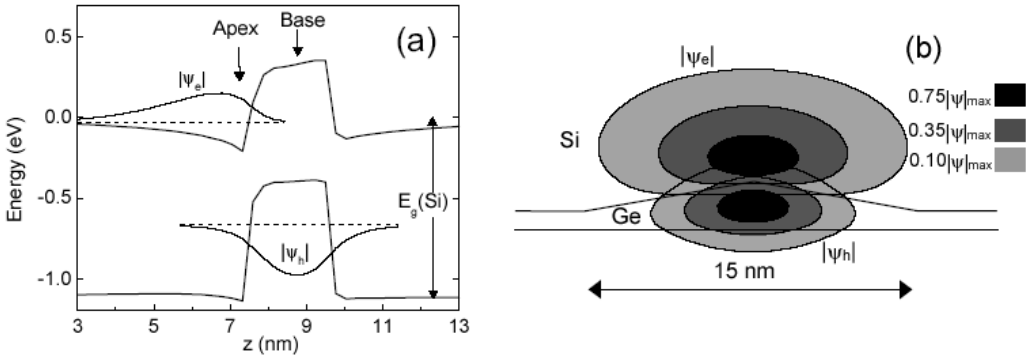

Figure 2.15: (a) Simplified band structure and wavefunctions of the electron an heavy hole of a Ge island embedded in Si. (b) Isosurface plots of electron and hole states. From Ref. [45].

of $E_g = 0.664eV$ while the one of Si is $E_g = 1.113eV$.

Whenever a film of material with a smaller bandgap is grown between material with a larger bandgap, localization of carriers is taking place in the growth direction, due to the band offsets. Depending on the relative position of conduction and valence bands, one distinguishes between type I and type II alignment. In type I both types of carriers, electrons and holes, are localized in the same layer while in type II the charge carriers are localized in different layers (Fig. 2.14). Strained SiGe on Si has been shown to have a type II structure [49].

Furthermore, it has been shown that for SiGe the valence band varies linearly with the Ge content [50]. Additionally, strain can cancel the degeneracy of the bands and depending on the sign of the strain the bands shift to higher or lower energies. In particular, for SiGe the degeneracy of the valence band maxima is lifted and the heavy hole valence band has a higher energy. Also the degeneracy of the sixfold degenerate Δ valleys in the conduction band is splitted into twofold degenerate $\Delta(2)$ and fourfold degenerate $\Delta(4)$ valleys.

Figure 2.15 (a) shows a simplified one-dimensional (1D) band structure of a Ge island embedded in Si, along the growth direction z [51]. It is seen that it is a type II structure; holes are confined in the Ge island while electrons in the Si matrix, in particular close to the apex of the island [Fig. 2.15 (b)]. The width of the box, which is defined by the valence band, is determined by

the height of the embedded structure while the depth (band offset) depends on the Ge content of the island and the strain.

Although both Si and Ge are indirect semiconductors prohibiting direct recombinations for bulk material, the situation changes drastically for the 3D islands. Due to the spatial confinement of the carriers a relaxation of the condition of momentum conservation can take place and direct in the k-space (optical) transitions are feasible. Indeed, in the past years many photoluminescence measurements have been performed for Ge islands embedded in Si showing no-phonon peaks at various wavelengths [7, 8, 52, 53].

From the above brief discussion about the electrical and optical properties of Ge islands the importance of size, shape, strain and composition becomes obvious. Actually the properties of the buried islands are the ones which finally determine their electronic and optical characteristics, since the nanostructures can be significantly altered during their embedding into the host matrix [54, 55].

Although there have been many studies investigating the morphology and strain of the uncapped islands, a general understanding of their compositional profiles is still missing. Furthermore, there are not many studies which have investigated buried islands. Therefore, the main goal of this work was to study the composition of the nominally pure Ge islands. In the first place the stoichiometry of uncapped islands was investigated and afterwards the effect of Si overgrowth on both the shape and the composition of islands was studied.

Chapter 3

Experimental Techniques

In this chapter the experimental techniques by which the samples have been grown and characterized are briefly discussed. The method of selective wet chemical etching is discussed in more detail, since it constitutes the key technique used throughout this work.

3.1 Molecular Beam Epitaxy

MBE is typically used in combination with UHV for growing high purity crystalline films, multilayers and 3D nanostructures. It is used both for research and for applications in semiconductor device fabrication. Material is deposited in form of atoms or molecules on a substrate which is kept at an elevated temperature. The temperature is chosen such as to guarantee on one hand a high enough mobility for getting smooth films and on the other hand to prevent interdiffusion between the arriving and the substrate atoms. The material, which is going to be deposited, is heated in an cell which is surrounded by several layers of radiation shielding. It is evaporated through a small opening in the end of the cell and the deposition rate is simply controlled by varying the temperature of the latter. The big advantage of MBE is that it permits slow growth rates compared to the other techniques and thus growth conditions close to thermodynamical equilibrium can be achieved. Typical growth rates are between 0.01-10 ML/sec, which in case of Ge corresponds to 5 nm-5 μm/hour.

All samples used in this study were grown by means of MBE on 4 inches Si (001) wafers by the MBE group of our institute. Prior to growth the wafers

were ex-situ chemically cleaned in order to remove the silicon oxide and the organic materials. Afterwards, they were in-situ deoxidized, this time by heating them at 900°C. Thereafter, the substrate temperature was reduced to the chosen growth temperature and different amounts of Ge at various rates and temperatures were deposited. During growth the pressure in the growth chamber was around 5×10^{-9} mbar guaranteeing a clean surface.

3.2 Scanning Probe Microscopy

3.2.1 Scanning Tunneling Microscope

STM is a technique which is used to obtain atomically resolved topographic information of conducting or semiconducting surfaces. An atomically sharp tip is positioned very close to the sample surface and it is scanned over it. Due to this very small distance d which is typically between 2-10 Å, a tunneling current can flow between the tip and the surface when a bias voltage is applied. In a very simplified form, the tunneling current is given by the following formula:

$$I \propto (V/d)exp(-Kd/\sqrt{\varphi}), \tag{3.1}$$

where V is the applied voltage between the tip and sample, φ is their average work function and K is a constant. Typically, the tunneling current is changing by one order of magnitude when the gap distance is varied by 1 Å.

It has to be stated that the STM technique is actually not sensitive to the position of the atoms but to the local density of electronic states. When the sample is negatively biased in respect to the tip the image represents a surface map of the filled electronic states. In the opposite case the empty states are visualized.

In particular, it can be shown that if the tip is hold at a fixed position above the surface and the voltage is varied, the resulting tunneling current or more precisely its derivative (dI/dV) corresponds closely to the local density of states around the Fermi energy. As a consequence, the STM can be also used as a tool for performing spectroscopy on the atomic level. In this case one speaks of Scanning Tunneling Spectroscopy (STS).

Returning to the topographic measurements, one distinguishes between two different modes:

- Constant current mode. In this mode the current and the bias voltage are kept constant and the distance between the tip and sample is measured while scanning the surface.

- Constant height mode. In this mode the voltage and distance between the sample and tip are kept constant and the variations in the tunneling current are measured.

The images presented in this work were taken in a homebuilt RT UHV-STM system [23]. The samples were transferred from the MBE machine to the STM by a portable vacuum suitcase in which the pressure was in the low 10^{-9} $mbar$ regime. Filled state images were obtained in the constant current mode and the typical used parameters were $I = 0.2$ nA for the tunneling current and $V_{bias} = -2.5$ V for the bias voltage.

3.2.2 Atomic Force Microscope

In the case of an AFM again a sharp tip is positioned very close to the sample surface but the principle of operation is different. In this case one uses, the interatomic forces exerted between the tip and the sample in order to obtain a topographic image of the surface. Thus not only conductive but also insulating samples can be investigated. The sharp tip is positioned at the end of a 100-300 μm long cantilever and the forces acting between the tip and the surface lead to a deflection of the cantilever. This deflection is then measured and an image of the surface is obtained. Deflections as small as 2-10 Å can be detected.

Depending on the tip-sample distance one distinguishes between:

- Contact mode. The AFM tip is in soft physical contact with the surface and repulsive forces are exerted. These forces cause the cantilever to follow the morphology of the surface.

- Non-contact mode. The distance between the tip and the sample is 10-100 Å and weak attractive forces are exerted. The cantilever in this case is not in contact with the sample but it is forced to oscillate close to its resonant frequency. While interacting with the sample this frequency changes slightly and these variations are used to obtain the topographical image. Since in this mode the forces acting on the sample are very weak it is suitable for soft specimens.

- Tapping mode. This mode is similar to the non-contact mode but usually a better resolution can be achieved. In this mode the tip barely touches the surface when the cantilever is at the lowest point in its oscillation and it is mainly used to obtain images of not atomically flat surfaces with high topographical corrugations.

All AFM images presented in this work were obtained in a "digital instruments Nanoscope IIIa Multimode" AFM, operated in tapping mode.

3.3 Transmission Electron Microscopy

In TEM the obtained image is created by electrons passing through the sample and its resolution is lower than 1 nm. It has the same principle of operation like the optical microscope with the difference that electrons instead of photons are used and that the beam is focused with electric and magnetic lenses. A beam of electrons (2-3 μm spot) is focused onto the specimen and the interaction of the crystalline sample with the electrons results in diffraction or scattering of the later. The part of the beam which is passing through the sample is then magnified and projected onto a screen in order to get the final image. Due to the fact that the penetration length of electrons is relatively small thin specimens are needed for TEM measurements.

Depending on which electrons are used in order to form the final image one distinguishes between:

- Bright field mode: in this mode the image is created by the electrons which are transmitted through the sample without diffraction. Areas of the sample with thicker regions or higher atomic number of the sample appear darker.

- Dark field mode: Electrons diffracted by the planes of atoms are used to create the diffraction pattern on the fluorescent screen.

For investigating buried interfaces and 3D structures cross-sectional TEM (X-TEM) is particularly useful. The samples are cut normal to their surface and they are thinned by means of ion milling and chemical etching.

The X-TEM images presented in this work were taken by Dr. Müller at the PSI Villigen in a Philips CM30ST electron microscope operated at 300 kV along the Si $< 110 >$ direction. The specimens were prepared by mechanical

prethinning and subsequent ion etching in a precision ion polishing system (PIPS) by Gatan, using Ar ions at 4.3 kV and an etching angle of 4°.

3.4 Selective Wet Chemical Etching

The procedure by which material is removed in a controlled way from a substrate is defined as etching and it can be divided in wet and dry etching. In the former the detachment of material is happening in a liquid, while in the latter the material is transferred into the gaseous phase.

The use of wet etching techniques has a long history in treating surfaces and materials. Already in prehistoric times liquids like citric acid and acetic acid were used for treating materials. In the past the chemical etching was mainly used for art and craftwork. An important step for its wider use was the discovery of hydrofluoric acid (HF) by Scheele in 1771, because it allowed the treatment of a variety of materials.

The first use of etching for "scientific" purposes seems to appear in the early 19th century, for studying crystallographic symmetries in crystals. For example, it was relatively easy to distinguish between right- and left-handed quartz by the use of wet etching. The etching figures for the faces of one form are quite distinctive from those of other forms when etched with HF. The interest in etching was raised when it became clear that by means of wet etching defects of imperfect surfaces could also be investigated. Due to the strain of a dislocation a faster etch rate at the point of its emergence at the surface was observed; this led to the formation of etch pits. From their shape, information about the inclination of the dislocations lines relative to the surface was obtained. By using this etch-pit technique also the movement of dislocations could be observed in a very clear way [56].

Nowadays the etching techniques have become a key process for the fabrication of semiconductor microdevices and microcomponents since they allow a much more refined removal from a solid surface compared to mechanical methods. This is very important since in modern microelectronics, structures in the sub-micrometer range are needed. The etching of semiconductors in liquid reactants is in fact widely used at all stages of the microsystem technology, such as for removing contaminants from the wafers, for creating three-dimensional structures, for revealing buried layers to define electrical contacts, etc. .

3.4.1 Basic Terminology of Etching

An important quantity to be known for each etching solution (etchant) is its etch rate r. It is defined as the ratio of the etched height h_{etched} and the etching time $t_{etching}$:

$$r = h_{etched}/t_{etching}. \tag{3.2}$$

For technological applications etchants which attack just one of the components of a given material combination would be desirable. Such a so called "specifically reacting etching medium" does usually not exist, and the etchants do not react on one material only. Thus one defines the etching selectivity of an etchant $S_{etching}$ for two materials A and B as:

$$S_{etching} = r_A/r_B, \tag{3.3}$$

were r_A and r_B are the etch rates for the materials A and B, respectively.

The temperature at which the etching takes place is an important parameter that influences both the etch rate and the selectivity. At low temperatures the etchants show slow etch rates but a high selectivity while at elevated temperatures the etch rates increase to the cost of the selectivity.

3.4.2 Calibration of the Etchants

The dependance of the etch rate on the Ge and Si content in Si_xGe_{1-x} alloys was determined by etching so-called virtual substrates [57]. These consist of strain-relaxed SiGe layers of different compositions grown on top of linearly graded SiGe buffers. The 1 μm thick virtual substrates used in this work were grown by means of low energy plasma enhanced chemical vapor deposition [58] by the group of Prof. von Känel. Prior to their exposure to the etchant, some portions of the virtual substrates were masked with Apiezon wax W100, which acts like a resist. Such samples were then etched for a given time, after which they were rinsed with deionized water and the wax was removed with dichloromethane. The height difference between the masked and unmasked regions was determined by using a DEKTAK profilometer and the ratio of this height to the etching time was used as an evaluation of the etch rate. In order to obtain representative values, we repeated this procedure for different etching times and we took the corresponding averages and standard deviations as indications for the etch rates and their uncertainties, respectively.

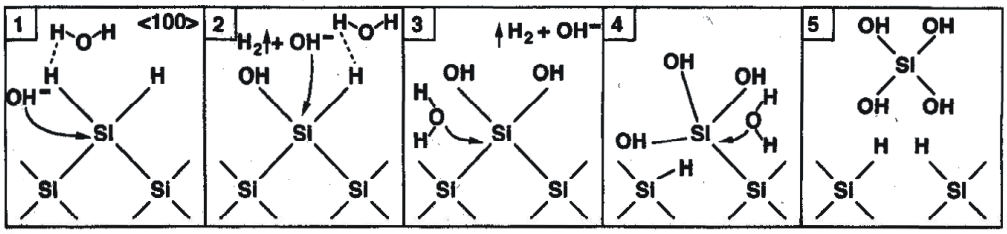

Figure 3.1: Etching mechanism of Si in alkaline solutions. From Ref. [63].

3.4.3 Selective Etching of Si over Ge

Etching of Si in alkaline solutions is widely used. Due to the fact that alkaline solutions show orientation-dependant etch rates [59] and quenching of the etch rates for heavily doped materials [60], they are used in micromachining of Si for creating cantilever beams [61], grooves [62], etc. .

Various alkaline etchants have been used to etch Si and it has been concluded that OH^- and H_2O are the chemically active species during the etching procedure, while the cation is of minor importance.

The following mechanism, shown schematically in Fig. 3.1, has been proposed for the etching of Si in such solutions [63]. As starting point a hydrogen passivated Si(001) surface is assumed. The $Si-H$ bond is attacked by an OH^- ion and a $Si-OH$ bond is created with the parallel evolution of a H_2 molecule. The second $Si-H$ bond is attacked by the same procedure leading to a further H_2 molecule. Due to the attraction of the electrons by the ligands, the $Si-Si$ backbonds become weaker and as a consequence they can be also attacked by water. The result is that Si is been removed from the surface and a surface still covered with $Si-H$ bonds is left behind. Figure 3.2 displays the etch rate diagram for a 2 molar (2M) potassium hydroxide (KOH) solution at RT for different Si_xGe_{1-x} compositions.

It is seen that the etch rate decreases drastically for increasing Ge contents and that the solution etches selectively Si over $Si_{0.8}Ge_{0.2}$ with a selectivity of about 100. As has been proposed by Fitzgerald et al. [64] the reason for this behaviour is the reduced tunneling barrier for holes through the etchant/Si interface, which is caused by the SiGe alloy. As a consequence an increased supply of holes does exist. These react with Si, form a passivating oxide which slows down the erosion and eventually etching is stopped for high Ge concentrations.

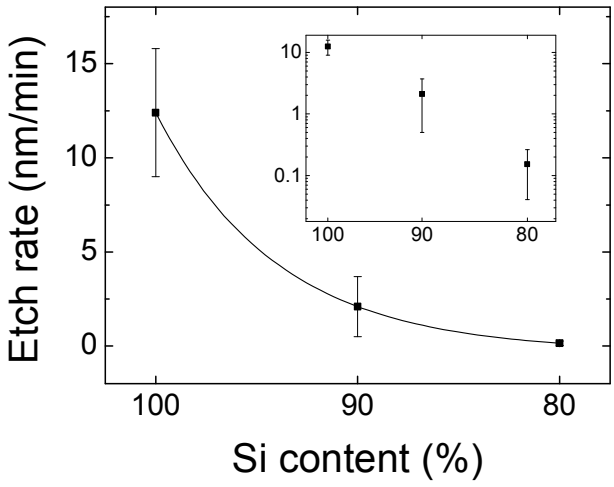

Figure 3.2: Etch rate diagram for a 2M KOH solution at RT. The inset shows the same plot in logarithmic scale.

3.4.4 Selective Etching of Ge over Si

Since Si/SiGe heterostructures have become very important in Si technology the interest of having etchants which etch also selectively Ge over Si has strongly increased. Thus, different etchants with this characteristic have been reported in the literature [65, 66]. In this study we have chosen to use a hydrogen peroxide solution (H_2O_2) [67]. Ge can be removed in aqueous H_2O_2 solutions since it is oxidized by the latter and its oxide is water soluble. Figure 3.3 displays the etch rate diagram of a 31% H_2O_2 solution (Merck) at RT for different Si_xGe_{1-x} compositions. The etch rate decreases monotonously for higher Si concentrations and shows a selectivity of Ge over $Si_{0.3}Ge_{0.7}$ of about 50.

The decrease of the etch rate for increasing Si contents can be understood as follows: when SiGe is etched in the H_2O_2 solution not only Ge but also Si oxide is formed. Contrary to the GeO_2, SiO_2 is stable in water and thus a porous silicon dioxide film is left behind. This film reduces the etch rate and for high enough Si concentrations it eventually stops the etching procedure [68].

For etching also Si_xGe_{1-x} alloys with higher Si content we have used a mixture consisting of ammonium hydroxide (NH_4OH), H_2O_2 and deionized

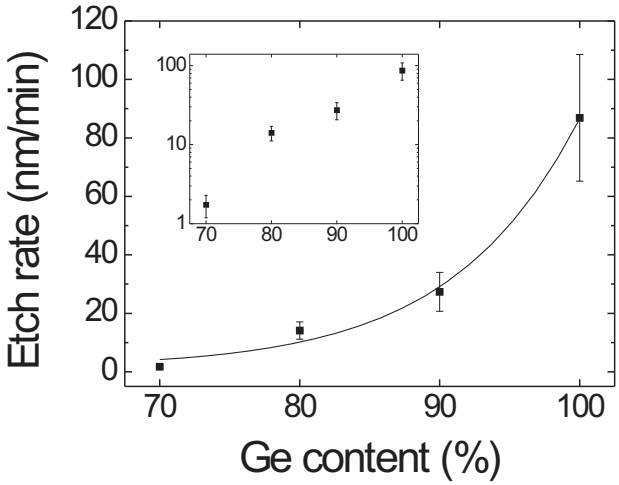

Figure 3.3: Etch rate diagram for a 31% H_2O_2 solution at RT. The inset shows the same plot in logarithmic scale.

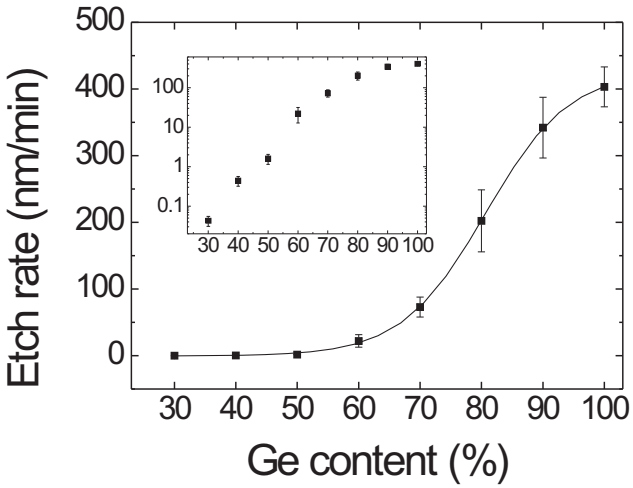

Figure 3.4: Etch rate diagram for the 1:1 volume 28% NH_4OH / 31% H_2O_2 solution at RT. The inset shows the same plot in logarithmic scale.

water. The same components, at a different ratio and temperature, are widely used for removing several metal contaminants from the surface of silicon wafers and are known with the name RCA standard clean 1 (RCA SC1) [69]. Figure 3.4 shows the etch rate diagram for a 1 : 1 volume solution consisting of 10 ml 31% H_2O_2 and 10 ml 28% NH_4OH solution. The etchant shows a selectivity of Ge over $Si_{0.7}Ge_{0.3}$ of about 10^4.

The high selectivity is not easily explained. In fact, as shown before, aqueous KOH solutions, etch Si_xGe_{1-x} with concomitant hydrogen evolution and increasing Ge content decreases the etching rate. Johnson et al. [70] showed that this is also true when aqueous NH_3, i.e. NH_4OH is used. But in the presence of H_2O_2, the scenario changes, and Ge is predominantly dissolved (without hydrogen evolution). The reasons are most probably the fast passivation of the Si by the Si oxide produced from Si and H_2O_2, and the strongly increased etching (oxidation) rate of Ge, which does not form passive layers.

When applying these two etchants on the islands a different behaviour can be observed. The 31% H_2O_2 solution shows a stop etch behaviour, i.e. the Ge-rich part of the island is removed within the first 10 minutes and the remaining non etched part of the island having a Ge content less than 65% is not attacked even for etching times longer than 24 hours. On the other hand the 1 : 1 volume 31% H_2O_2/28% NH_4OH solution does not show this behaviour. The Ge rich parts are removed gradually but eventually for long etching times the complete island is removed from the surface.

Chapter 4

Composition of as-grown Ge Islands

The composition of self-organized Ge islands grown on Si(001) has been the subject of intense investigations during the past years because, as already mentioned, it determines to a large extent the optical and electronic properties of the islands. High-resolution Rutherford backscattering spectroscopy studies performed on samples grown at 300°C showed that already before the first ML is completed intermixing of Ge and Si is taking place [71]. Thus it is not surprising that the nominally pure Ge islands do contain a considerable amount of Si.

The majority of the studies concerning the QD composition relied on diffractive [72, 74, 75] or spectroscopic techniques [73, 76, 77, 78] that give an average value over a large number of islands. They are therefore restricted to samples with a monomodal island distribution and they do not allow the addressing of individual islands so as to investigate compositional variations from island to island. The general conclusions on which these studies agreed were that the composition of the dots becomes richer in Ge closer to the apex of the islands [72, 74, 75, 79, 80] and that the overall Si content is increasing monotonously with the growth temperature [73, 81] (Fig. 4.1).

In order to measure compositional variations throughout individual dots Floyd et al. [79] performed electron microscopy based experiments but no lateral variations were observed.

An alternative method that combines selective chemical etching and AFM was used by Schmidt et al. [84] and Denker et al. [82] in order to probe the composition of Ge hut clusters and pyramids in single and stacked layers.

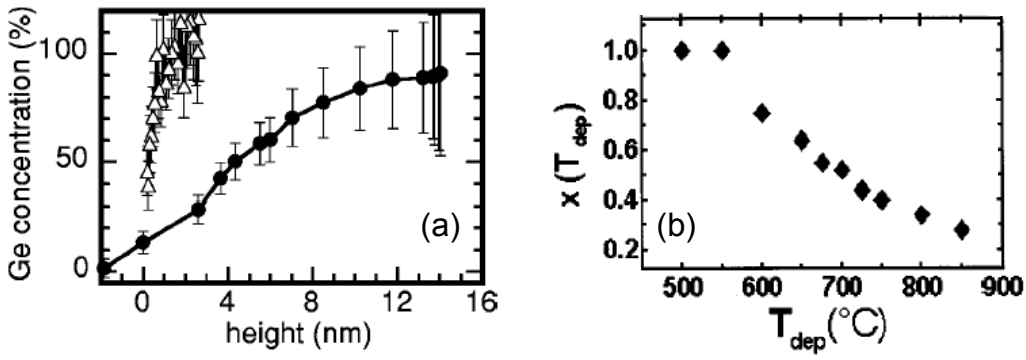

Figure 4.1: (a) Plot showing the Ge concentration of pyramid (triangle) and dome (circle) islands as a function of height. From Ref. [72]. (b) Ge content x included in the islands as a function of the growth temperature. From Ref. [73].

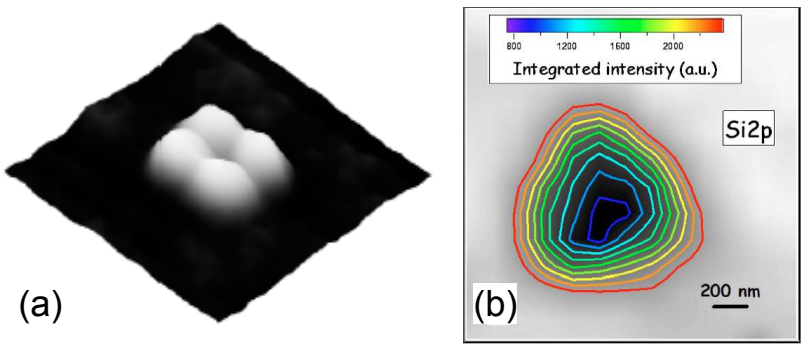

Figure 4.2: Lateral variation in the composition of Ge islands. (a) 3D AFM image of an etched Ge island grown on Si(001) showing the Si enrichement of the pyramid corners (see section 4.1.1). From Ref. [82]. (b) X-ray photoemission electron microscopy (XPEEM) Si2p image of a Ge island grown on Si(111). Again a Si richer periphery is observed. From Ref. [83].

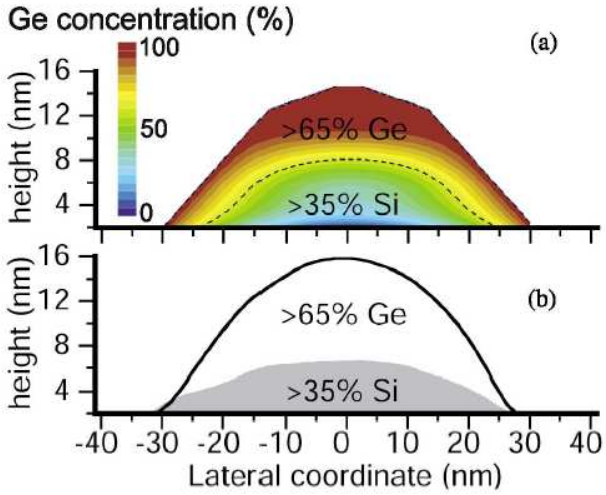

Figure 4.3: (a) Chemical composition map of dome islands showing a Si-rich core. (b) AFM line scans taken before and after etching, displaying the Si-rich core. From Ref. [80].

Denker et al. [82] showed that there is a lateral variation in the island composition and that the corners of pyramid islands have a higher content in Si. Later, X-ray microscopy [83] experiments performed on individual Ge islands grown on the Si(111) surface, showed also a lateral variation in the composition of the islands with their periphery having a higher Si content (Fig. 4.2).

At variance with these results, recent experiments based on selective chemical etching together with a set of diffraction techniques [80], showed the existence of dome islands with a Si-rich core (Fig. 4.3).

It becomes thus evident that there is controversy about the stoichiometry of the islands. On the one hand there are reports claiming that the islands have a Si-rich periphery and on the other there are studies giving evidence of islands with a Si-rich core. It is important to notice that in the majority of the above mentioned studies, just islands grown at one specific temperature and deposition rate were investigated; the effect of varying the growth parameters was not addressed. Furthermore, it should be pointed out that it is not straightforward to compare the results obtained by different groups since a slightly different calibration of the temperature or growth rate can give different results for nominally the same conditions. Thus, a more general

study investigating the compositional profiles as a function of different growth conditions is needed.

Apart from the debate about the islands' compositional profiles, also their interpretation has not been straightforward and no agreement on their origin has been achieved. Due to the increased strain at the substrate/island interface it has been proposed that the Si included in the island could originate from bulk interdiffusion phenomena triggered by the non-uniform stress fields [32, 33, 79, 85, 86]. On the other hand, it has been also proposed that a Si-rich periphery can derive from surface mediated diffusion processes [82, 83, 84, 87]. Thus also the origin of the experimentally observed profiles is still under discussion.

In this chapter the effects of substrate temperature and growth rate on the composition of Ge islands grown on Si(001) is investigated with a combination of selective wet chemical etching and AFM. It will be shown that a simple kinetic model comprising only surface diffusion processes can explain all the experimentally observed compositional profiles for pyramid and dome islands grown in the 560°-740°C range.

4.1 Samples Grown in the 560-620°C Temperature Range

The samples used for this study were grown by solid source MBE. After chemical cleaning and deoxidation at 950°C in UHV, a 100 nm thick Si buffer was grown while ramping the substrate temperature from 480°C to the island growth temperature (560-620°C). The samples were grown by depositing 6 MLs of Ge with a rate of 0.04 ML/s. After the formation of a wetting layer (WL), the appearance of 3D islands was monitored by reflection high energy electron diffraction (RHEED). So as to investigate the effect of the growth rate, another set of samples was prepared by depositing 11 MLs of Ge with growth rates of 0.04 ML/s and 0.08 ML/s. The etching experiments were performed at RT by dipping the samples for 10 minutes in a commercial (Merck) 31% H_2O_2 solution, which, as has been shown in Chapter 3, etches selectively Ge over Si and stops etching for SiGe alloys with Ge concentrations less than about 65%. Longer etching times did not significantly change the morphology of the remaining structures. After being etched, the samples were rinsed in deionized water and their morphology was investigated by

means of AFM in tapping mode.

4.1.1 Effect of Growth Temperature

Figures 4.4 (a)-(c) show AFM topographies of QD samples grown at 580°C, 600°C and 620°C, respectively. With increasing growth temperature, the size of the islands increases and their density decreases, as expected. The sample grown at 580°C shows a coexistence of hut clusters, pyramids and domes. At 600°C we observe mainly domes and transition islands [88] while at 620°C the surface is covered by a monomodal distribution of domes.

The lower row of Fig. 4.4 shows the corresponding surface morphologies after the chemical etching in a 31% H_2O_2 solution. The huts become shallower [84] and the pyramids show a cross-like shape as has been already reported previously [82] [left inset in Fig. 4.4 (d)]. The selectivity of the etchant implies that the remaining parts of the islands (in the case of pyramids, the corners) have a larger Si content. Etched domes exhibit a ring-like structure up to a temperature of 600°C. At 620°C the rings transform into a convex mound-like structure, that occurs also at higher growth temperatures. The 560°C sample (not shown) is very similar to that grown at 580°C, both before and after etching. A careful inspection of the etched pyramids grown at 560°C and 580°C, reveals that a few of them do not exhibit the characteristic cross shape but still have a protruding apex [left and right inset in Fig. 4.4 (d), respectively]. This observation indicates that these latter pyramids have an increased Si content at their top.

4.1.2 Growth Simulations

In order to interpret the experimental results we performed growth simulations similar to those reported in Ref. [82]. The simulated pyramids have a base which consists of 360 × 360 atoms and a height corresponding to 36 atoms, giving thus rise to a facet inclination of around 11°. For reducing the simulation time just one corner of the pyramid was simulated and the size of the total simulation field was 360 × 360. No reconstruction of the facets has been taken into account; the facets are actually stepped. The shape of the dome island has been simplified even more. Its base is actually a circle and just two facet orientations have been taken into account; one steep at the base with an angle of about 25° and one at the top with an angle of about 11°. The dome has a diameter of 344 and a height of 56 atoms. Since

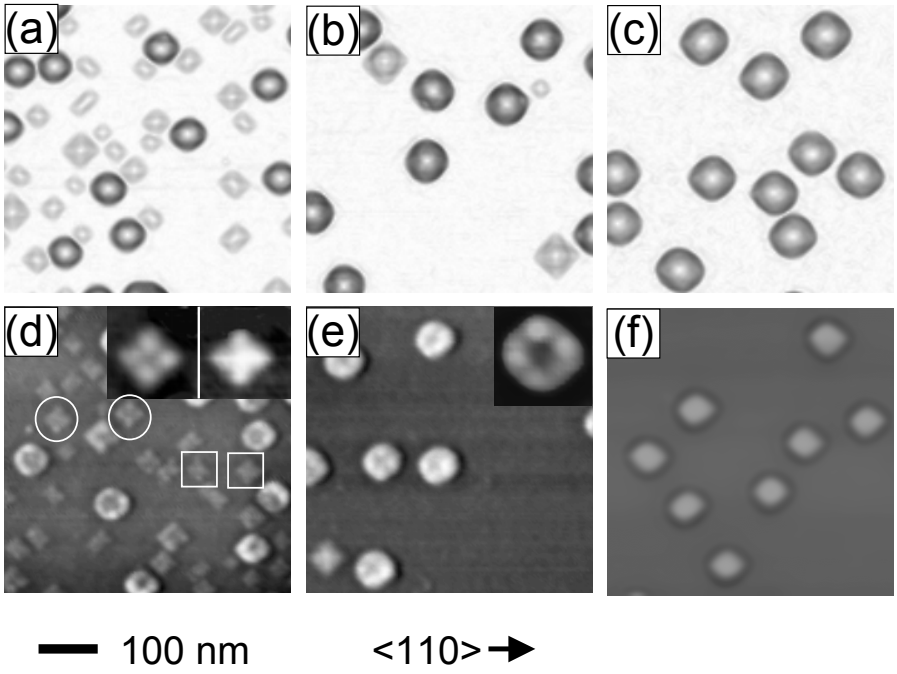

Figure 4.4: AFM topographies showing the morphology of Ge islands grown on Si(001) before (upper row) and after 10 minutes of H_2O_2 etching (lower row). The growth temperatures are 580°C for (a) and (d), 600°C for (b) and (e) and 620°C for (c) and (f). The insets show a higher magnification (80×80 nm^2) of: (d) the two different observed etched structures for pyramid islands, and (e) the protrusions in the ring structures of the etched domes. The encircled islands in (d) are examples of pyramids without apex while the ones enclosed by squares correspond to pyramids with apex. The gray scale in (a)-(c) is related to the local surface gradient while in (d)-(f) it represents a combination of local surface height and gradient so as to enhance small-scale morphological details.

it is known that the nominally pure Ge islands are actually intermixed, we took into account that apart from Ge atoms also Si atoms participate in the growth. We furthermore took into account that at the temperatures used in our experiments islands are growing in a shell-like manner: a new facet is added to the existing island as soon as enough atoms are present for forming this new facet. As free parameters we have used the diffusion length of the Si adatoms and the ratio between the number of Si and Ge atoms participating to the island growth. This ratio represents the composition of the WL that is assumed to be uniform and infinite (like an infinite reservoir of constant composition). Also for the WL no reconstruction is taken into account. The simulation starts with a very small Ge nucleus (a 2D island consisting of few atoms) to which Si and Ge atoms are randomly added according to the following steps:

1. Atoms located outside of the already existing nucleus are supposed to diffuse freely on the WL according to the random walk model. We neglect thus the anisotropy in the diffusivity due to strain and due to the M × N reconstruction of the WL. In the simulation algorithm an atom is considered at its starting position x_o and its final position x is randomly chosen according to the normal probability distribution:

$$P_x \propto exp((x - x_o)^2/2\lambda^2), \tag{4.1}$$

where λ is the diffusion length.

2. The atoms which have a new position within the "growing" island, are used for the formation of the new facets. First it is decided whether the arriving atom is Si or Ge. This is done by comparing a randomly created number for each atom (between 0 and 1) with the WL composition (0 for 100% Ge, 1 for 100% Si). Depending on the nature of the atom one distinguishes between two cases: The Si atoms deposited on the island remain at the place where they "land" while Ge atoms are just used to fill the empty "places" in the growing facet. This is equivalent to assume a much higher diffusion length of the Ge atoms compared to the Si ones. This assumption is reasonable since Cherepanov et al. [89] have shown that the diffusion length of Ge is 2-3 times higher than that of Si on (111) surfaces. Furthermore, Si has to diffuse out of the thin WL before diffusing towards the islands. Thus, these two factors can lead to such a different diffusivity between Si and Ge. Just very recently [90], first-principle calculations showed that indeed there is a difference in the diffusivity between Ge and Si on the Ge/Si(001) surface

which is additionally enhanced on the Ge {105} facets.

3. As soon as enough atoms are present for growing a new facet, this is considered to be completed and the simulation proceeds with the formation of the new facet. This whole procedure continues up to the point when the island reaches its a priori chosen final size.

4. For each set of parameters more than 200 of such simulations are performed and their results are averaged so as to obtain a composition value for each different part of the island.

By simulating the growth in such a way, it is implied that the composition of each part is determined at the moment this part is being created. Thus no material exchange within the island is allowed and bulk diffusion is forbidden.

We have performed simulations for a large range of diffusion lengths and WL compositions so as to investigate their effect on the final composition of the islands.

4.1.3 Comparison between Experiment and Simulation

Pyramids Fig. 4.5 (a) shows a 2D cross section through a simulated compositional map along the $< 100 >$ direction for a pyramid with a high Ge composition and a Si diffusion length equal to 25% of the pyramid base. For a direct comparison with the etching experiments, we have to consider all the points of this map with a Ge composition lower than 65%, a so-called 65% Ge isocompositional profile. This is shown in Fig. 4.5 (b), which agrees fairly well with the experimental cross-like structure shown in Fig. 4.5 (c).

The reason for the increased Si content of the corners can be understood in terms of simple geometrical arguments. For diffusion lengths which are small compared to the width of the pyramid, the corners have a bigger "capture zone", implying that a higher number of randomly diffusing atoms reaches the corners in respect to the sides (Fig. 4.6). This fact, together with the higher diffusion length for the Ge atoms leads to a high number of Si atoms incorporated close to corner positions and thus to the observed Si enrichment of the corners.

If we consider a pyramid with a higher overall average Si content, i.e. a pyramid that is grown on a Si-richer WL, a different result is obtained: the isocompositional profile is now showing a protruding apex [Fig. 4.5 (e)], in good agreement with the second type of experimentally observed etched pyramids [Fig. 4.5 (f)].

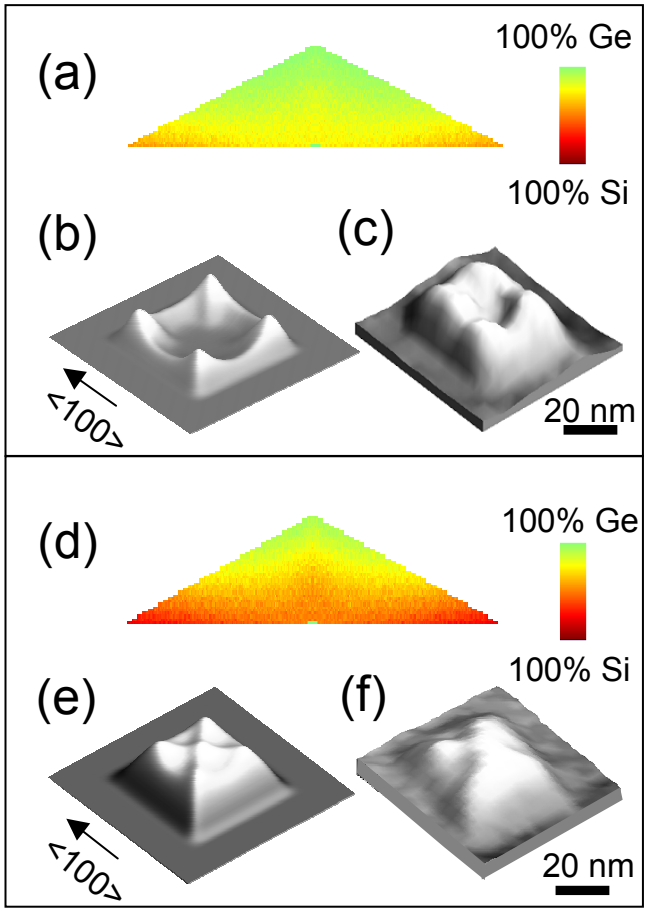

Figure 4.5: (a) 2D cross section through the compositional map of a simulated pyramid with a Si diffusion length corresponding to 1/4 of its base and an average Ge composition of 75%. The cross section is along $< 100 >$, i.e. along the pyramid side and passes through its center. (b) 65% Ge isocomposition surface profile of the same pyramid. For comparing the simulated data with the AFM images, the former were smoothened by means of a gaussian convolution (σ=4 atoms). (c) Experimental etched structure of a pyramid without apex. (d) Same as (a) but with an average Ge composition 52%. (e) 65% Ge isocomposition surface profile of the pyramid in (d). (f) Experimental etched structure of a pyramid with protruding apex.

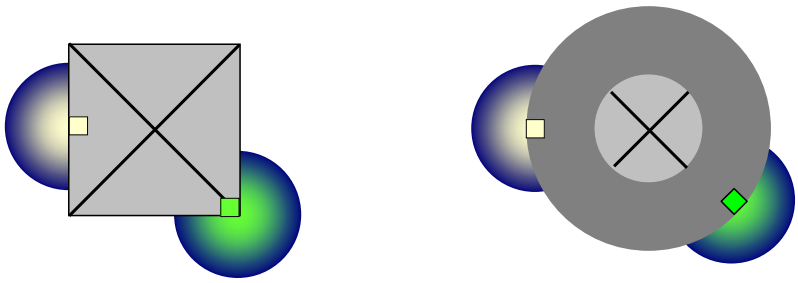

Figure 4.6: (left) Schematic representation of the bigger capture zone for the corners of the pyramids. For the dome islands (right) this geometrical effect does almost not exist since domes have a much more symmetric octagonal base. The shape of the dome shown here is the one used for the simulation. The island has a circular base and just two type of facets do exist: a steep one (dark grey) and a shallow one (light grey).

To understand the origin of this latter result we have to consider that, as recently demonstrated [88], pyramids grow by a successive overlay of {105} facets, involving predominantly surface diffusion processes. During the formation of a new {105} facet, the probability that a Si atom is incorporated at a certain position is thus proportional to the probability that it reaches that position by diffusing from the WL. Points A and B in Fig. 4.7 were incorporated into the pyramid at different times at which the pyramid had different sizes. The distance Si atoms had to travel for reaching A is on average larger than for B, resulting in a higher Si composition of B (pyramid center) with respect to A. Evidently, the geometrical argument presented above is true also for Ge atoms. However, as already mentioned previously, the diffusion length of Ge is larger than that of Si and thus the motion of the Ge atoms is not significantly restricted by this geometrical effect. The increase of the Si content in the center is always present but it appears more clearly for a higher overall Si composition [compare Figs. 4.5 (a) and (d)]. This result implies that those pyramids, which after etching still have a protruding central part, have also a higher total Si content. In other words, although the pyramids look morphologically identical before etching, they do not have the same composition. This could be caused by local fluctuations of the WL composition [91] induced by the non-uniform distribution and density of the islands.

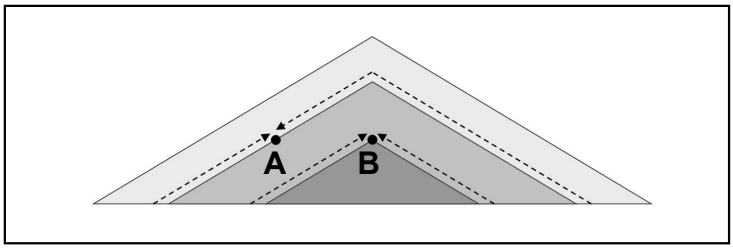

Figure 4.7: Schematic representation for the origin of the higher Si content close to the pyramid center. The arrows indicate the path that atoms starting from the WL have to follow in order to reach different positions of the pyramid at different moments of the pyramid growth. See text for details.

Domes The etched domes grown in the 560-600°C temperature range show a ring-like structure [see Fig. 4.4 (d) and (e)] whose height increases with increasing temperature: at 560°C it is of 1.4 nm, at 580°C of 3.6 nm and at 600°C of 6.5 nm. This implies that also in the case of domes the periphery has a higher Si content compared to the center. The actual difference is that while for the square-based pyramids the Si-richer regions are mainly concentrated in the corners, this geometrical effect is almost absent for the domes which have a much more symmetric octagonal base [92] (see Fig. 4.6). Nevertheless, a careful inspection reveals that for many of the domes a tiny modulation of the ring does exist in the form of four protrusions, located at the same position of the pyramids' corners [inset in Fig. 4.4 (e)].

This can be easily understood when considering that domes evolve from pyramids through a transformation that involves primarily surface diffusion processes [88]. It is thus not surprising that the composition of a dome 'remembers' that of the pyramid from which it has originated.

At 620°C the ring is replaced by a convex mound structure having a height of about 13 nm [Fig. 4.4 (f)]. In order to rationalize this change we have to consider that the increase of the substrate temperature has two main effects. First, it augments the Si content of the WL (see Appendix A) and second, it increases the adatom surface diffusivity. This is particularly important for Si atoms, since the diffusion of Ge atoms is already activated at lower temperatures [88]. As a consequence, at higher temperatures more

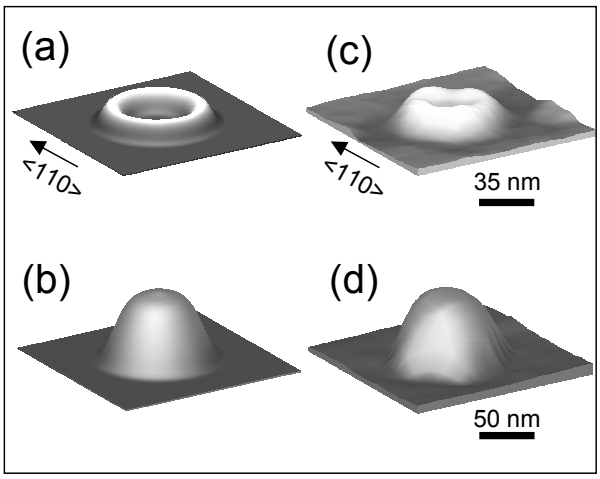

Figure 4.8: (Left column) Simulated 65% Ge isocompositional profiles for (a) a dome with small Si content and diffusion length and (b) a dome with a higher Si content and diffusion length. For comparing the simulated data with the AFM images, the former were smoothened by means of a gaussian convolution (σ=4 atoms). (c) and (d) experimental etched structures of domes grown at 580°C and 620°C, respectively.

Si atoms can reach even high-lying points of the island, thus producing a "Si-filling" of the central hole and creating the mound structure. By including these two effects into the growth simulations for dome-shaped islands, the transition from a ring- to a mound-like isocompositional profile can indeed be reproduced rather well (Fig. 4.8). This result further confirms, that the inhomogeneous Si distribution of islands grown at lower temperatures is produced by kinetic limitations. Moreover, it demonstrates the generality of our simple model and proves that bulk diffusion driven by stress fields is not necessary for justifying the experimentally observed compositional profiles.

4.1.4 Effect of the Growth Rate

The effect of the growth rate on the island composition was investigated by growing 11 MLs of Ge at a fixed substrate temperature (620°C) but with different deposition rates, 0.04 and 0.08 ML/s, respectively. The samples are characterized in both cases by a monomodal distribution of domes, but

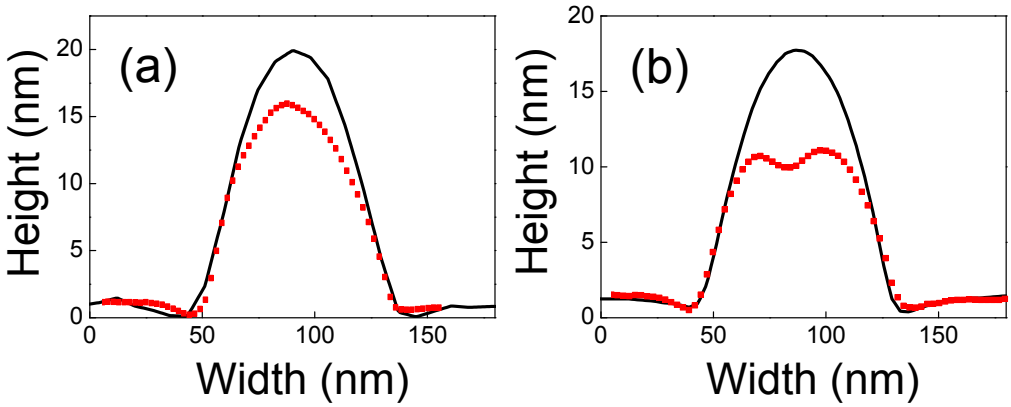

Figure 4.9: Representative AFM linescans of domes grown at 620°C with two Ge deposition growth rates: (a) 0.04 ML/s and (b) 0.08 ML/s before (solid black line) and after (dotted red line) selective chemical etching.

their composition appears to be different. In the first sample the etched islands show a mound-like structure with an average height of 14.6±0.7 nm, while in the second they show a ring-like profile with a height of 10.1±1.3 nm (Fig. 4.9). The influence of the Ge growth rate on the island composition can be also understood within a kinetically determined growth model. In fact, while the Ge supply rate for a growing island is doubled, that of Si remains almost unchanged, being principally determined by the substrate temperature. This leads to a back transformation of the etched morphologies from mound to ring-like structures as also verified by the simulation. Summarizing, we have so far demonstrated that a simple kinetic growth model can qualitatively reproduce the complex inhomogeneous alloying of self-organized 3D islands.

Despite its simplicity, the model is able to grasp the essential features of the compositional profiles of pyramids as well as domes and it correctly describes their evolution as a function of the substrate temperature and of the growth rate. Its basic assumptions are clearly over-simplified and other important effects (strain release, surface energy, etc.) should be included in a true comprehensive description of the island growth. For example, the kinetic accumulation of Si at the pyramid edges could possibly be amplified due to the energy gain that Si atoms experience when attaching to already Si-rich regions. Nevertheless, the good agreement with the experimental results lets

us expect that, even by taking into account these further effects, the main origin for the measured composition profiles would still be of kinetic nature.

4.1.5 Comparison with the Results Reported in the Literature

By comparing our results with the compositional profiles reported in the literature, we notice that there is a good agreement on the observation that the composition of the dots becomes richer in Ge closer to the apex of the islands and that the overall Si content is increasing with increasing growth temperature. Recently Malachias et al. [80] obtained a detailed 3D map of the Si and Ge distribution within dome islands by using grazing incidence anomalous x-ray scattering. Their reported experimental profile fits well with the mound-like structure described above and we therefore believe that it could be explained by a growth model similar to that presented here. By combining transmission electron microscopy and electron energy-loss spectroscopy, Floyd et al. [79] investigated the composition of dome islands with both lateral and height resolution. Although they expected a lateral modulation in the island composition caused by a strain-driven bulk interdiffusion, they did not observe it. A possible reason could be that small variations are not detected by a transmission technique that integrates over 100-200 nm thick sample slices. In our study, for nominally similar growth temperatures, we do observe lateral variations in the island composition in the form of ring structures for domes and of cross-like structures for pyramids. Nevertheless, the growth model we have introduced to explain these effects is based just on surface processes and does not need to take into account any bulk interdiffusion. This is supported by the values of the corresponding diffusion energy barriers reported in the literature [93, 94, 95]: according to them, in the 560-620°C temperature range, bulk interdiffusion is kinetically limited and much too small to explain the amount of Si that we observe in the islands. Thus, bulk interdiffusion should not be considered as the main factor responsible for island intermixing.

4.2 Samples Grown at 740°C

The samples investigated at this temperature were grown by deposition of 10 MLs of Ge on Si (001) and they were directly cooled to room temperature at

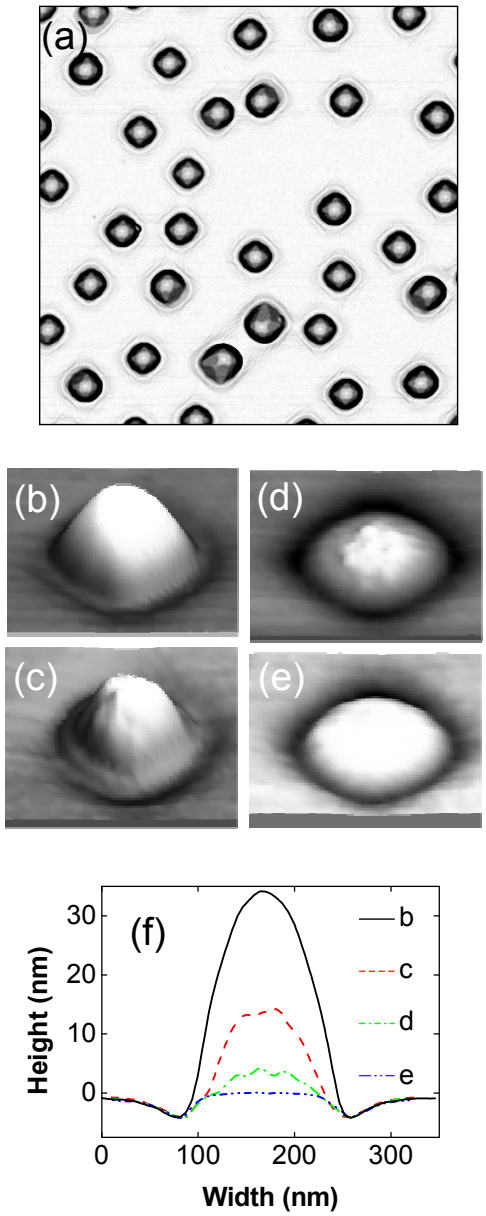

Figure 4.10: (a) 2×2 μm^2 AFM image of the sample grown by deposition of 10 MLs of Ge at 740°C. (b)-(e) AFM images of the *same* island after 0 (b), 40 (c), 60 (d) and 150 (e) minutes of etching in a 1:1 volume (31% H_2O_2)/ (28% NH_4OH) solution. Their size is 260×260 nm^2. The corresponding linescans in (f) demonstrate that the island is etched almost isotropically. All AFM images have their sides parallel to the $< 110 >$ directions.

a rate of 1°C/s. Since the etching of these islands in the 31% H_2O_2 solution did not show any effect we etched them in a 1:1 volume (31% H_2O_2)/ (28% NH_4OH) solution (VLSI Selectipur, Merck) (see section 3.4.4).

4.2.1 Composition of Islands

Figure 4.10 (a) shows an AFM image of the sample grown at 740°C which consists of domes and barns. (b)-(e) display the etching of the same island for different etching times in a 1:1 volume (31% H_2O_2)/ (28% NH_4OH) solution (for details about how to locate the same sample area see Appendix B). One can easily recognize that the etching proceeds in an almost isotropic way. For long etching times the island is completely removed and a circular plateau which was buried below the island can be observed on the surface. [Figure 4.10 (e)]. These plateaus are surrounded by almost square shaped trenches with sides aligned along the $< 100 >$ directions [30].

Due to the fact that this etchant does not show any stop-etch behaviour no quantitative information about the composition of these islands can be obtained. It can be only stated that their composition is higher than 35% Si since they cannot be attacked by the 31% H_2O_2 solution and that their compositional profile does not show any substantial asymmetry.

4.2.2 Comparison between Simulation and Experiment

For simulating islands grown at these high temperatures we take into account that the WL has a higher Si concentration and that the diffusion length of the Si atoms is substantially increased. Indeed, by performing such kind of simulations a more uniform and Si richer alloying of the islands is obtained because the Si atoms can now access every point of the island with high probability. The geometrical arguments having an important influence for the lower growth temperatures, i.e. for low diffusivities, do not play any significant role for these conditions.

4.2.3 Origin of the Incorporated Si

Again the question arises whether the Si included in the islands is originating from surface processes or if, especially at these high temperatures, bulk diffusion is activated. As already stated above, after complete removal of the islands circular plateaus can be observed on the surface, that lie on average

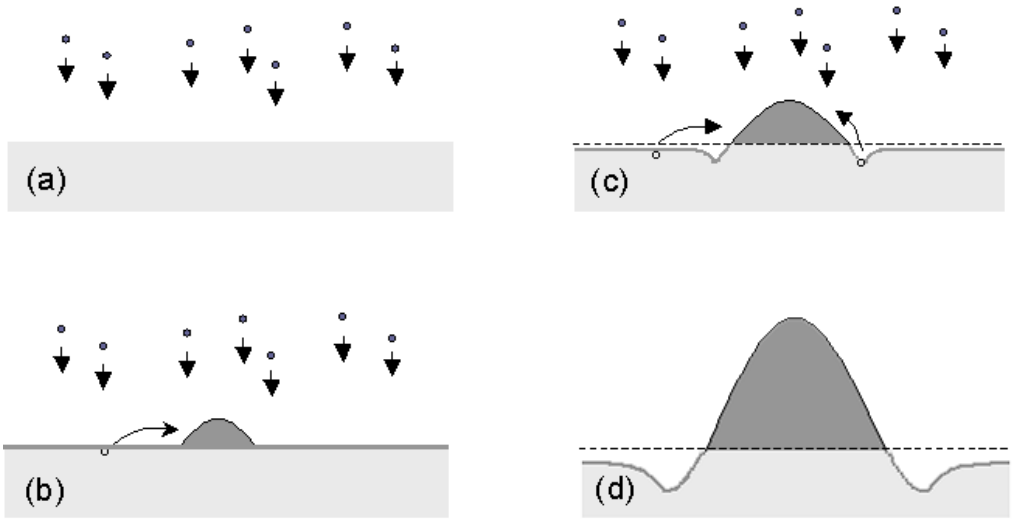

Figure 4.11: Schematic representation of the lowering of the substrate level during growth. (a) Ge atoms are deposited on Si. (b) islands grown from Ge atoms and Si diffusing through the WL. (c) islands continue to grow and induce an out diffusion of the surrounding highly strained material that produces a trench. In this way Si-rich material from the trenches gets incorporated into the islands. Due to the incorporation of substrate Si atoms, the lowering of the WL level has already started. (d) Final situation with the island surrounded by its trench and its interface lying higher than the neighboring surface.

1.1 nm higher than the surrounding surface. These are interpreted as the original interface between the islands and the Si substrate. An experimental support for this interpretation derives from exposing the sample to the etching solution for 1700 minutes. The etch rates reported in Fig. 3.4 were measured for Si contents up to 70%, since for higher concentrations the etching time required to obtain a measurable height difference with the profilometer becomes very long and the height measurements unreliable. Nevertheless, by extrapolation, we can evaluate an etching rate of about 1×10^{-3} nm/min for a $Si_{0.9}Ge_{0.1}$ alloy. Thus, if the composition of the plateaus was of $Si_{0.9}Ge_{0.1}$, their height should be reduced by more than 1 nm after 1700 minutes of etching. On the contrary, the plateaus remained almost unchanged, indicating that they consist of at least 90% Si.

We interpret this observed height difference between the plateaus and the substrate as the result of an overall lowering of the substrate surface, taking place during growth (Fig. 4.11). In order to support this hypothesis, we first note that the as-grown islands shown in Fig. 4.10 (a) are highly intermixed. Indeed, their total volume corresponds to the volume of a film of circa 2.9 nm as determined by AFM, while the deposited 10 MLs of Ge are only equivalent to 1.4 nm. This indicates an average Si composition higher than 50%, consistently with anomalous x-ray scattering measurements performed on similar samples [81]. The trenches surrounding the islands cannot be the only source of Si, since their volume amounts only to 0.3 nm. Thus there is 1.2 nm of "missing" material. This "missing" 1.2 nm of Si material must necessarily come from the substrate region located between the islands. On the other hand, if Si reaches the islands by surface diffusion after having moved through a thin and intermixed wetting layer, a uniform substrate lowering would occur except for in the regions below the islands. This is exactly what we observe in the etched sample and the measured height difference of 1.1 nm between the plateaus and the surrounding substrate is in good agreement with the value of the "missing" Si evaluated above. Thus, from mass conservation, we conclude that bulk diffusion, if present, does not play any significant role for the island composition.

Chapter 5

Composition of Annealed Islands

In the previous chapter we have investigated the composition of the as-grown islands and we have seen the influence of two growth parameters on their composition: temperature and Ge deposition rate. Another important parameter in the growth of self-organized quantum dots is the so-called growth interruption or post growth annealing, during which the sample is heated for a certain time after the deposition flux has been stopped. All the profiles for the as-grown islands which have been reported in the literature have a fourfold or cylindrical symmetry. This is completely different for annealed islands. Already in 1998, Kamins et al. showed that annealed islands do not have a symmetric compositional profile [85]. Some years later, Denker et al. [82] found also an asymmetric compositional profile for annealed dome islands (Fig. 5.1). In a detailed study performed by Kamins et al. [28], it was shown that during annealing smaller islands dissolve while the bigger ones grow. Moreover, the authors also demonstrated that the total volume of the system increases, implying that Si originating from the substrate must be incorporated into the islands. But up to now, no systematic study about the composition of annealed islands has been performed and the observed "strange" asymmetric compositional profiles have been attributed to transition islands (Fig. 2.11).

In this chapter we investigate the compositional profiles of annealed islands grown at relatively low temperatures (580°C) as well as at higher temperatures (740°C).

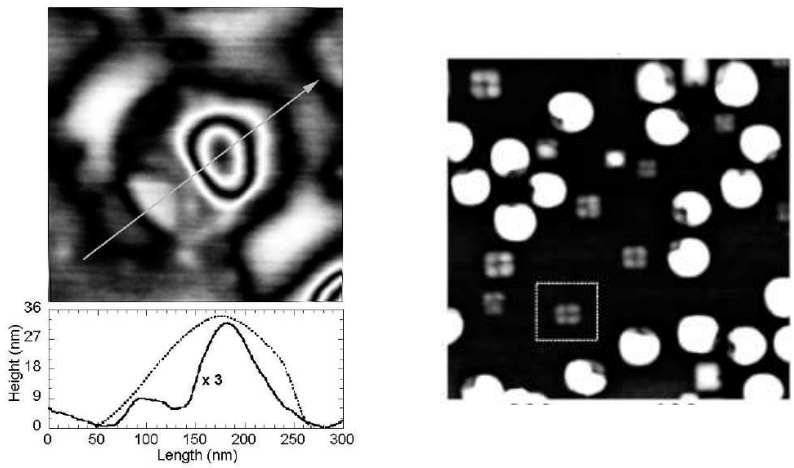

Figure 5.1: (left) AFM image and corresponding line scan of a transition island after annealing for 20 min at 650°C and partially etching with an HCl/H_2 gas mixture. From Ref. [85]. (right) 500 × 500 nm^2 AFM image of a sample grown at 650°C, annealed for 10 minutes and etched in a H_2O_2 solution. From Ref. [82]. Also here an anisotropic etching profile is observed for dome islands.

5.1 Samples Annealed at 740°C

In order to investigate the effect of annealing, 10 MLs of Ge were deposited at a rate of 0.04 ML/s at 740°C and the samples were kept at this temperature for different times. For investigating their composition we used the 1:1 volume (31% H_2O_2)/ (28% NH_4OH) solution (see section 3.4.4).

Figure 5.2 (a) and (d) show the surface morphology of the as-grown and the 10 minutes annealed samples, respectively (the as-grown samples are shown only for comparisons). While the as-grown sample, as already mentioned before, consists of domes and barns, the annealed sample includes also mainly transition islands and pyramids. This is so, because postgrowth annealing is known to cause coarsening and strong SiGe intermixing, which leads to a reverse transition from domes to pyramids passing through the transition island shapes [28, 85]. Indeed a quantitative comparison of the two samples reveals that, upon annealing, the island density decreases from 8.8 to 6.7 mm^2 and that the total island volume increases from 2.9 to 3.2 nm. The SiGe intermixing is further supported by the observation that, after

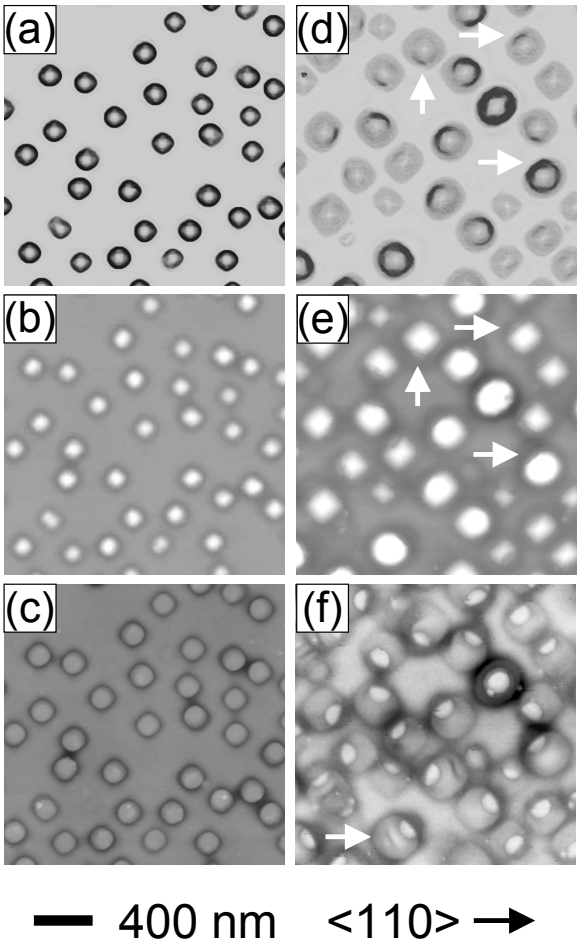

Figure 5.2: AFM images showing as-grown (left column) and annealed islands (right column) before and after different etching times. In both cases exactly the same region was imaged after successive etching experiments (see Appendix B). In (a)-(c) the as-grown islands are shown after 0, 40 and 150 minutes of etching, respectively. (d)-(f) display the annealed islands after 0, 80 and 620 minutes of etching, respectively. For the images (a) and (d) the grayscale is related to the local surface slope so that steep (darker) and shallow (brighter) facets can be distinguished. For the remaining images the grayscale represents the local surface height and is separately adjusted in order to get the highest contrast. For the annealed islands the etching is always asymmetric and starts at the steeper facets as indicated by the arrows in (d) and (e). The arrow in (f) shows a secondary trench, probably created by a temporary interruption in the island movement (see text).

70 minutes of etching, two times more material has been removed from the as-grown sample with respect to the annealed one.

While the as-grown sample is etched almost symmetrically [Fig. 5.2 (a)-(c)], the annealed sample is asymmetrically etched [Fig. 5.2 (d)-(f)]. Moreover, after the complete removal of the islands the annealed sample presents characteristic half-moon-like structures [Fig. 5.2 (f)]. Also the morphology of the trenches surrounding the islands differs significantly after sample annealing. Upon annealing they become much more irregular and deeper and wider on one side [darker areas next to the 'half-moons' in Fig. 5.2 (f)].

The anisotropic etching observed in Fig. 5.2 (e), as well as the peculiar half-moon plateaus visible in Fig. 5.2 (f) indicate a rather complex SiGe material distribution within the annealed islands. In order to understand its microscopic origin, we examined the island erosion at different etching stages by focusing on particular islands and taking line scans after various etching times (Fig. 5.3). Both dome (left column) and pyramid-like (right column) annealed islands are etched quicker from one side. In particular, this is the steeper side of the island, below which the half-moon like structure can be found. Based on the selectivity of the etchant, we conclude that this part of the island is Ge-richer. Figs. 5.3 (d) and (h) clearly show the morphology of the trenches surrounding the annealed islands, which actually consist of two distinct regions. The first is smaller and deeper and surrounds only the half-moon, while the second is shallower and larger and completely encircles the island. The evolution of the island etching is summarized by the AFM line-scans taken at the different stages of the etching process [Fig. 5.3 (i) and (j)]. By comparing the halfmoons with the plateaus obtained after the complete etching of the as-grown islands [Fig. 5.2 (c)] we find that they have a similar diameter, i.e. the half-moon shaped plateaus can be interpreted as remnants of the original circular plateaus. However, we notice that while the apex of the island lies above the center of the plateau for the as-grown sample, it is significantly displaced from the plateau center after annealing.

The above observations can be interpreted as a consequence of a lateral motion of the islands [96]. It has been recently shown, that for nearby positioned islands the region between them has a high strain energy density. Under these conditions Ge atoms prefer to migrate away from the region located between two neighboring islands [97]. The Ge atoms are redeposited on the opposite side of the island where they intermix with Si, via only surface diffusion processes, simply by producing a new atomic layer on top of an already existing one. The Si which contributes to the intermixing is always

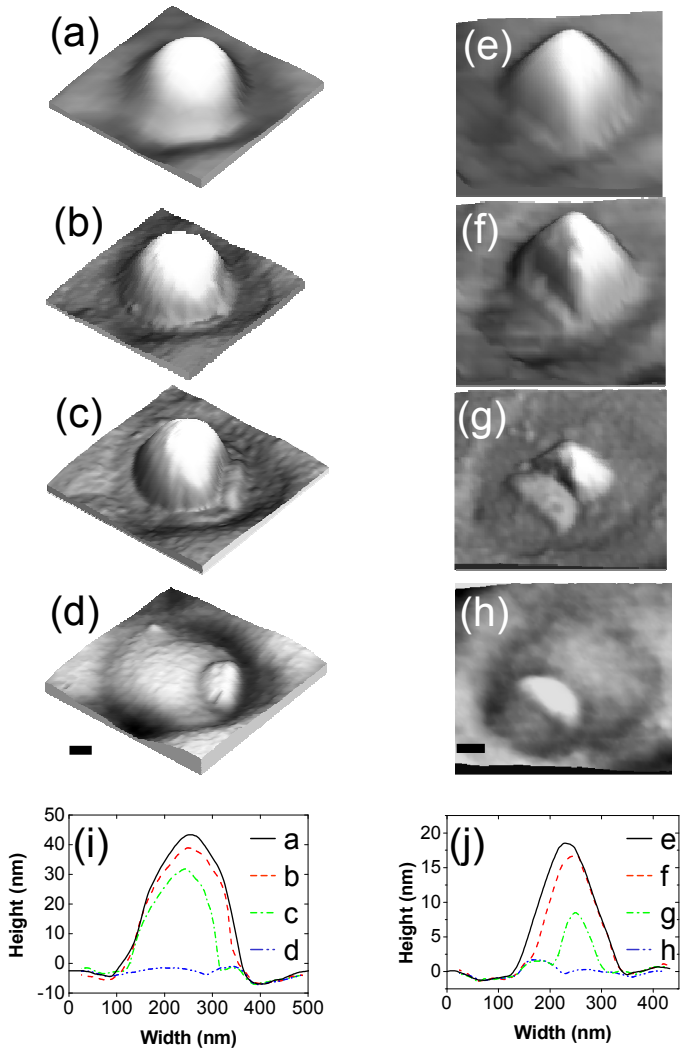

Figure 5.3: AFM topographies showing successive stages of the erosion of two different islands. (a)-(d) for an annealed dome and (e)-(h) for an annealed pyramid-like island. The corresponding linescans (i) and (j) demonstrate that the annealed islands are etched quicker from their steeper side, below which the half-moon shaped plateaus are finally emerging. The scale bars correspond in each case to 50 nm. The etching times are 0, 80, 170 and 620 minutes respectively.

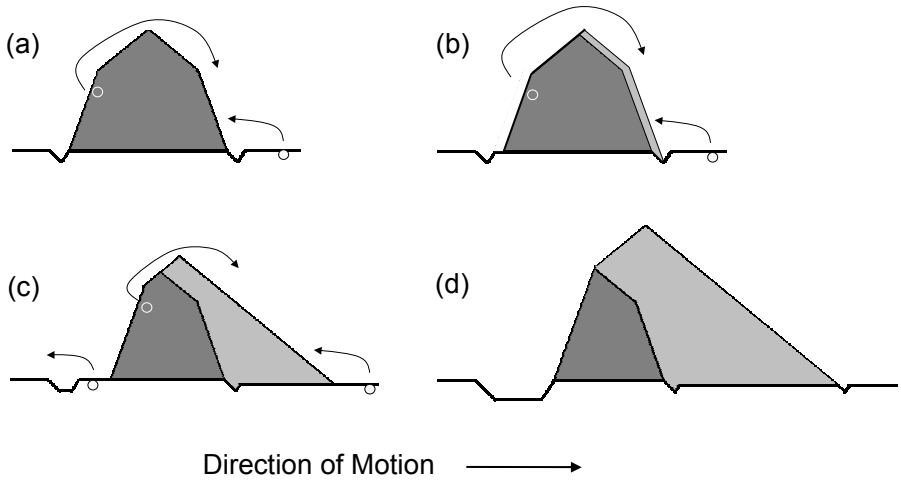

Figure 5.4: Schematic representation of the lateral island movement during annealing. (a) Initial island. Ge rich material (dark gray) is diffusing from one side of the island to the opposite one, where it intermixes with Si atoms (light gray) originating from the substrate, and (b) creates a SiGe alloy (gray). (c) The part of the Si plateau, which is uncovered diffuses away. Moreover, because of the lower strain, the new alloyed side of the island assumes a shallower shape. (d) The final island has a deeper and wider trench on the Ge rich side (remnant of the initial island) and a shallower trench surrounding its newly grown part.

available from the substrate through surface diffusion.

In the following it is shown that a self-sustaining process is initiated since the alloyed region turns out to be energetically favorable also for further Si atoms originating from the substrate [96].

In order to understand this self-sustaining mechanism, one can consider an initially pure Ge island in which a new alloyed layer has been formed on one side. This layer consists of Ge removed of the opposite side of the islands and of Si originating from the substrate through surface diffusion [Fig. 5.4 (b)]. If x is the Ge content of the alloyed layer, the difference in Ge chemical potential between the mixed side and the pure-Ge side is:

$$\Delta\mu_{Ge} = K_b T ln(x) - U(1-x)^2, \tag{5.1}$$

where U is the strain energy per atom for pure Ge. The two terms correspond

to entropy and strain energy, respectively and both are always negative, favoring the process. (Ge motion alone contributes no change in volume or surface energy.) Since the difference in the Ge chemical potential in negative, Ge is drawn from the bare side to add to the mixed side, if Si is supplied simultaneously. During annealing, the substrate acts as a reservoir for Si. The difference in Si chemical potential between the substrate and the alloyed side of the island is

$$\Delta\mu_{Si} = K_b T ln(1-x) - Ux^2 + \Gamma V^{1/3}. \tag{5.2}$$

V is the island volume and Γ reflects the surface energy and also includes geometrical factors that account for the island shape. The first two terms on the right side of this equation are always negative, so Si is always drawn from the substrate to add to the island, unless the surface energy term becomes dominant.

Note that the alloy covers the growing side of the island, so on that side the pure-Ge core is not accessible by surface diffusion, only the alloyed layer. But on the shrinking side of the island, Si cannot be incorporated, so the pure-Ge core remains exposed and can continue to diffuse away.

Consequently, while the islands are growing during the post-growth annealing, their center of mass is moving because of the internal redistribution of Ge and the asymmetric incorporation of Si (see Fig. 5.4). Moreover, during the lateral displacement, part of the island interface with the original Si substrate is revealed. The atoms belonging to this region are under compressive strain generated by the receding islands' edges and thus diffuse away as soon as they are uncovered [Fig. 5.4 (c)]. As a result, a wide and deep trench is created on this side of the islands, while the portion of the interface that is still covered remains unchanged. This explains why, when the islands of the annealed sample are completely removed by etching, instead of full plateaus only fractions of them - the above mentioned "half-moons" - appear [Fig. 5.2 (f)]. The advancing part of the islands, as discussed above, is highly intermixed and less strained and can therefore be delimited by a shallower surface orientation [20]. Thus, the annealed islands exhibit an asymmetric shape [Fig. 5.2 (d)]. The trenches formed around the relaxed parts of the islands are shallower and are constantly overgrown during further island movement. The island/substrate interface of the newly formed portion of the island is therefore slightly lower than the surrounding substrate. It appears that in some cases the island movement is interrupted for some time so that a

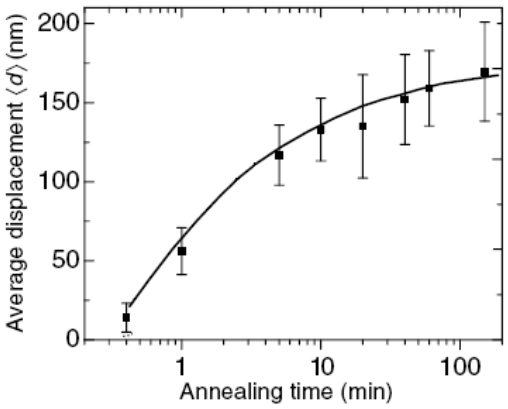

Figure 5.5: Average displacement of the islands versus annealing time. The displacement is taken as the distance between the centers of the island base before and after annealing. From Ref. [96].

deeper trench is formed between the initial and the final one as can be sometimes observed in the etched samples [see arrow in Fig. 5.2 (f)]. The above reported complex mechanism, schematically shown in Fig. 5.4, fits quite well with all the experimentally observed features.

The lateral motion can proceed until much of the original island has intermixed with Si from the substrate. This is seen in Fig. 5.5 were it is shown that the displacement of the islands starts to saturate for long annealing times.

Again Si incorporated into the island by bulk diffusion seems to be negligible since for annealing times as long as 10 hours the half-moon structures can be observed clearly. If bulk diffusion would have taken place the island/substrate interface would have smeared out and as a consequence the half-moon structures would not be any more visible.

5.2 Samples Annealed at 580°C

In order to investigate if the same mechanism is active also at lower temperatures, a series of samples were grown by deposition of 6 MLs of Ge at 580°C and in situ annealing at the same temperature for 10 and 20 minutes [Fig. 5.6]. The comparison between Fig. 4.4 (a) and Figs. 5.6 (a) and 5.6 (b) reveals that a coarsening process has taken place in which the hut clusters

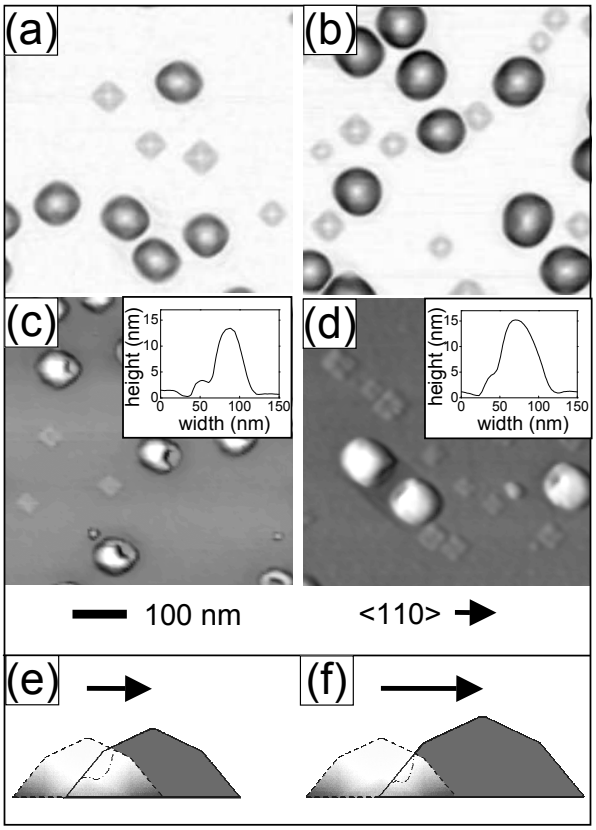

Figure 5.6: AFM topographies showing the morphology of 580°C annealed Ge islands before (upper row) and after (lower row) 10 minutes of 31% H_2O_2 etching. The annealing times are 10 minutes for (a) and (c) and 20 minutes for (b) and (d). The insets in (c) and (d) show representative linescans across the etched islands. The gray scale in (a) and (b) is related to the local surface slope while in (c) and (d) it represents a combination of local surface height and gradient so as to enhance small-scale morphological details. (e), (f) represent a schematic model of the island movement and of its effect on the island composition. The dashed border includes the original island and its compositional profile taken from the actual simulation (darker regions are Si rich and not attacked by the etchant). The dash-dotted line inside the final island (dark grey) indicates the linescan that is expected after etching. The arrows indicate the direction and the "magnitude" of the island motion.

have disappeared and the average island size has increased. After annealing the etched pyramids show qualitatively the same compositional profile like the as-grown ones. Conversely, the domes display a completely different compositional profile after the growth interruption (for both 10 and 20 minutes). The symmetric Si-rich ring typical of 580°C as-grown domes [see Fig. 4.8 (c)] is replaced by a strongly asymmetric structure in which the part removed by the etching is close to the island border. Moreover, linescans as those shown in the insets of Figs. 5.6 (c) and 5.6 (d) reveal that the Ge-rich part of these domes becomes smaller with increasing annealing time. These very peculiar compositional profiles cannot be easily explained without considering that Ge islands move laterally during annealing, as has been described above. Figure 5.6 (e) schematically shows the effect of this movement on the composition of domes that initially had a Si-rich ring. The right side of the island is highly alloyed and will therefore not be affected by the etchant. The left side is constituted by the material of the original island with a lower lying Si-rich region that corresponds to the original ring and a higher lying Ge-rich part that will be removed after etching. The total resulting compositional profile is thus very similar to the experimentally measured one [see line scan in inset of Fig. 5.6 (c)]. The observation that the island displacement scales with the annealing time further explains why the etched part of the island becomes smaller for longer growth interruptions [Fig. 5.6 (f)]. For islands close to each other, we observe a clear correlation between the direction of motion and the direction away from the nearest neighbor. A very similar behaviour is also seen when the annealing is performed at higher temperatures, and this supports the above interpretation. Since the compositional profile of pyramids is qualitatively the same for the as-grown and the annealed islands, a movement seems not to be plausible in this case. The origin of the different behavior of pyramids and domes cannot be unambiguously derived from our experiments. One reason could be that in the case of pyramids the repulsive strain fields needed to trigger the island motion [97] are not strong enough [34].

Chapter 6

Growth and Shrinking Paths of SiGe Islands

As already discussed in Chapter 2, detailed studies about the morphological evolution of Ge islands on Si(001) islands have been reported in the literature [4, 24, 25, 26, 27, 28]. Despite all this work, an issue which is still under debate is whether the shape of the islands is determined by kinetics [46] or by thermodynamics [43, 98]. An approach to answer this question is to study the shrinkage of islands. Islands that while shrinking follow the reverse path of their growth would be a strong indication that their shape is governed by thermodynamics.

It is known that island coarsening, i.e. the growth of large islands at the expense of smaller ones, is occuring not only as a consequence of annealing [28, 31] but also during growth [45, 46]. Ross et al. [45] observed this coarsening by real-time LEEM measurements and they were able to distinguish the growing from the shrinking islands. Nevertheless, the limited spatial resolution of electron microscopy did not allow to precisely determine the island shapes while these were shrinking.

In this chapter the coarsening phenomenon will be analyzed by ex-situ STM and AFM measurements which offer a much better lateral resolution. It is shown that shrinking islands can be distinguished from growing ones by using as "markers" their surrounding trenches [99].

Samples grown at 740°C and 840°C were investigated since the islands grown at such high temperatures are big enough to be precisely solved by STM as well as by AFM. Both as-grown and annealed samples were examined.

The SiGe islands were obtained by depositing 5 MLs of Ge at 740°C and 840°C with a rate of 0.04 ML/s. A second set of samples was grown by deposition of 10 MLs of Ge and subsequent post-growth annealing for 20 minutes. After growth, all samples were cooled to room temperature at a rate of about 1°C/s. Some of them were analyzed ex-situ by means of AFM, while others were transferred under UHV conditions to a homemade STM.

6.1 Coarsening during Growth

Figure 6.1 (a) shows an AFM image of the sample grown by deposition of 5 MLs of Ge at 740°C. The sample contains islands of different shapes. It includes domes (D), transition domes (TD), pyramids (P), truncated pyramids (TP), prepyramids (not shown in the image) and trenches, which do not encircle any island. For this reason, we call the latter empty trenches (ET). The different island shapes represent different stages of the island evolution. Some islands grow while others dissolve, as it is happening in every coarsening process. Figures 6.1 (b)-(d) are STM images showing the growth of islands, which is happening through the pyramid to dome transition. Also at these high temperatures the transition seems to follow the same pathway reported for samples grown at 560°C [88]. Incomplete {105} facets start to form at the top of pyramids and these bunch together at their lower step edges [Fig. 6.1 (b)]. These bunches transform into steeper dome facets [Fig. 6.1 (c)] and finally a mature dome develops [Fig. 6.1 (d)]. Each of the three islands shown in the transition path of Fig. 6.1, is surrounded by a trench whose base area is comparable to the island diameter. This is actually the critical feature which allows the distinction between growing and shrinking islands. The existence of ET on the surface proves that while islands can completely dissolve this is not true for their trenches; the latter do remain on the surface even after the complete disappearance of their island. Thus, it is natural to assume that islands having a base area smaller than the trench area are shrinking. Pyramids at different stages of the shrinking process can be seen in more detail in Fig. 6.2. Fig. 6.2 (a) is a STM image of a pyramid that has already started to shrink. Actually, not only the base area of the island is an indication of its dissolution but also its position relatively to the trench. The island center is clearly displaced with respect to the trench center and part of its interface with the Si substrate is getting revealed. This is seen much better in Fig. 6.2 (b), where the pyramid has transformed into a truncated

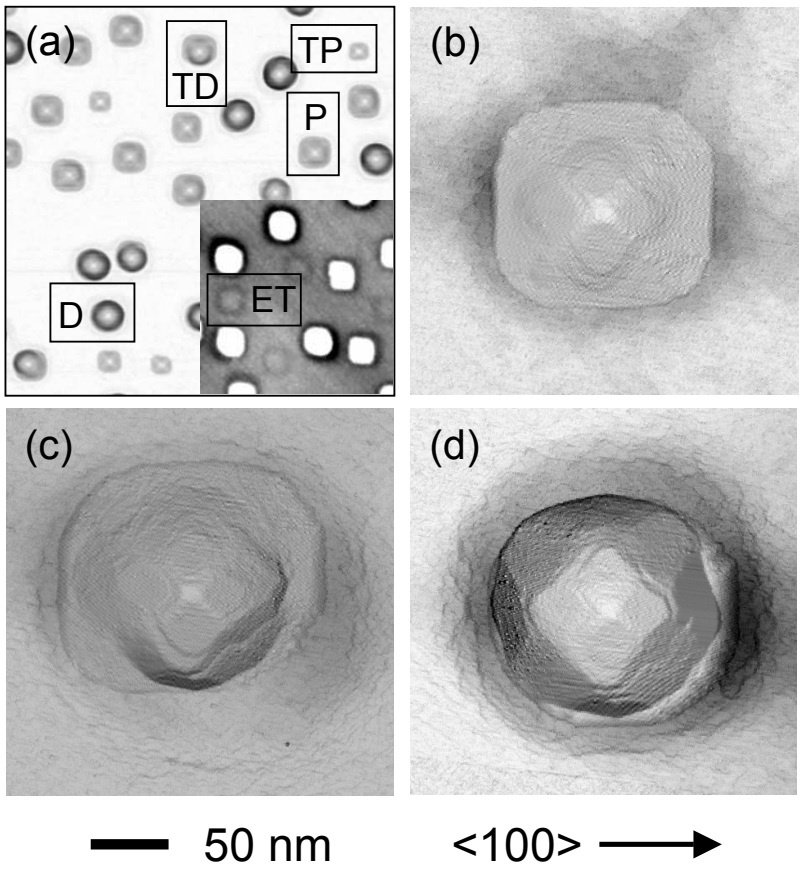

Figure 6.1: (a) AFM scan (2×2 μm^2) of the sample grown by deposition of 5 MLs of Ge on Si(001) at 740°C. Different types of islands can be found: domes (D), transition domes (TD), pyramids (P) and truncated pyramids (TP). The inset is a 1×1 μm^2 AFM image displayed with modified contrast in order to make the empty trenches (ET) visible. (b)-(d) STM images showing the pyramid to dome transition. On the top of the pyramid a step bunching of incomplete {105} facets takes place (b). This leads to the formation of steeper facets (c), which grow further until the complete transformation to a dome island (d). The gray scale in (a) is related to the local surface slope, while in (c)-(d) it represents a combination of local surface height and slope in order to contemporarily visualize morphological details of the islands and of the surrounding trenches.

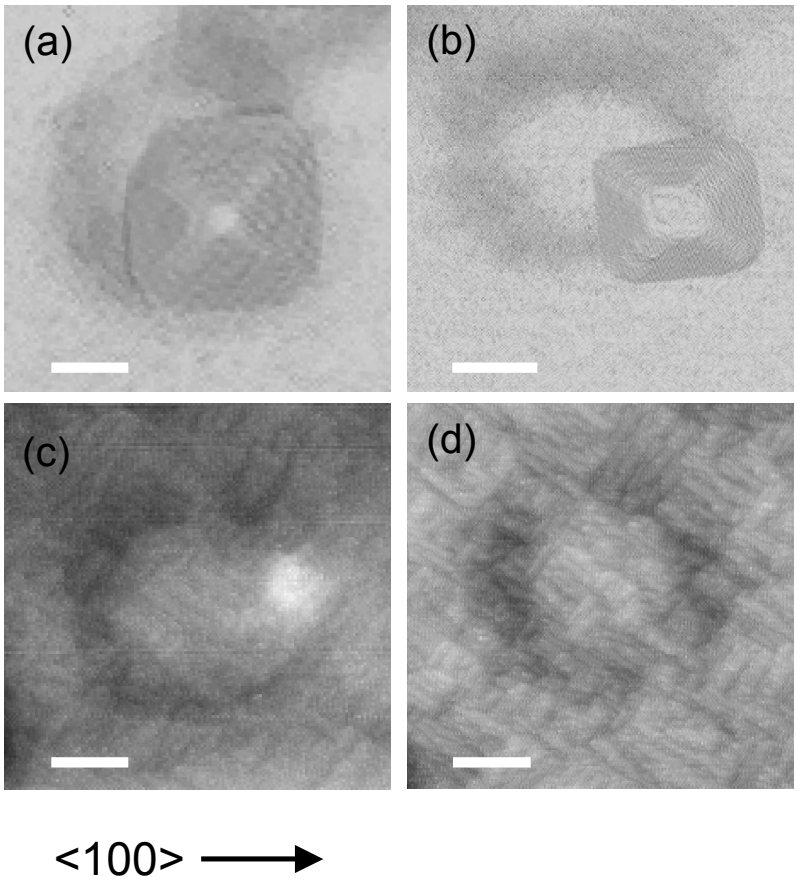

Figure 6.2: STM images showing the path islands follow while shrinking. (a) Pyramid, which has already started to shrink. (b) Truncated pyramid, which is clearly shifted in respect to the trench center and extends significantly over its border. (c) Prepyramid, located at the right side of the trench and which corresponds to the last stage of the island shrinkage and (d) empty trench remaining on the surface after the island has completely disappeared. The scale bar in each image corresponds to 50 nm.

pyramid. The origin of this displacement cannot be unambiguously derived from our experiments. It is not clear if the observed displacement is connected with a Si-enrichment of the islands as has been shown in the previous chapter for the growing islands. Figure 6.2 (c) shows the final stage before the complete disappearance of the island, i.e. a 3D unfaceted mound, a so-called prepyramid [25]. After the disappearance of the unfaceted mounds, empty trenches remain on the surface [Fig. 6.2 (d)]. The same route was observed also for the samples grown at 840°C.

The path which is described above, i.e. the shrinkage of the pyramids through the stages of truncated pyramid and prepyramid, is actually the inverse of their growth [22], proving thus that the shape of the islands is thermodynamically determined.

6.2 Coarsening during Annealing

In the previous section the coarsening during growth was investigated. In order to check whether the shrinking route reported above is general, also annealed samples were analyzed. Figure 6.3 (a) shows an AFM image of a sample which was grown by deposition of 10 MLs of Ge at 740°C and subsequent annealing for 20 minutes. The inset shows the surface morphology just after the Ge deposition flux has been stopped and demonstrates that before annealing the sample is characterized by a monomodal distribution of domes. On the annealed sample, as for the 5 ML Ge as-grown sample in Fig. 6.1 (a), truncated pyramids surrounded by a larger trench can be observed (encircled island). According to what discussed in the previous section, such islands are clearly shrinking ones. Figure. 6.3 (b) displays the same area of the sample after 1000 minutes of etching in a 1:1 volume NH_4OH/H_2O_2 solution. After the complete etching of the islands a half-moon like feature can be observed below *each* island, also below the shrinking ones. As has been shown in Chapter 5, this characteristic half-moon structure is an indication of the movement the islands undergo while growing during post-growth annealing. As a consequence, on the annealed sample we have indications of islands that are both growing and shrinking. This apparent contradiction can be reconciled by assuming that after the Ge flux has been stopped, some of the domes transform into truncated pyramids by following the evolution path schematically shown in Fig. 6.4. In the initial stages of annealing, domes transform into asymmetric transition islands while moving

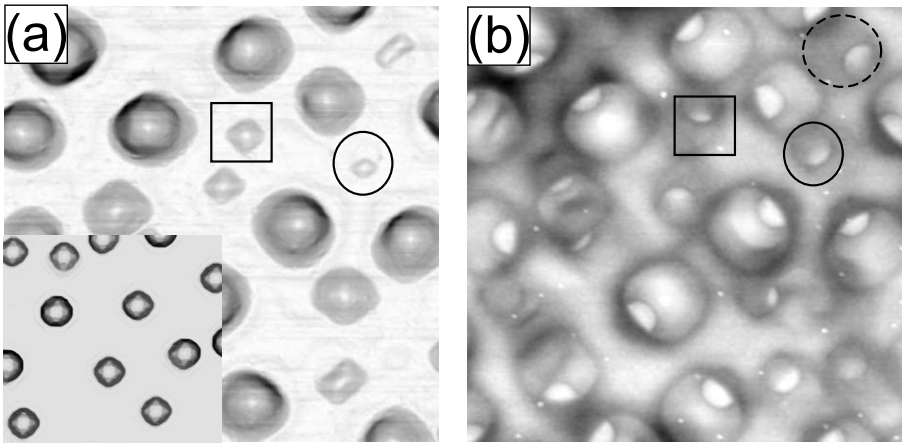

Figure 6.3: AFM scans (2×2 μm^2) showing the same area of a sample grown by deposition of 10MLs of Ge at 740°C and subsequent annealing for 20 minutes, before (left) and after (right) 1000 minutes of etching in a NH_4OH/H_2O_2 solution. It can be seen that below the encircled truncated pyramid a half-moon like structure exists. The inset in (a) is an AFM image (1×1 μm^2) of the same sample prior to annealing. The images have their sides parallel to the $< 110 >$ directions.

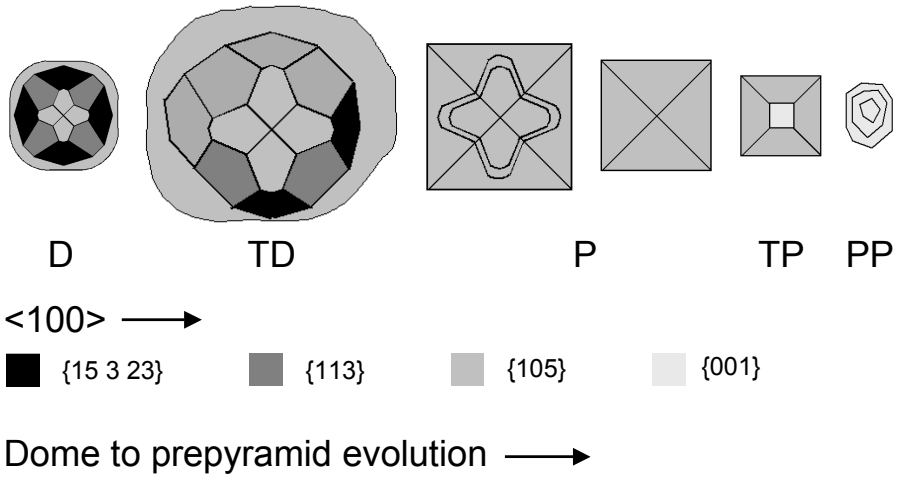

Figure 6.4: Schematic representation of the path followed by a dome island during annealing when transforming first into a transition dome and then in a prepyramid.

according to the mechanism explained in section 5.1. Thus in this first shape transformation the islands are growing by incorporation of Si originating from the substrate. After a certain critical volume has been reached, coarsening sets in and some of the islands start to shrink assuming the shape of a pyramid [the square shown in Fig. 6.3 (a) displays an island which is shrinking and has a pyramidal shape]. As a next step, the transformation towards the truncated pyramid is taking place and finally unfaceted mounds appear on the surface prior to the complete disappearance of the islands. The first step in the transition shown in Fig. 6.4, i.e. the growth and contemporary transformation of a dome into a transition dome, is most probably occurring to all islands. In fact all pyramids and truncated pyramids that we have observed on this sample are surrounded by slightly depressed areas that are much larger than the base area of the as-grown domes [darker area included in the dashed circle in Fig. 6.3 (b)]. This indicates that the shrinking starts only after the initial as-grown island has increased its size.

The observation that also on this annealed sample the islands do not shrink in a self-similar way but through various shape transformations, suggests that the transformation path that islands follow when they become smaller and disappear is thermodynamically determined.

Chapter 7

Shape and Composition of Buried Islands

In Chapters 4 and 5 the composition of the free-standing (uncapped) islands has been thoroughly investigated. As already stated in Chapter 2 section 2.5, whenever the optical end electronic properties of the QDs are to be exploited, they have to be embedded in a host matrix. This is because the recombination centers created by the surface states have to be passivated. During the islands' overgrowth (capping) by the host material significant morphological and compositional changes occur [54, 55, 100] that affect significantly the QDs' optoelectronic properties. As a consequence, the structural characteristics defining the properties of the system are the shape, size, strain and composition not of the free-standing but of the buried islands.

Despite their importance, it has not been possible up to now to get precise quantitative data about the 3D shape of buried SiGe islands. Furthermore, not much is known about their composition apart from the general trend that overgrowing them at high temperatures leads to an increase of the average Si content [101].

The initial stages of overgrowth during which some MLs of Si are deposited on the islands have been studied by means of LEEM [54] and STM [55]. In these studies it was shown that the islands become flatter and obtain a bigger base area (Fig. 7.1).

As a standard technique, X-TEM is used to address the shape of buried islands. However, apart from the difficulty in preparing thin X-TEM specimen, especially for low density samples, the created section might include any part of the islands, making TEM thus helpful for obtaining only qual-

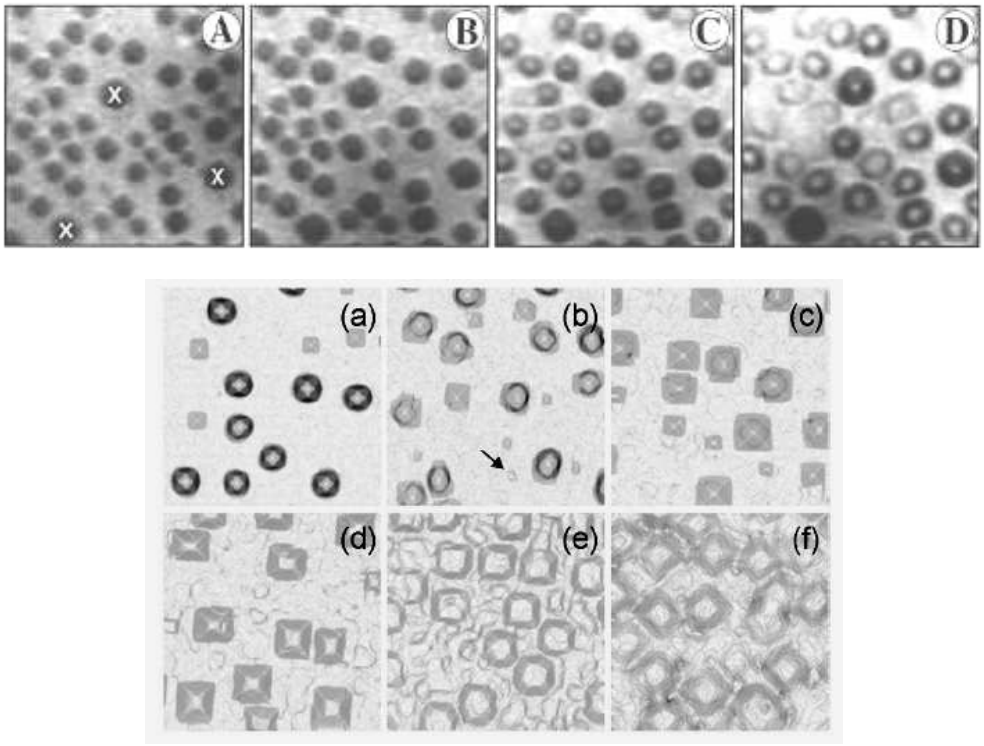

Figure 7.1: (upper row) Sequence of LEEM images showing the overgrowth of Ge islands at 650°C. From Ref. [54]. (lower row) STM images showing the overgrowth of Ge islands at 450°C. From Ref. [55]. In both cases a flattening of the islands' top and a widening of their base can be observed.

itative information. The access to the full 3D shape of the islands is not feasible with this technique. The same problems are faced when performing cross sectional STM studies, which for SiGe islands have not been possible up to now. Scanning TEM in combination with electron energy-loss spectroscopy (EELS) can be additionally used in order to investigate the 2D compositional profiles of the capped islands [79] but clearly one faces the same type of problems. Alternatively, X-ray scattering measurements have been used to evaluate the shape and composition of buried SiGe islands. This method provides information about the 2D profile of the islands and their average composition, but the interpretation of the measurements is not straightforward since a comparison with a structural and compositional

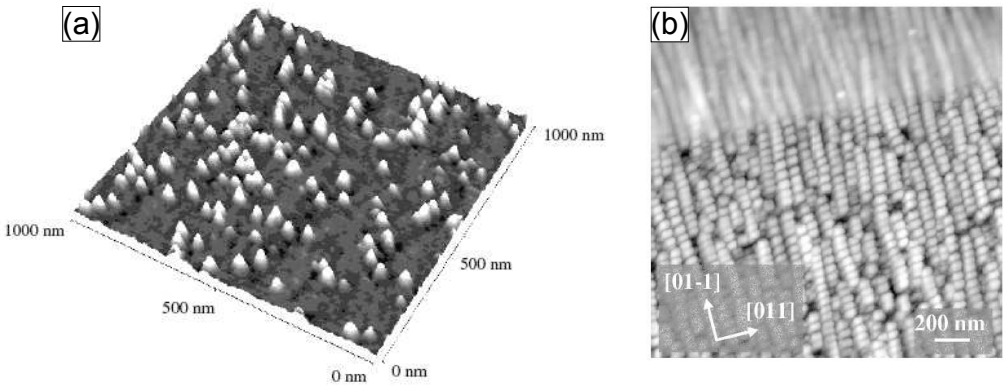

Figure 7.2: AFM images displaying disclosed islands: (a) InAs islands which were capped with GaAs at 550°C. From Ref. [104] (b) InGaAs islands which were overgrown with GaAs at 540°C. From Ref. [105].

model is needed [102]. Karpovich et al. [103, 104] and later Wang et al. [105] investigated the morphology of buried In(Ga)As QDs grown on GaAs by removing the GaAs host matrix using selective chemical etching. Not much information about the morphological changes upon overgrowth was given (Fig. 7.2).

In this chapter both the morphology and the composition of buried islands for different overgrowing temperatures is studied. Selective wet chemical etching is used once more as the experimental method for removing in the first place the Si overlayers and, in a second step, to address the composition of the disclosed islands.

7.1 Removing the Si cap from the Islands

The buried SiGe QD samples were grown by depositing 6.7 MLs of Ge on Si(001) at 620°C; subsequently 20 nm of Si were deposited at two overgrowth temperatures: 300°C and 620°C. As already seen in Fig. 4.4 (c), the deposition of Ge under such growth conditions produces a monomodal distribution of dome islands. The overgrown specimens were dipped in a 50% hydrofluoric acid (HF) solution for about 30 seconds so as to remove the native silicon oxide formed on the samples and to get reproducible initial conditions for the experiments. Subsequently, they were dipped for about 2 minutes in a 2M

KOH solution which, as has been shown in section 3.4.3, removes selectively Si over Ge and shows a selectivity of Si over $Si_{0.8}Ge_{0.2}$ of about 100 at RT.

Figures 7.3 (a) and (b) display AFM images of the as-grown samples after they have been overgrown at 300°C and at 620°C, respectively. It can be seen that while capping at 300°C results in a replica of the buried islands, covering the islands at 620°C restores a flat Si surface above the coherent dome islands. The lower row of Fig. 7.3 shows the morphology of the samples after the Si layers have been removed. While the islands which were overgrown at 300°C show no difference within the statistical error in respect to the uncapped ones, those overgrown at 620°C have a much bigger base area and a flatter top.

The question which naturally arises is whether the disclosed islands in Fig. 7.3 (d) are actually equivalent to the embedded ones or if their morphology results from a combined effect of the buried island structure and the etching action. As has been recently reported [106], islands grown at 620°C have a Ge content between 50% and 76%. After overgrowth, their Ge content decreases to 40-50%. Thus, according to the etch rates of the used solution which were reported in section 3.4.3, the islands should not be attacked by the etchant. In order to verify this, X-TEM images of the sample which was overgrown at 620°C were taken. Figure 7.4 displays such an image where additionally an AFM line-scan of a disclosed island along the $< 110 >$ direction is superposed. The heights of the buried islands measured from the X-TEM images were between 5.5 and 6.5 nm. By performing a statistical analysis over more than 100 disclosed islands an average height of 6 ± 0.5 nm was found. Thus, the disclosed islands are a reliable representation of the embedded ones, implying that the selective etching method can be used to investigate the shape of the buried islands.

Fig. 7.5 shows a statistical analysis of the structural properties of as-grown and disclosed islands. By plotting the height of each island as a function of its base area, a direct comparison between the different samples becomes possible. From this graph one can quantitatively recognize that while for the low temperature overgrown sample no statistically relevant morphological changes take place, the sample overgrown at 620°C contains islands with much lower height (6 ± 0.5 nm instead of 18.5 ± 0.8 nm for the as-grown islands) and much bigger base area ($9.4\pm1.2\times10^3$ nm^2 instead of $4.6\pm0.2\times10^3$ nm^2). The base area of the disclosed islands is not only larger, but also much more broadly distributed than that of the as-grown islands. A gaussian fit of these distributions results in a full width at half maximum (FWHM) of about

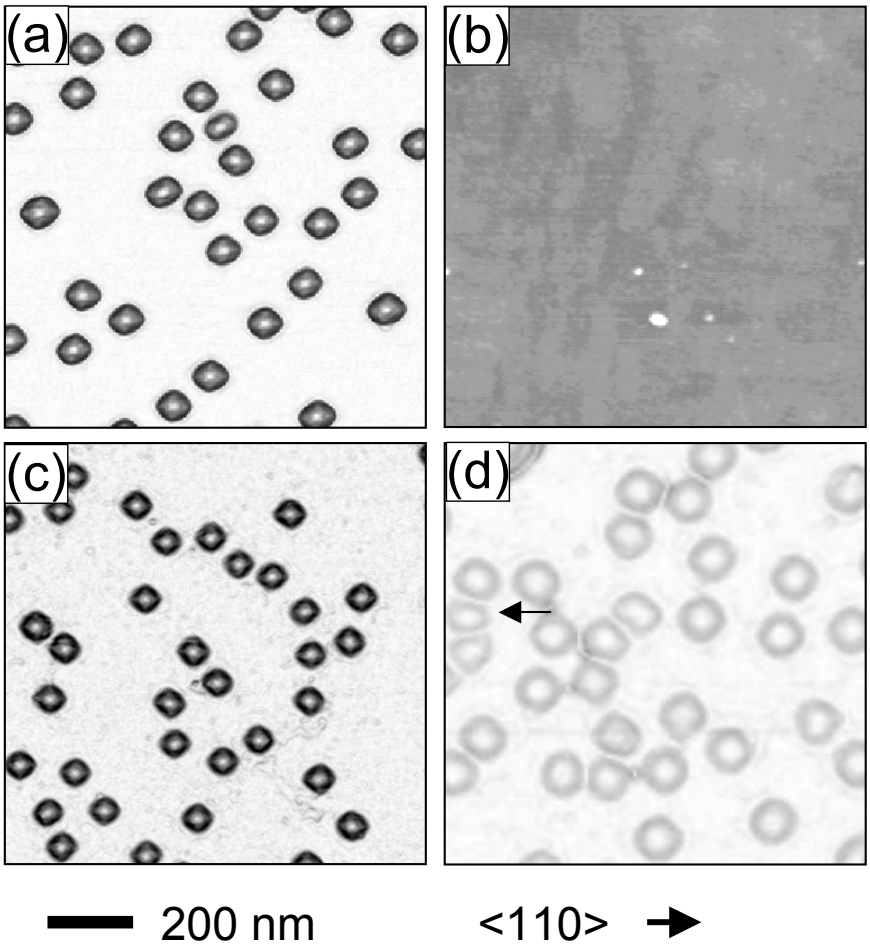

Figure 7.3: (upper row) AFM images showing the surface morphology after overgrowing the islands at 300°C (a) and at 620°C (b), respectively. (lower row) Corresponding AFM images displaying the disclosed islands after the Si layers have been removed. Again (c) was capped at 300°C and (d) at 620°C. The arrow in (d) points towards a "squeezed" island (see text for details). The gray scale in (a), (c) and (d) is related to the local surface slope while in (b) it represents the local surface height.

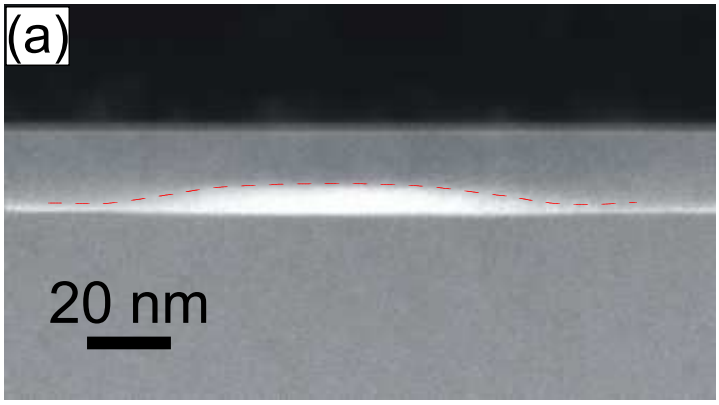

Figure 7.4: X-TEM image of the sample grown at 620°C and capped with 20 nm of Si at the same temperature. The dashed line is a representative AFM line scan of a disclosed island along the $< 110 >$ direction. Data courtesy of Dr. E. Müller.

10% for the as-grown and the 300°C overgrown sample and of about 20% for the 620°C overgrown islands. A possible explanation for this broadening is the following: it is known that while overgrowing the islands, Ge material from the top is removed towards the base were it is getting intermixed with the deposited Si [54]. During this procedure the width of the islands is getting larger and the distance between next neighbors is decreasing. As has been recently shown [97], the strain energy density in the region between islands is increasing for reduced distances and Ge atoms tend to migrate away from this region. Thus, if the initial distance of the islands prior overgrowth is small, the expansion of islands during capping is hindered. This can be clearly seen for the island indicated by an arrow in Fig. 7.3 (d). Since it is located between two islands, during overgrowth it cannot expand and its shape appears squeezed. On the other hand, the height distribution of the disclosed islands is much narrower than that of the as-grown islands.

7.1.1 Correlation between the Surface and Island Morphology

After verifying that the applied method can be used for investigating the buried SiGe islands, a more systematic study was performed on a second set of samples. 5.9 MLs of Ge were deposited at a rate of 0.04 ML/sec while the

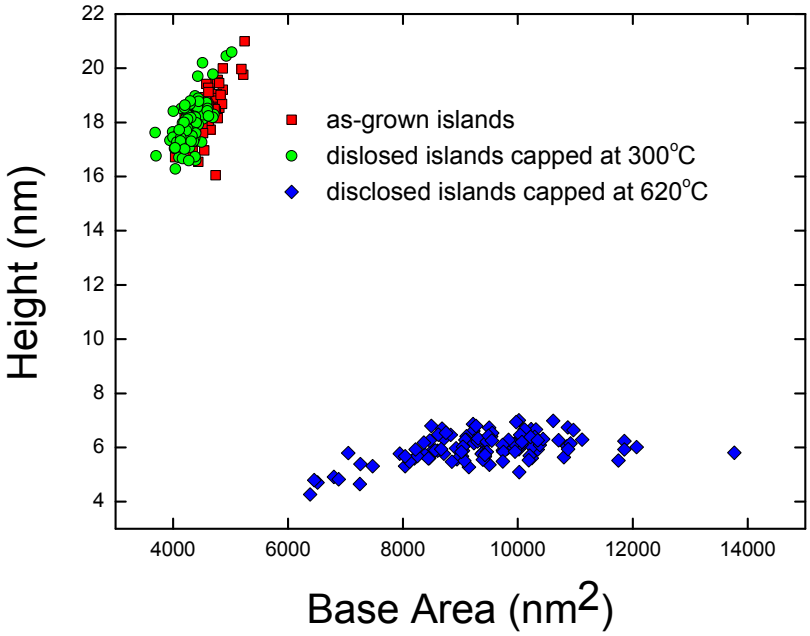

Figure 7.5: Statistical analysis of the as-grown and disclosed islands capped at two different temperatures. The height of each island is plotted as a function of its base area.

substrate was kept at a temperature of 580°C. Subsequently, 20 nm of Si were deposited at a rate of 1Å/sec (0.2 ML/sec) at three different temperatures: 300°C, 450°C and 580°C.

Figure 7.6 shows AFM images of the as grown islands before (a) and after covering them with 20 nm of Si at 300°C (b), 450°C (c) and 580°C (d). The as-grown sample consists of a trimodal island distribution of hut clusters, pyramids and domes. After Si capping at 300°C [Fig. 7.6 (b)] the surface displays no significant morphological changes. The capped surface is essentially a replica of the buried islands but the structures have a flatter top, in accordance to what has been recently reported [107]. Furthermore, by comparing the dome-like Si structures with the dome islands on the uncapped sample it is seen that their base area and volume have increased by 18% and 17%, respectively, while their height is reduced by 4%. On the other hand, after Si capping at 450°C [Fig. 7.6 (c)], the surface morphology evolves towards truncated pyramids with edges aligned along the $< 110 >$ directions, as reported previously [55] [Fig. 7.1, (f)]. Their base area is roughly three

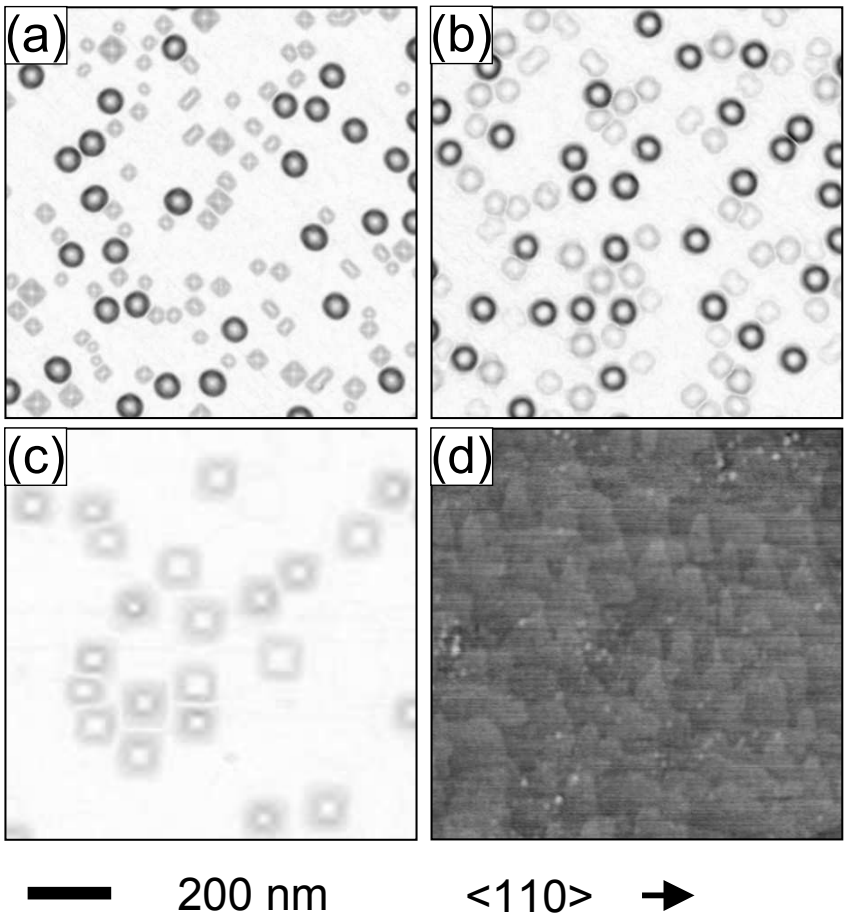

Figure 7.6: AFM images displaying the surface morphology before (a) and after overgrowing the islands with 20 nm of Si at 300°C (b), 450°C (c) and at 620°C (d), respectively. The gray scale in (a)-(c) is related to the local surface slope while in (d) it represents the local surface height.

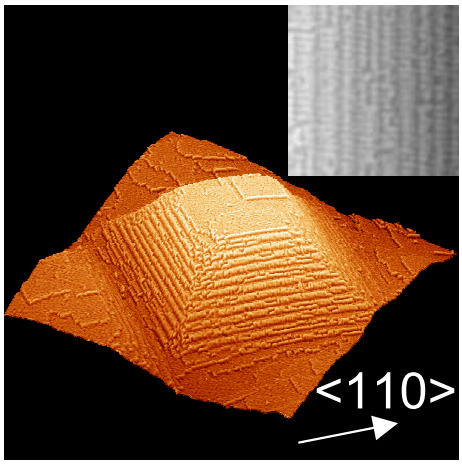

Figure 7.7: 3D STM image of a "ziqqurat" structure (160×160×5.1 nm^3). The inset is a 15×15 nm^2 2D STM image which displays the B-type double steps aligned along the < 110 > directions. Data courtesy of Dr. A. Rastelli.

times larger than the base area of the uncapped dome islands while their height is roughly the half of it (5.3±0.8nm). Finally, the surface morphology of the sample which was capped at 580°C is again flat [Fig. 7.6 (d)].

Figure 7.7 is a 3D STM image of such a rotated truncated pyramid and shows that it consists of a staircase of steps. The high resolution inset shows that they are double B-type Si-steps. Due to the similarity of these structures with the terraced pyramidal temples of ancient mesopotamia, we call them for simplicity *"ziqqurat"*. These ziqqurats are actually observed for a wide range of overgrowth temperatures [100] and for different growth techniques, such as MBE [100], chemical vapor deposition (CVD) [108] and magnetron sputtering epitaxy (MSE) [55, 109].

In order to reveal the buried islands, the Si layers were removed by exposing the sample in the 2M KOH solution, as described in the previous section. Figure 7.8 (a) displays the 300°C buried islands after the Si cap has been removed. Also in this case no difference to the as-grown ones can be observed. Indeed, by performing the facet plot analysis [92] on the disclosed islands it can be seen that *the facets can be still distinguished* [inset in Fig. 7.8 (a); the steep {15 3 23} facets of the dome islands cannot be resolved due to the small dimensions of the islands]. Surprisingly, the morphology of the islands which

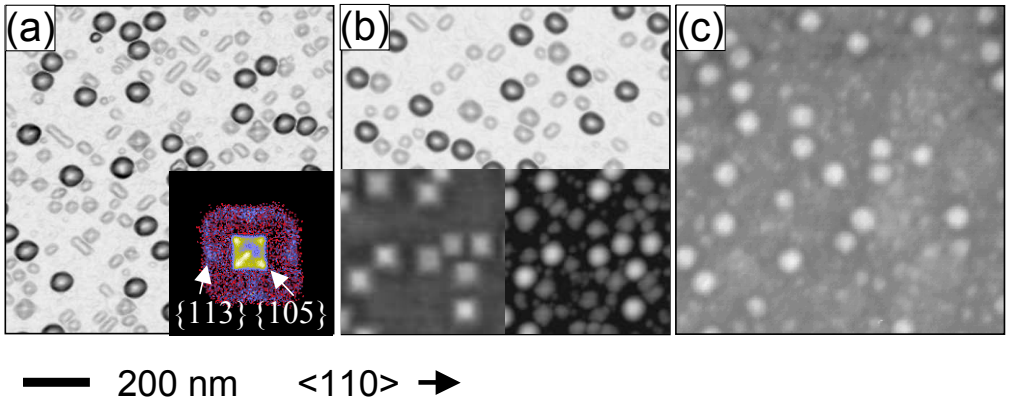

Figure 7.8: AFM images displaying the disclosed islands after the Si cap layer has been etched away for samples overgrown at 300°C (a), 450°C (b) and 580°C (c), respectively. The inset in (a) shows the facet plot of the islands, revealing that after the Si removal the facets of the islands are still present. The insets in (b) display AFM images showing the same area of the sample before (left) and after the 450°C Si cap has been removed (right). A one-to-one correlation between the position of the dome islands and the ziqqurat structures can be seen. The gray scale in (a) and (b) is related to the local surface slope while in (c) and in the insets of (b) it represents the local surface height.

were overgrown at 450°C has also not changed. Although the covering Si surface looks completely different, the buried islands have not experienced any substantial morphological change. This simple experiment proves that the ziqqurat structures observed on the surface *do not* represent the morphology of the underlying island. By measuring the density of the dome islands on the as-grown sample and that of the ziqqurats, similar values are obtained. In order to check whether there is any correlation between the position of the dome islands and the observed ziqqurats, an uncapping experiment was performed by locating the same sample area before and after etching (see Appendix B). The result of this experiment is shown in the insets of Fig. 7.8 (b). A clear correlation is found between the position of underlying shape preserved domes and that of ziqqurat structures, while the surface above hut clusters and pyramids is flat.

On the other hand, the disclosed islands which were overgrown at the

growth temperature (580°C) show obvious morphological changes. Actually just the dome islands are clearly visible. By analyzing them it can be seen that, as already shown in the previous section, their height is drastically reduced (roughly to one third of the initial value before capping) and the width has increased by about 10-20 nm.

7.1.2 Composition of Buried Islands

Since the above described etching method permits the access to the buried islands by simply removing the Si layers above them, it opens also a path to investigate the composition of the disclosed islands. This is simply done by dipping the disclosed islands in the 31% H_2O_2 solution. In other words, first the Si layers are removed by etching selectively Si over Ge and then the composition of the disclosed islands is investigated by selectively etching Ge over Si.

Figure 7.9 shows the result of such an experiment: AFM images of disclosed islands which were capped at 300°C (a), at 450°C (b) and at 580°C (c), after they have been additionally etched for 10 minutes in the 31% H_2O_2 solution. In all cases the dome islands show the ring-like structure which was reported in section 4.1.3 for the uncapped domes. This is a clear indication that also during overgrowth no bulk diffusion is occurring at these temper-

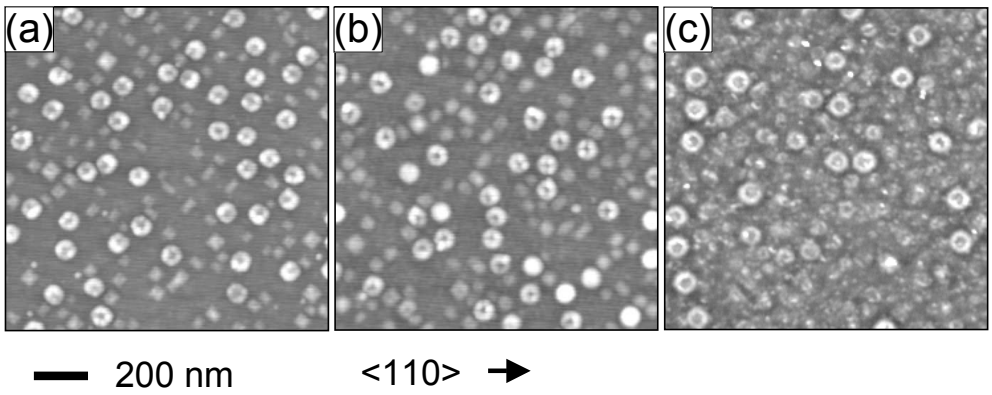

Figure 7.9: AFM images displaying the disclosed islands after etching them for 10 minutes in the 31% H_2O_2 solution. The overgrowth temperatures are 300°C for (a), 450°C for (b) and 580°C for (c).

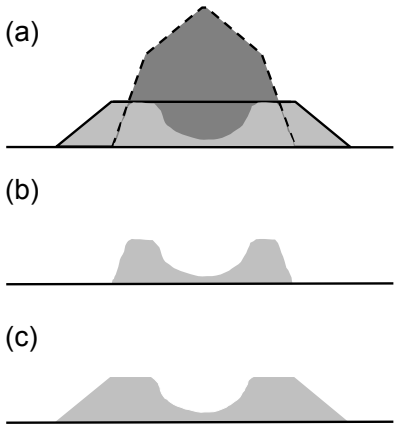

Figure 7.10: Schematic representation of the island morphology and composition. (a) shows the morphological and compositional profile of a dome island before (dashed line) and after overgrowth at 580°C (solid line). Light gray represents Si-rich, dark grey Ge-rich regions. (b) Si-ring remaining on the surface after etching an as-grown or low temperature overgrown dome island. (c) Si-ring remaining on the surface after etching a disclosed island which was overgrown at 580°C. It is seen that the Si-rich base area has become bigger but the Ge-rich region (missing part) does still exist proving thus that no bulk diffusion has taken place.

atures. In fact, if no exchange of atoms can take place within the islands, their composition cannot be altered.

This is very clearly seen in Fig. 7.9 (c). The compositional profile for the disclosed islands overgrown at 580°C shows that although their morphology has drastically changed [see Fig. 7.8 (c)] this is not the case for their composition; the Ge-rich region enclosed by the Si-rich ring does still exist.

In conclusion, it can be stated that under capping conditions such that just surface diffusion can take place, the composition of a morphologically modified buried island can be constructed by the compositional profile of the as-grown one (cut at the reduced new height) with the addition of Si-rich material around the initial base area (see Fig. 7.10). From this compositional profile it emerges that the real, electronically active QD is actually the Ge rich part surrounded by the Si-ring.

Chapter 8

Conclusions and Outlook

In this work the properties of SiGe islands grown on Si(001) were investigated by a combination of selective chemical etching and scanning probe microscopy. The main goal was to determine the stoichiometry of SiGe QDs, i.e. buried SiGe islands.

In the first part of this thesis the composition of free-standing islands was thoroughly investigated. It was shown that as-grown islands show compositional profiles which have a fourfold or cylindrical symmetry. For low growth temperatures, Si is mainly located at the periphery of the islands while for higher temperatures islands with a considerable amount of Si in the center were observed. The compositional profiles of both pyramid and dome islands were explained within a very simple model based on surface diffusion processes and which assumes that the composition of each part of the island is determined at the moment of its growth. No material intermixing within the island was allowed, prohibiting thus any kind of bulk diffusion. This model can not only explain our results but also the results obtained by other groups can be understood within this framework.

During post-growth annealing, the symmetry of the compositional profiles breaks down because the SiGe islands move laterally. This motion is induced by alloying driven energy minimization. Ge-rich material leaves one side of the island by surface diffusion, and mixes with additional Si from the surrounding surface as it redeposits on the other side. Thus while moving the islands become larger and Si-richer.

By analyzing samples grown at high temperatures, coarsening was observed for as-grown as well as for annealed samples. It was shown that also at these temperatures the pyramid to dome transition path, followed by the

islands while growing, is similar to the one reported for lower temperatures. Furthermore, by investigating the shrinking of both as-grown and annealed islands it was revealed that they do not shrink in a self-similar way but they undergo various shape transformations before they "disappear" from the surface. The path the islands follow while shrinking is the reverse of their growth, thus proving that their shape is thermodynamically determined.

Finally, the shape and composition of buried islands was investigated in detail. The Si capping layers were removed and the disclosed islands were analyzed. It was shown that up to the temperature of 450°C the islands undergo neither morphological nor compositional changes. At an overgrowth temperature of 580°C the islands become wider and shallower. Despite these morphological changes, their compositional profile shows that the Ge-rich area present in the as-grown islands, does still exist.

The results obtained in this work demonstrate that at least up to the temperature of 740°C no significant bulk diffusion is taking place. As a consequence, our experiments discard the models which explain the compositional profiles of islands based on bulk diffusion through the basal interface. What is lacking in the literature is a comprehensive model, based just on surface diffusion processes, which will be able to explain the compositional profiles of islands for different growth parameters. Such a model has to be much more sophisticated than the simple one presented in this work, since it has to include also strain, surface energies and the different reconstructions observed on the wetting layer and the facets.

Outlook

The experimental method presented in chapter 7, with which the shape and the composition of embedded islands were revealed, opens further perspectives for performing interesting experiments. In particular, it can allow the experimental determination of the temperature at which bulk diffusion becomes active. The result of a preliminary experiment towards this direction is displayed in Fig. 8.1. A sample which was grown at 580°C, capped at 300°C and subsequently annealed to 750°C was dipped in the 2M KOH solution and the disclosed islands were revealed. No morphological changes can be observed also for the disclosed islands contained in this sample, indicating once more that no bulk diffusion has taken place. A more systematic study, i.e. overgrowing islands at 300°C and post-growth annealing them at different temperatures, will allow the determination of the temperature at which

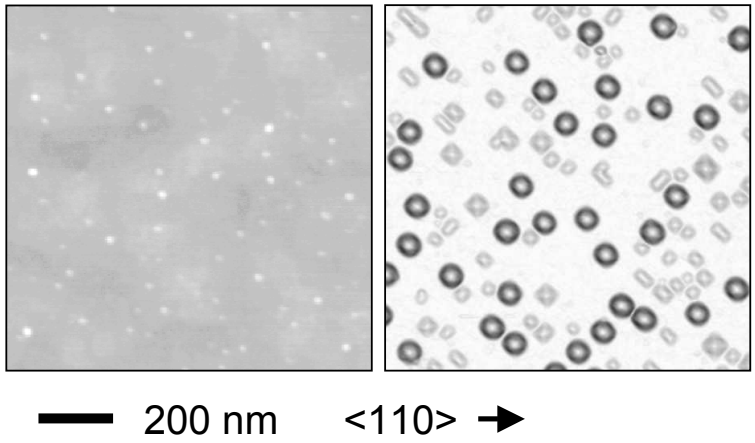

Figure 8.1: (left) AFM image taken after depositing 5.9 ML of Ge at 580°C, 20 nm Si capping at 300°C and subsequent post growth annealing at 750°C. (right) AFM image of the same sample after removing the Si layers. It is seen that the disclosed islands have not experienced morphological changes. The gray scale in the left image represents the local surface height while in the right image the local surface slope is displayed.

bulk diffusion is taking place for the Ge/Si(001) system and in this way a highly discussed issue could be solved.

Additionally, by imaging the same sample areas in closely stacked layers, the vertical island correlations can be characterized. Preliminary results for a double stack of islands shown in Fig. 8.2 demonstrate that indeed these measurements are feasible. The left image in Fig. 8.2 displays second layer islands which have been grown by deposition of 10 ML of Ge at 740°C on a 30 nm Si spacer covering the first layer of islands. In order to reach the buried islands the islands covering the surface are removed by etching the sample in a 1 : 1 volume 31% H_2O_2/28% NH_4OH solution for a long time. After removing the islands the sample is dipped in a 2M KOH solution and the disclosed islands are revealed. By comparing the two images of Fig. 8.2 (both images correspond to exactly the same area) a one-to-one correlation between the position of the islands in the two layers can be observed. This experiment demonstrates that the proposed method offers an easy and cheap alternative to conventional X-TEM measurements and it provides additional

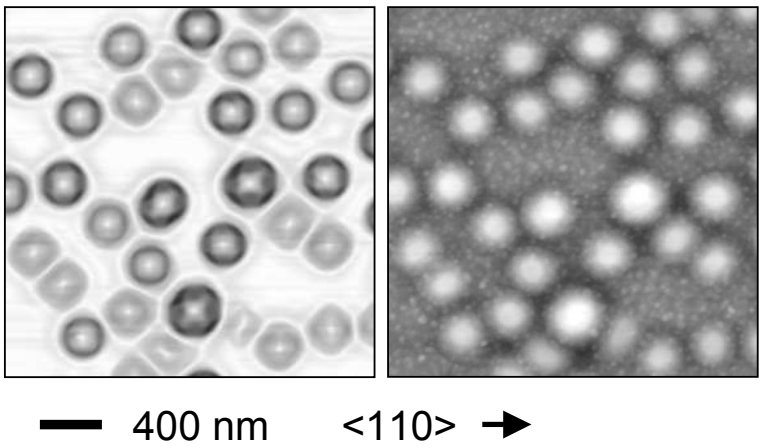

Figure 8.2: Studying the correlation of islands in stacked layers. (left) AFM image of islands contained in the second layer (surface). The islands were grown by deposition of 10ML of Ge at 740°C and the Si spacer had a thickness of 30 nm. (right) AFM image displaying the buried islands contained in the first layer. A one-to-one correlation between the positions of the islands in the two layers does exist. The gray scale in the left image represents the local surface slope while in the right image the local surface height is displayed.

statistical information not available from the latter.

We expect that by proper choice of the selective etchant the etching technique can be applied also to different material systems and thus help to obtain information about the shape and composition of strained islands, that is of fundamental importance for predicting the electronic properties of semiconductor nanostructures.

Appendix A

Surface Reconstruction

The surface reconstruction of the Ge/Si(001) system has been widely investigated [110]. It is known that Si(001) shows a (2×1) reconstruction which forms in order to reduce the number of dangling bonds. After the deposition of 1 ML of Ge this changes to (2×N) and eventually after 2.5-3 MLs of Ge the widely known (M×N) reconstruction appears. Already very early it was shown that the composition of the WL is not 100% Ge but some Si is included in it [71]. Intuitively, it is expected that the Si content in the WL should increase monotonously with the temperature, but this has not been proven up to now. An easy experiment to verify this trend, is to investigate the WL reconstruction of samples grown at different temperatures by means of STM. For this purpose samples grown by deposition of 5 MLs of Ge at 740°C and 840°C were prepared.

Figure A.1 (upper row) shows the WL of samples grown at 740°C (a) and at 840°C (b). The surface reconstruction for the 740°C sample is (M×N), indicating that still for this high temperature the WL is Ge rich. On the other hand, the sample grown at 840°C shows the characteristic (2×N) reconstruction. The difference in the reconstruction pattern proves in a direct way that the Si content of the WL grown at 840°C is higher than the corresponding one at 740°C. We believe that this trend, i.e. the higher the growth temperature the higher the Si content in the WL, is valid also for lower temperatures. By comparing the measured reconstructions with the results of ab-initio and classical molecular dynamics simulations, an estimate of the WL structure and composition might be obtained [111].

Another interesting point about the surface reconstruction is whether it is preserved inside the deep trenches.

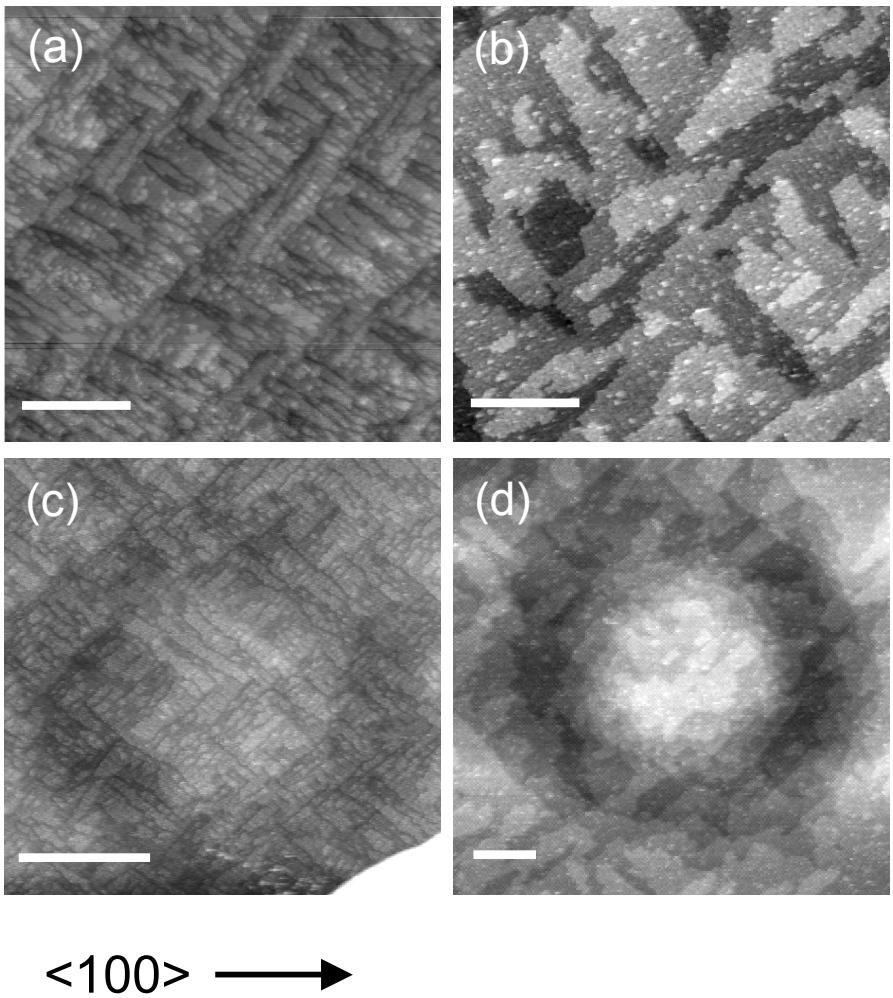

Figure A.1: (upper row) STM images of the WL which show that the surface reconstruction is changing from (M×N) at 740°C (a) to (2×N) at 840°C (b). The white spots in (b) are probably due to a local oxidation of the sample. (lower row) STM images of empty trenches observed on samples grown at (c) 740°C and (d) 840°C. The same reconstruction can be observed on the surface and inside the trenches. The scale bar in each image corresponds to 50 nm.

The lower row of Fig. A.1 shows high resolution STM images of empty trenches remaining on the surface after the islands have disappeared during coarsening: samples grown at (c) 740°C and at (d) 840°C. It can be seen that the reconstruction is the same on the surface and inside the trench. This means that, despite the fact that the trenches extend inside the Si substrate (up to about 1 nm), they are always covered by a Ge-rich layer. The same observation was made also for trenches surrounding islands.

As has been shown in section 4.2.3 for the sample grown at 740°C, the total volume of material incorporated into the islands, is larger than the sum of the volume of the deposited material and the volume of the trenches. It was stated that since at these temperatures bulk diffusion is not significant [96], the "missing" material must be Si originating from below the WL. It was further proposed that Si atoms can out-diffuse through the thin WL and get incorporated into the islands in order to lower their chemical potential [96]. Actually, the real microscopic mechanism governing this phenomenon is not known. But the fact that the same reconstruction is covering also the trench, for which it is accepted that it provides the islands with Si, indicates that such an out-diffusion through the WL is not hindered and can indeed take place. Recently [111] it has been shown that dimer row vacancies are likely to represent preferential channels for diffusion of Si towards the substrate during the Si-capping of the WL. These channels could also be important for the reverse path, i.e. the path that Si follows when it diffuses from the substrate through the WL and towards the islands.

Appendix B

Locating the Same Sample Area

In the first studies where selective etching was applied to self-organized semiconductor islands, the information was obtained by comparing the average morphology of the islands before and after etching [82, 84]. A further improvement of this method is to study the same area, i.e. exactly the same islands, before and after etching. This allows to obtain not only statistical information about the behavior of the island ensemble but also to address individual islands. Moreover, by locating the same island several times it becomes possible to observe not only the final etched morphology, but also the intermediate stages.

In order to find the same surface region after successive etching experiments, prior to etching a cross-like mark is scratched on the surface. Actually, since usually 5×5 mm^2 wafer pieces are used, one of the lines is double in order to break the four-fold symmetry. As a next step the AFM cantilever is positioned close to the marked cross by employing an optical microscope connected with the AFM head and the relative horizontal and vertical distances between the cantilever tip and the cross-mark are measured. Figure B.1 shows such a micro-photograph of the sample displaying the AFM cantilever positioned close to such a mark. After each etching experiment the cantilever is positioned at the same relative position to the cross and the same region is located again.

Figure B.2 shows the etching on the same SiGe island obtained by using this technique.

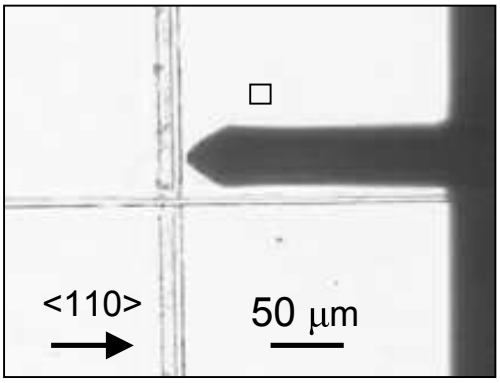

Figure B.1: Micro-photograph (magnification factor 180) showing the positioning of the AFM cantilever at the upper-right corner of the cross-mark. This allows the measurement of the same area after every etching experiment. The square area shown above the cantilever corresponds to the maximum scan range of the AFM (13.4×13.4 μm^2).

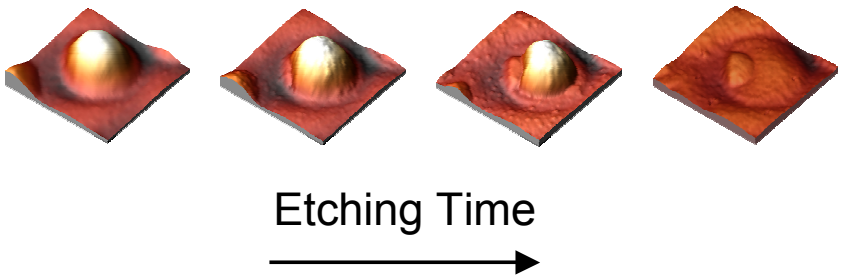

Figure B.2: AFM images showing the same island after 0, 80, 170 and 620 minutes of etching.

Appendix C

Low Temperature Etching

All etching experiments described in this thesis were performed at RT. When using the 1:1 volume (31% H_2O_2)/ (28% NH_4OH) solution on samples grown at high temperatures, intermediate erosion stages can be observed since this solution has a slow etching rate for Si-rich SiGe alloys. On the other hand, etching with the 31% H_2O_2 solution does not allow the observation of the intermediate etching stages since the etching is very fast. As already showed in Chapter 5, the observation of the intermediate stages can be important for getting valuable additional information about the composition of the islands.

In order to be able to address the intermediate stages of etching also when using the 31% H_2O_2 solution, etching experiments at lower temperatures were performed. Figure C.1 shows the etch rate diagram of the 31% H_2O_2 solution at RT and at -10°C. Although the selectivity of Ge over $Ge_{0.7}Si_{0.3}$ is not substantially changed (around 50 at room temperature versus 55 at -10°C), a reduction of the etching rates by a factor about 20-30 can be observed at -10°C. Due to these reduced etch rates, the observation of intermediate etching stages becomes possible.

Low temperature (LT) etching experiments were performed on samples which were grown at 560°C by deposition of 6 MLs of Ge and subsequent annealing for 500 s. The sample contains hut clusters, pyramids and dome islands. For the etching experiment 5×5 mm wafer pieces from adjacent regions were cut so as to have statistically identical samples. The pieces were etched at -10°C for different times (5, 15 and 60 minutes) in a 31% H_2O_2 solution and the morphology of the etched pyramids was subsequently investigated by means of AFM.

Figure C.2 shows the different types of structures (labeled from 1 to 3),

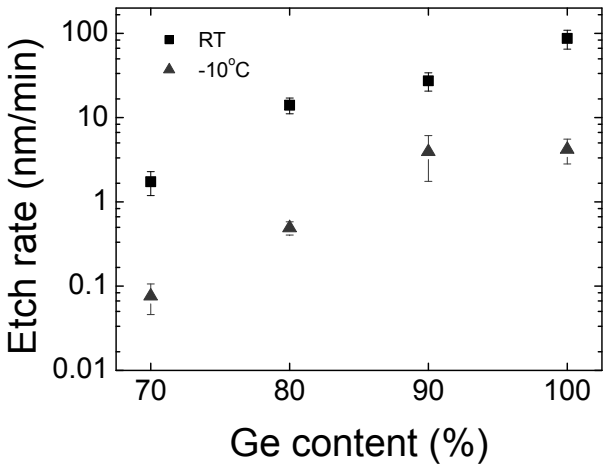

Figure C.1: Etch rate diagram of a 31% H_2O_2 solution at room temperature (squares) and at -10°C (triangles).

which can be found on all the etched samples independently of the etching time. As type 2 we have characterized all the islands in which at least one of the facets has already been attacked by the etchant, but the apex is still protruding. For every different etching time there is a peak in the statistical distribution of these types, which is shifting from type 1 to type 3 while the etching time increases from 5 to 60 minutes. This is clearly seen in Fig. C.3, where the relative frequency of each type for the different etching times is shown. The diagram shown in Fig. C.3 allows us to interpret Fig. C.2 as the route which is followed during the etching procedure. The etchant initially attacks the facets of the pyramid while also the top of the island is being consumed. Eventually, both facets and island top are removed and just the periphery of the pyramid, mainly its corners, are remaining. From Fig. C.3 one important observation can be made. Not every pyramid is reaching type 3 structure even after etching for a long time. Some of them stop to be etched while they have a structure of type 2. It was furthermore verified that the final structure after etching does not depend on the initial size of the pyramid. Since not all the pyramids show the same structure after etching, we can conclude that they have a different composition although they look identical. Not only a compositional difference between pyramids of the same sample does exist but also facets of the same pyramid seem to have a different composition.

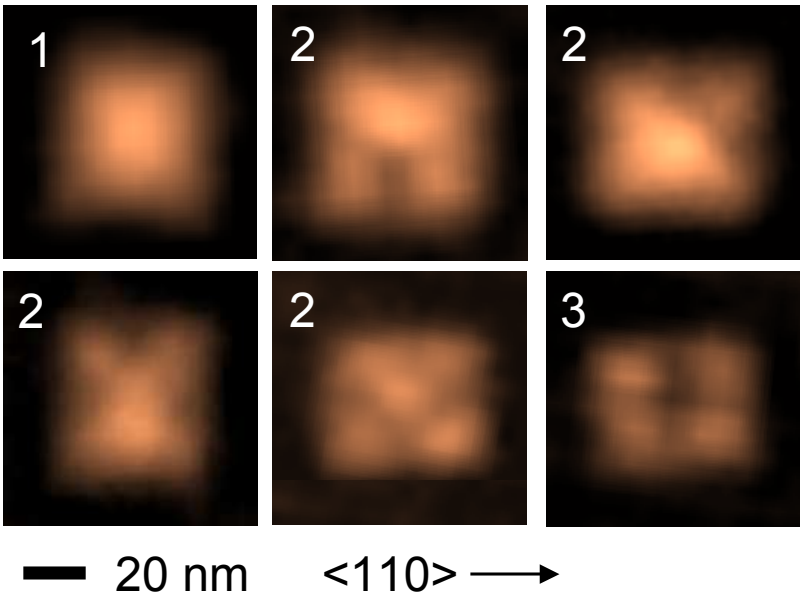

Figure C.2: Images of the different pyramid structures (labeled from 1 to 3) observed with AFM after etching.

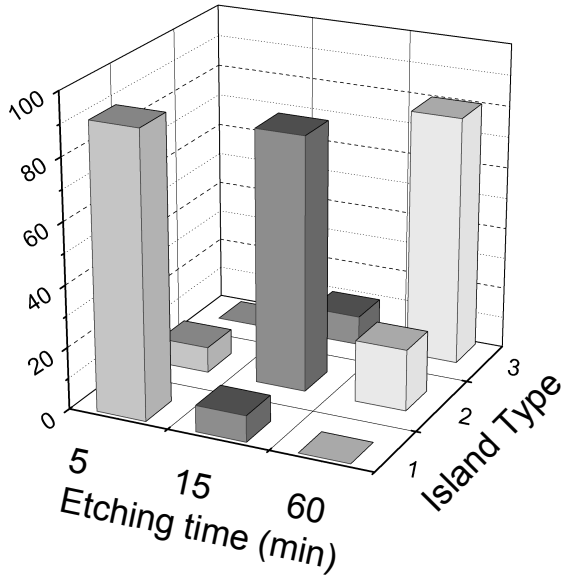

Figure C.3: Diagram showing the relative frequency of each etched structure as a function of the etching time. Island types correspond to the definition given in Fig. C.2.

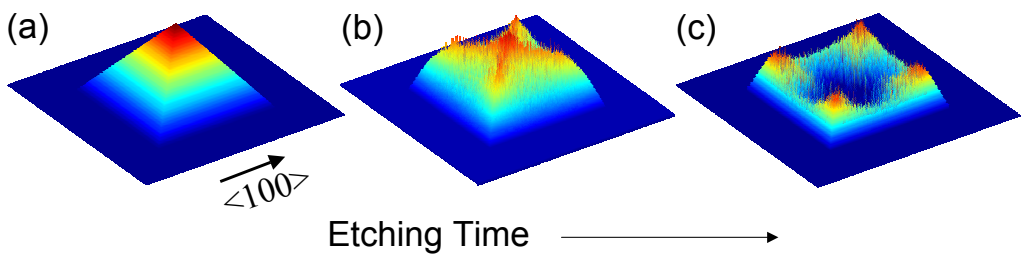

Figure C.4: Images showing snapshots from the simulated etching. A good similarity to the experiment can be observed. The vertical scale of (a) has been reduced by 50% compared to the other two images.

In Chapter 4 a compositional map for Ge pyramids grown on Si(001) was simulated. It was proposed that the pyramids have a Si rich periphery (more pronounced at the corners) and that their composition while going from the base to the apex of the island is getting Ge richer. Additionally, we reported that there is a local increase in the Si content at the center of the pyramid at some height from the substrate. Afterwards, in Chapter 5 it was shown that the compositional profiles of the pyramids do not change upon annealing.

For being able to make a comparison between the compositional map and the experimental results on the successive etching stages, also the erosion of the pyramid islands was simulated. In this simulation the atoms which are getting in contact with the etchant are removed, with a probability that depends on the average composition of each point. This probability is 1 for a 100% Ge composition, scales down for Si richer parts and eventually becomes 0 for Ge concentrations less than 65%. By performing the simulated etching it can be seen that the experimental etching route can be indeed reproduced [Fig. C.4]. The islands, even when their Si content is low, are passing through a structure of type 2 before the final type 3 structure is appearing, where mainly the four corners protrude. For a Si richer pyramid the etching will stop at a structure similar to Fig. C.4 (b).

Bibliography

[1] L. Canham. Silicon optoelectronics at the end of the rainbow? *Physics World*, 5(3):41, 1992.

[2] M. Arienzo, S. S. Iyer, B. S. Meyerson, G. L. Patton, and M. C. Stork. Si-Ge alloys - growth, properties and applications. *Applied Surface Science*, 48/49:377, 1991.

[3] D. J. Eaglesham and M. Cerullo. Dislocation-free Stranski-Krastanow growth of Ge on Si(100). *Physical Review Letters*, 64:1943, 1990.

[4] Y.-M. Mo, D. E. Savage, B. S. Swartzentruber, and M. G. Lagally. Kinetic pathway in Stranski-Krastanov growth of Ge on Si(001). *Physical Review Letters*, 65:1020, 1990.

[5] B. Delley and E. F. Steigmeier. Quantum confinement in Si nanocrystals. *Physical Review B*, 47(3):1397, 1993.

[6] M. Stoffel, U. Denker, and O. G. Schmidt. Electroluminescence of self-assembled Ge hut clusters. *Applied Phyiscs Letters*, 82:3236, 2003.

[7] U. Denker, M. Stoffel, O. G. Schmidt, and H. Sigg. Ge hut cluster luminescence below bulk Ge band gap. *Applied Physics Letters*, 82:454, 2003.

[8] M. Stoffel, U. Denker, G. S. Kar, H. Sigg, and O. G. Schmidt. Extended wavelength region of self-assembled Ge/Si(001) islands capped with Si at different temperatures. *Applied Physics Letters*, 83:2910, 2003.

[9] J. Konle, H. Presting, H. Kibbel, K. Thonke, and R. Sauer. Enhanced performance of silicon based photodetectors using silicon/germanium nanostructures. *Solid State Electronics*, 45(11):1921, 2001.

[10] P. Boucaud, V. Le Thanh, S. Sauvage, D. Dbarre, and D. Bouchier. Intraband absorption in Ge/Si self-assembled quantum dots. *Applied Physics Letters*, 74:401, 1999.

[11] H. Presting, J. Konle, and H. Kibbel. Self-assembled Ge-dots for Si solar cells. *International Journal of Modern Physics B*, 16(28-29):4347, 2002.

[12] O. G. Schmidt and K. Eberl. Self-assembled Ge/Si dots for faster field-effect transistors. *IEEE Transactions on Electron Devices*, 48(6):1175, 2001.

[13] F. C. Frank and J. H. van der Merwe. *Proc. Roy. Soc. London A*, 198:205, 1949.

[14] Z. Zhang, F. Wu, and M. G. Lagally. An atomistic view of Si(001) homoepitaxy. *Annual Review of Materials Science*, 27:525, 1997.

[15] M. Vollmer and A. Weber. *Zeitschrift für Physikalische Chemie*, 119:277, 1926.

[16] A. Dragoset, P. N. First, J. A. Stroscio, D. T. Pierce, and R. J. Celotta. *MRS Symposia Proceedings*, 151:193, 1989.

[17] I. N. Stranski and L. Krastanov. Zur Theorie der orientierten Ausscheidung von Ionenkristallen aufeinander. *Akad.Wiss. Lit. Mainz Math.-Natur. Kl.*, IIb:797, 1939.

[18] J. Stangl, V. Holý, and G. Bauer. Structural properties of self-organized semiconductor nanostructures. *Review of Modern Physics*, 76:725, 2004.

[19] E. Bauer and J. H. van der Merwe. Structure and growth of crystalline superlattices: from monolayer to superlattice. *Physical Review B*, 33:3657, 1986.

[20] Hull and Bean. Germanium Silicon: Physics and Materials. *Academic Press 1999.*

[21] Taken from the webpage of the MBE group of our Institute: www.fkf.mpg.de/mbe/.

[22] A. Rastelli, H. von Känel, B. J. Spencer, and J. Tersoff. Prepyramid-to-pyramid transition of SiGe islands on Si(001). *Physical Review B*, 68:115301, 2003.

[23] C. Manzano. Scanning Tunneling Microscopy of self-organized semiconductor quantum dots. *PhD Thesis, Lausanne, EPFL*, 2004.

[24] E. Sutter, P. Sutter, and J. E. Bernard. Extended shape evolution of low mismatch $Si_{1x}Ge_x$ alloy islands on Si(100). *Applied Physics Letters*, 84:2262, 2004.

[25] A. Vailionis, B. Cho, G. Glass, P. Desjardins, D. G. Cahill, and J. E. Greene. Pathway for the Strain-Driven Two-Dimensional to Three-Dimensional Transition during Growth of Ge on Si(001). *Physical Review Letters*, 85:3672, 2000.

[26] J. Tersoff, B. J. Spencer, A. Rastelli, and H. von Känel. Barrierless Formation and Faceting of SiGe Islands on Si(001). *Physical Review Letters*, 89:196104, 2002.

[27] M. Tomitori, K. Watanabe, M. Kobayashi, and O. Nishikawa. STM study of the Ge growth mode on Si(001) substrates . *Applied Surface Science*, 76-77:322, 1994.

[28] T. I. Kamins, G. Medeiros-Ribeiro, D. A. A. Ohlberg, and R. Stanley. Evolution of Ge islands on Si(001) during annealing. *Journal of Applied Physics*, 85:1159, 1999.

[29] S. A. Chaparro, Y. Zhang, J. Drucker, D. Chandrasekhar, and D. J. Smith. Evolution of Ge/Si(100) islands: Island size and temperature dependence. *Journal of Applied Physics*, 87:2245, 2000.

[30] U. Denker, O. G. Schmidt, N. Y. Jin-Phillipp, and K. Eberl. Trench formation around and between self-assembled Ge islands on Si. *Applied Physics Letters*, 78:3723, 2001.

[31] T. I. Kamins, E. C. Carr, R. S. Williams, and S. J. Rosner. Deposition of three-dimensional Ge islands on Si(001) by chemical vapor deposition at atmospheric and reduced pressures. *Journal of Applied Physics*, 81:211, 1997.

[32] X. Z. Liao, J. Zou, D. J. H. Cockayne, J. Oin, Z. M. Jiang, X. Wang, and R. Leon. Strain relaxation by alloying effects in Ge islands grown on Si(001). *Physical Review B*, 60:15605, 1999.

[33] S. A. Chaparro, J. Drucker, Y. Zhang, D. Chandrasekhar, M. R. McCartney, and D. J. Smith. Strain-Driven Alloying in Ge/Si(100) Coherent Islands. *Physical Review Letters*, 83:1199, 1999.

[34] P. Raiteri, L. Miglio, F. Valentinotti, and M. Celino. Strain maps at the atomic scale below Ge pyramids and domes on a Si substrate. *Applied Physics Letters*, 80:3736, 2002.

[35] C. Ratsch, A. Zangwill, and P. Šmilauer. Scaling of heteroepitaxial island sizes. *Surface Science*, 314:L937, 1994.

[36] D. Kandel and E. Kaxiras. Surfactant mediated crystal growth of semiconductors. *Physical Review Letters*, 75:2742, 1995.

[37] Ph. Sonnet and P. C. Kelires. Physical origin of trench formation in Ge/Si(100) islands. *Applied Physics Letters*, 85:203, 2004.

[38] E. Bauer. *Zeitschrift für Kristallographie*, 110:372, 1958.

[39] E. Bauer and H. Popper. *Thin Solid Films*, 12:167, 1972.

[40] H. Lüth. Surfaces and Interfaces of Solid Materials. *Springer Verlag 1993.*

[41] J. Tersoff and F. K. LeGoues. Competing relaxation mechanisms in strained layers. *Physical Review Letters*, 72:3570, 1994.

[42] V. A. Shchukin, N. N. Ledentsov, P. S. Kopev, and D. Bimberg. Spontaneous Ordering of Arrays of Coherent Strained Islands. *Physical Review Letters*, 75:2968, 1995.

[43] G. Medeiros-Ribeiro, A. M. Bratkovski, T. I. Kamins, D. A. A. Ohlberg, and R. S. Williams. Shape Transition of Germanium Nanocrystals on a Silicon (001) Surface from Pyramids to Domes. *Science*, 279:353, 1998.

[44] W. Ostwald. *Z. Phys. Chem.*, 34:495, 1900.

[45] F. M. Ross, J. Tersoff, and R. M. Tromp. Coarsening of Self-Assembled Ge Quantum Dots on Si(001). *Physical Review Letters*, 80:984, 1998.

[46] F. M. Ross and R. M. Tromp. Transition States Between Pyramids and Domes During Ge/Si Island Growth. *Science*, 286:1931, 1999.

[47] A. Rastelli. Structural evolution of nanoscopic islands of Ge and SiGe on Si(001). *PhD Thesis, Universitá degli Studi di Pavia*, 2002.

[48] Ashcroft and Mermin. Solid State Physics. *Thomson Brooks/Cole 1976*.

[49] M. L. W. Thewalt, D. A. Harrison, C. F. Reinhart, J. A. Wolk, and H. Lafontaine. Type II Band Alignment in $Si_{1-x}Ge_x$/Si(001) Quantum Wells: The Ubiquitous Type I Luminescence Results from Band Bending. *Physical Review Letters*, 79:269, 1997.

[50] C. G. van de Walle and R. M. Martin. Theoretical calculations of heterojunction discontinuities in the Si/Ge system. *Physical Review B*, 34:5621, 1986.

[51] A. I. Yakimov, N. P. Stepina, A. V. Dvurechenskii, A. I. Nikiforov, and A. V. Nenashev. Excitons in charged Ge/Si type-II quantum dots. *Semiconductor Science and Technology*, 15:1125, 2000.

[52] H. Sunamura, N. Usami, Y. Shiraki, and S. Fukatsu. Island Formation During Growth of Ge on Si(100) - a Study Using Photoluminescence Spectroscopy. *Applied Physics Letters*, 66:3024, 1995.

[53] P. Schittenhelm, M. Gail, J. Brunner, J. F. Nützel, and G. Abstreiter. Photoluminescence Study of the Crossover from 2-Dimensional to 3-Dimensional Growth for Ge on Si(100). *Applied Physics Letters*, 67:1292, 1995.

[54] P. Sutter and M. G. Lagally. Embedding of Nanoscale 3D SiGe Islands in a Si Matrix. *Physical Review Letters*, 81:3471, 1998.

[55] A. Rastelli, M. Kummer, and H. von Känel. Reversible Shape Evolution of Ge Islands on Si(001). *Physical Review Letters*, 87:256101, 2001.

[56] W. Zulehner, D. Huber, R. G. Seidensticker, and R. B. Heimann. Crystals: Growth, Properties, and Applications. Silicon Chemical Etching. *Springer-Verlag 1982*.

[57] E. A. Fitzgerald, Y.-H. Xie, M. L. Green, D. Brasen, A. R. Kortan, J. Michel, Y.-J. Mii, and B. E. Weir. Totally relaxed Ge_xSi_{1x} layers with low threading dislocation densities grown on Si substrates. *Applied Physics Letters*, 59:811, 1991.

[58] G. Isella, D. Chrastina, B. Rossner, T. Hackbarth, H. Herzog, U. Konig, and H. von Känel. Low-energy plasma-enhanced chemical vapor deposition for strained Si and Ge heterostructures and devices. *Solid-State Electronics*, 48(8):1317, 2004.

[59] P. J. Holmes. The electrochemistry of semiconductors. *Academic Press, Ltd., London*.

[60] E. D. Palik, V. M. Bermudez, and O. J. Glembocki. Ellipsometric study of the etch-stop mechanism in heavily doped Silicon. *Journal of the Electrochemical Society*, 132(1):135, 1985.

[61] P. M. Sarro and A. W. Vanherwaarden. Silicon cantilever beams fabricated by electrochemically controlled etching for sensor applications. *Journal of the Electrochemical Society*, 133(8):1724, 1986.

[62] E. Bassous and E. F. Baran. Fabrication of high precision nozzles by anisotropic etching of (100) Silicon. *Journal of the Electrochemical Society*, 125(8):1321, 1978.

[63] V. Lehmann. Electrochemistry of Si. *Wiley-VCH 2002*.

[64] E. A. Fitzgerald, K. C. Wu, M. Currie, N. Gerrish, D. Bruce, and J. Borenstein. Silicon-Based Epitaxial Films for MEMS. *Mat. Res. Soc. Symp. Proc.*, 518:233, 1998.

[65] A. H. Krist, D. J. Godbey, and N. P. Green. Selective removal of a $Si_{0.7}Ge_{0.3}$ layer from Si(100). *Applied Physics Letters*, 58(17):1899, 1991.

[66] T. K. Carns, M. O. Tanner, and K. L. Wang. Chemical etching of $Si_{1-x}Ge_x$ in HF-H_2O_2-CH_3COOH. *Journal of the Electrochemical Society*, 142(4):1260, 1995.

[67] W. Primak, R. Kampwirt, and Y. Dayal. Peroxide etching of Germanium. *Journal of the Electrochemical Society*, 114(1):88, 1967.

[68] B. L. Bircumshaw, M. L. Wasilik, E. B. Kim, Y. R. Su, H. Takeuchi, C. W. Low, G. Liu, A. P. Pisano, T.-J. King, and R. T. Howe. Hydrogen peroxide etching and stability of p-type poly-SiGe films. *Technical Digest, 2004 IEEE, 17th International Conference on Micro Electro Mechanical Systems*, page 514, 2004.

[69] W. Kern. Handbook of semiconductor wafer cleaning technology. *Noyes Publications 1993*.

[70] F. S. Johnson, D. S. Miles, D. T. Grider, and J. J. Wortman. Selective chemical etching of polycrystalline SiGe alloys with respect to Si and SiO_2. *Journal of Electronic Materials*, 21(8):805, 1992.

[71] K. Nakajima, A. Konishi, and K. Kimura. Direct Observation of Intermixing at Ge/Si(001) Interfaces by High-Resolution Rutherford Backscattering Spectroscopy. *Physical Review Letters*, 83:1802, 1999.

[72] R. Magalhães-Paniago, G. Medeiros-Ribeiro, A. Malachias, S. Kycia, T. I. Kamins, and R. S. Williams. Direct evaluation of composition profile, strain relaxation, and elastic energy of Ge:Si(001) self-assembled islands by anomalous x-ray scattering. *Physical Review B*, 66:245312, 2002.

[73] G. Capellini, M. De Seta, and F. Evangelisti. SiGe intermixing in Ge/Si(100) islands. *Applied Physics Letters*, 78:303, 2001.

[74] T. U. Schülli, J. Stangl, Z. Zhong, R. T. Lechner, M. Sztucki, T. H. Metzger, and G. Bauer. Direct Determination of Strain and Composition Profiles in SiGe Islands by Anomalous X-Ray Diffraction at High Momentum Transfer. *Physical Review Letters*, 90:066105, 2003.

[75] J. Stangl, A. Daniel, V. Holý, T. Roch, G. Bauer, I. Kegel, T. H. Metzger, Th. Wiebach, O. G. Schmidt, and K. Eberl. Strain and composition distribution in uncapped SiGe islands from x-ray diffraction. *Applied Physics Letters*, 79:1474, 2001.

[76] F. Boscherini, G. Capellini, L. Di Gaspare, F. Rosei, N. Motta, and S. Mobilio. GeSi intermixing in Ge quantum dots on Si(001) and Si(111). *Applied Physics Letters*, 76:682, 2000.

[77] N. Motta, F. Rosei, A. Sgarlata, G. Capellini, G. Mobilio, and F. Boscherini. Evolution of the intermixing process in Ge/Si(111) self-assembled islands. *Materials Science and Engineering B*, 88:264, 2002.

[78] A. V. Kolobov, H. Oyanagi, S. Wei, K. Brunner, G. Abstreiter, and K. Tanaka. Local structure of Ge quantum dots self-assembled on Si(100) probed by x-ray absorption fine-structure spectroscopy. *Physical Review B*, 66:075319, 2002.

[79] M. Floyd, Y. T. Zhang, K. P. Driver, J. Drucker, P. A. Crozier, and D. J. Smith. Nanometer-scale composition measurements of Ge/Si(100) islands. *Applied Physics Letters*, 82:1473, 2003.

[80] A. Malachias, S. Kycia, G. Medeiros-Ribeiro, R. Magalhães-Paniago, T. I. Kamins, and R. S. Williams. 3D Composition of Epitaxial Nanocrystals by Anomalous X-Ray Diffraction: Observation of a Si-Rich Core in Ge Domes on Si(100). *Physical Review Letters*, 91:176101, 2003.

[81] T. U. Schülli, M. Stoffel, A. Hesse, J. Stangl, R. T. Lechner, E. Wintersberger, M. Sztucki, T. H. Metzger, O. G. Schmidt, and G. Bauer. Influence of growth temperature on interdiffusion in uncapped SiGe-islands on Si(001) determined by anomalous x-ray diffraction and reciprocal space mapping. *Physical Review B*, 71:035326, 2005.

[82] U. Denker, M. Stoffel, and O. G. Schmidt. Probing the Lateral Composition Profile of Self-Assembled Islands. *Physical Review Letters*, 90:196102, 2003.

[83] F. Ratto, F. Rosei, A. Locatelli, S. Cherigi, S. Fontana, S. Heyn, P.-D. Szkutnik, A. Sgarlata, M. De Crescenzi, and N. Motta. Composition of Ge(Si) islands in the growth of Ge on Si(111) by x-ray spectromicroscopy. *Journal of Applied Physics*, 97:043516, 2005.

[84] O. G. Schmidt, U. Denker, S. Christiansen, and F. Ernst. Composition of self-assembled Ge/Si islands in single and multiple layers. *Applied Physics Letters*, 81:2614, 2002.

[85] T. I. Kamins, G. Medeiros-Ribeiro, D. A. A. Ohlberg, and R. S. Williams. Dome-to-pyramid transition induced by alloying of Ge islands on Si(001). *Applied Physics A*, 67:727, 1998.

[86] G. Hadjisavvas and P. C. Kelires. Critical aspects of alloying and stress relaxation in Ge/Si(100) islands. *Physical Review B*, 72:075334, 2005.

[87] N. Liu, J. Tersoff, O. Baklenov, A. L. Holmes Jr., and C. K. Shih. Nonuniform Composition Profile in $In_{0.5}Ga_{0.5}As$ Alloy Quantum Dots. *Physical Review Letters*, 84:334, 2000.

[88] F. Montalenti, P. Raiteri, D. B. Migas, H. von Känel, A. Rastelli, C. Manzano, G. Costantini, U. Denker, O. G. Schmidt, K. Kern, and L. Miglio. Atomic-Scale Pathway of the Pyramid-to-Dome Transition during Ge Growth on Si(001). *Physical Review Letters*, 93:216102, 2004.

[89] V. Cherepanov and B. Voigtländer. Influence of material, surface reconstruction, and strain on diffusion at the Ge(111) surface. *Physical Review B*, 69:125331, 2004.

[90] L. Huand, F. Liu, G.-H. Lu, and X. G. Gong. Surface Mobility Difference between Si and Ge and Its Effect on Growth of SiGe Alloy Films and Islands. *Physical Review Letters*, 96:016103, 2006.

[91] F. Ratto, F. Rosei, A. Locatelli, S. Cherifi, S. Fontana, S. Heun, P.-D. Szkutnik, A. Sgarlata, M. De Crescenzi, and N. Motta. Composition of Ge(Si) islands in the growth of Ge on Si(111). *Applied Physics Letters*, 84:4526, 2004.

[92] A. Rastelli and H. von Känel. Surface evolution of faceted islands. *Surface Science Letters*, 515:493, 2002.

[93] J. Räisänen, J. Hirvonen, and A. Antilla. The diffusion of silicon in germanium. *Solid State Electronics*, 24:333, 1981.

[94] G. L. McVay and A. R. DuCharme. The diffusion of germanium in silicon. *Journal of Applied Physics*, 44:1409, 1973.

[95] J. Wan, Y. H. Luo, Z. M. Jiang, G. Lin, J. L. Liu, K. L. Wang, X. Z. Liao, and J. Zou. Ge/Si interdiffusion in the GeSi dots and wetting layers. *Journal of Applied Physics*, 90:4290, 2001.

[96] U. Denker, A. Rastelli, M. Stoffel, J. Tersoff, G. Katsaros, G. Costantini, K. Kern, N. Y. Jin-Phillipp, D. E. Jesson, and O. G. Schmidt. Lateral Motion of SiGe Islands Driven by Surface-Mediated Alloying. *Physical Review Letters*, 94:216103, 2005.

[97] M. Stoffel, A. Rastelli, S. Kiravittaya, and O. G. Schmidt. Strain mediated SiGe island motion in single and stacked layers. *Physical Review B*.

[98] R. E. Rudd, G. A. D. Briggs, A. P. Sutton, G. Medeiros-Ribeiro, and R. S. Williams. Equilibrium Model of Bimodal Distributions of Epitaxial Island Growth. *Physical Review Letters*, 90:146101, 2003.

[99] A. Rastelli, M. Stoffel, J. Tersoff, G. S. Kar, and O. G. Schmidt. Kinetic Evolution and Equilibrium Morphology of Strained Islands. *Physical Review Letters*, 95:026103, 2005.

[100] M. Stoffel, G. S. Kar, U. Denker, A. Rastelli, H. Sigg, and O. G. Schmidt. Shape, facet evolution and photoluminescence of Ge islands capped with Si at different temperatures. *Physica E*, 23:421, 2004.

[101] J. Stangl, A. Hesse, V. Hóly, Z. Zhong, G. Bauer, U. Denker, and O. G. Schmidt. Effect of overgrowth temperature on shape, strain, and composition of buried Ge islands deduced from x-ray diffraction. *Applied Physics Letters*, 82:2251, 2003.

[102] A. Hesse, J. Stangl, V. Holý, T. Roch, G. Bauer, O. G. Schmidt, U. Denker, and B. Struth. Effect of overgrowth on shape, composition, and strain of SiGe islands on Si(001). *Physical Review B*, 66:085321, 2002.

[103] I. A. Karpovich, N. V. Baidus, B. N. Zvonkov, D. O. Filatov, S. B. Levichev, A. V. Zdoroveishev, and V. A. Perevoshikov. Investigation of the Buried InAs/GaAs Quantum Dots by Atomic Force Microscopy Combined with Selective Chemical Etching. *Physics of Low-Dimensional Structures*, 3/4:341, 2001.

[104] I. A. Karpovich, N. V. Baidus, B. N. Zvonkov, S. V. Morozov, D. O. Filatov, and A. V. Zdoroveishev. Morphology and photoelectronic properties of InAs/GaAs surface quantum dots grown by metal-organic vapour-phase epitaxy. *Nanotechnology*, 12:425, 2001.

[105] Zh. M. Wang, L. Zhang, K. Holmes, and G. J. Salamo. Selective etching of InGaAs/GaAs(100) multilayers of quantum-dot chains. *Applied Physics Letters*, 86:143106, 2005.

[106] J. Stangl, T. Schülli, A. Hesse, V. Holý, G. Bauer, M. Stoffel, and O. G. Schmidt. Structural properties of semiconductor nanostructures from x-ray scattering. *DPG Proceedings 2004*.

[107] A. Rastelli, E. Müller, and H. von Känel. Shape preservation of Ge/Si(001) islands during Si capping. *Applied Physics Letters*, 80:1438, 2002.

[108] S. Decossas, J. J. Marchand, and G. Brémond. Electrical characterisation of local electronic properties of self-assembled semiconductor nanostructures using AFM. *Physica E*, 23:396, 2004.

[109] M. Kummer, B. Vögeli, and H. von Känel. Si overgrowth of self-assembled Ge clusters on Si(001) - a scanning tunnelling microscopy study. *Materials Science and Engineering B*, 69-70:247, 2000.

[110] B. Voigtländer. Fundamental processes in Si/Si and Ge/Si epitaxy studied by scanning tunneling microscopy during growth. *Surface Science Reports*, 43:127, 2001.

[111] D. B. Migas, P. Raiteri, L. Miglio, A. Rastelli, and H. von Känel. Evolution of the Ge/Si(001) wetting layer during Si overgrowth and crossover between thermodynamic and kinetic behavior. *Physical Review B*, 69:235318, 2004.

Publications

- G. Katsaros et al., *"Revealing the 3D shape and composition of buried SiGe islands"*, in preparation.
- G. Katsaros, A. Rastelli, M. Stoffel, P. Acosta-Diaz, O. G. Schmidt, G. Costantini and K. Kern, *"Growth and shrinking paths of SiGe islands during high temperature coarsening"*, in preparation.
- G. Costantini, A. Rastelli, C. Manzano, P. Acosta-Diaz, G. Katsaros, R. Songmuang, O. G. Schmidt, and K. Kern, *"Interplay between thermodynamics and kinetics in the capping of InAs/GaAs(001) quantum dots"*, submitted.
- G. Katsaros, A. Rastelli, M. Stoffel, G. Isella, H. von Känel, A. Bittner, U. Denker, O. G. Schmidt, G. Costantini, and K. Kern, *"Revealing the lateral motion of self-organized islands by selective chemical etching"*, submitted.
- Z. Zhong, G. Katsaros, M. Stoffel, G. Costantini, K. Kern, O. G. Schmidt, N. Y. Jin-Phillipp, G. Bauer, *"Periodic pillar structures formed by Si etching of multilayer GeSi/Si"*, Appl. Phys. Lett., 87, 263102 (2005).
- G. Katsaros, G. Costantini, M. Stoffel, R. Esteban, A. M. Bittner, P. Acosta-Diaz, A. Rastelli, U. Denker, O. G. Schmidt, and K. Kern, *"Kinetic origin of island intermixing during the growth of Ge on Si(001)"*, Phys. Rev. B 72, 195320 (2005).
- U. Denker, A. Rastelli, M. Stoffel, J. Tersoff, G. Katsaros, G. Costantini, K. Kern, N. Y. Jin-Phillipp, D. E. Jesson, and O. G. Schmidt, *"Lateral motion of SiGe islands driven by surface-mediated alloying"*, Phys. Rev. Lett. 94, 211603 (2005).

- G. Costantini, A. Rastelli, C. Manzano, P. Acosta-Diaz, G. Katsaros, R. Songmuang, O. G. Schmidt, H. v. Känel, and K. Kern, *"Pyramids and domes in the InAs/GaAs(001) and Ge/Si(001) systems"*, J. Crystal Growth 278, 38 (2005).

Acknowledgments

I would like to thank the following people without whom this work would have not been possible:

- Prof. Klaus Kern for giving me the opportunity to perform my PhD thesis on such an exciting subject and to be a member of his research group.
- Prof. G. Schatz and Prof. M. Fuchs for judging this thesis and for being so kind to participate in my PhD exam.
- Giovanni Costantini for being my supervisor and for his support during this 3 1/2 years of my PhD.
- The MBE group of Oliver Schmidt for the very nice collaboration we had. In particular I would like to thank Mathieu Stoffel for the numerous samples he grew for me, for the very pleasant and nice working atmosphere and for making my papers readable!
- Carlos Manzano for the great time we spent together during my 1 1/2 years in Stuttgart. "Thank you for everything my friend".
- Paola Acosta, for "enduring" me and my bad mood all this time working together. "Thanks!"
- Ruben Esteban, for his help in setting up the simulations.
- E. Müller, for performing for us TEM measurements.
- G. Isella from the group of Prof. von Känel, for growing the virtual substrates needed for the calibration of the etchants.

- J. Tersoff, for the very nice collaboration and the helpful discussions which hopefully "developed" a bit my brain.

- Gero Wittich, Lucia Vitali, Alpan Bek and Michael Vogelgesang, for they support during the attempts to fix the STM and not only.

- My colleagues and friends in the office: Frank Stadler, Thomas Classen, Stephan Rauschenbach and Thomas Weitz. "Lust auf ein Spielchen?"

- Alex Bittner for his guidance in my chemical experiments, but even more important, for the many private discussions we had and the advices he gave me.

- Ruben Esteban (please don't forget to mention me and my car you know when!), Tilman Assmus (be aware a hacker is among us), Eduardo Lee (in the end you will accept that Karagounis is the best football player ever), Alicia Forment (Denia-Valencia is not so far away!), Diego Repetto (please send me a picture of Vieri's girlfriend), Kannan Balasubramanian (don't worry you will get kourabiedakia also in the future), Jens Böttcher (famous also for his greek surname Bocha!) and all the other people of the Kern's group.

- Wolfgang Heinz, Wolfgang Stiepany, and Mr. Chaikevitch for their help in solving any kind of technical problems, also the very "stupid" ones.

- Dimitris Paroglou, the "psychologist", for being always such a nice company.

- My friend and colleague Armando Rastelli for teaching me so many things during my thesis but even more for the nice "sad" times we spent this last 3 1/2 years in Stuttgart. "Geia mas, Armando!!"